

An *in vivo* structure-function analysis of the pathogenesis of triosephosphate isomerase deficiency.

by

Bartholomew P. Roland

Bachelor of Science, Central Michigan University, 2004

Submitted to the Graduate Faculty of
the School of Medicine in partial fulfillment
of the requirements for the degree of
Doctor of Philosophy

University of Pittsburgh

2014

UNIVERSITY OF PITTSBURGH

School of Medicine

This dissertation was presented

by

Bartholomew P. Roland

It was defended on

December 13th, 2013

and approved by

Donald B. DeFranco, Professor, Department of Pharmacology & Chemical Biology

Edwin S. Levitan, Professor, Department of Pharmacology & Chemical Biology

William C. deGroat, Distinguished Professor, Department of Pharmacology & Chemical
Biology

Yang Hong, Associate Professor, Department of Cell Biology

Dissertation Advisor: Michael J. Palladino, Associate Professor, Department of

Copyright © by Bartholomew P. Roland

2014

**AN *IN VIVO* STRUCTURE-FUNCTION ANALYSIS OF TRIOSEPHOSPHATE
ISOMERASE DEFICIENCY PATHOGENESIS**

Bartholomew P. Roland, PhD

University of Pittsburgh, 2013

Triosephosphate isomerase (TPI) is a glycolytic enzyme that catalyzes the isomerization of dihydroxyacetone phosphate into glyceraldehyde 3-phosphate, a non-linear step in glycolysis not required for the production of pyruvate. Dysfunction within TPI elicits a disease called TPI deficiency; a severe, rare, autosomal recessive disorder characterized by neurological dysfunction, shortened longevity, and hemolytic anemia. Previous studies questioned whether this disease was caused by changes in metabolism or protein conformation. To address this, we have used a genomic engineering strategy in *Drosophila* to study the relationship between the structure of TPI and pathology. We have generated and analyzed novel high-resolution crystal structures of TPI mutant proteins, yielding basic insights into TPI dysfunction. Our data suggest the pathogenesis of TPI deficiency is unrelated to its general role in metabolism. Further, *in vitro* experiments demonstrate that a toxic *Drosophila* TPI allele is characterized by a defect in protein dimerization. Using our genomic engineering system, we have generated several novel TPI alleles that further support the hypothesis that a conformational change at the dimer interface is sufficient to elicit TPI deficiency. We have conclusively shown that gross TPI activity is not predictive of disease presence or severity. Finally, we have identified a synaptic defect caused by a dimer interface mutant that we propose is the source of neurological dysfunction in *Drosophila* and TPI Deficiency patients.

TABLE OF CONTENTS

PREFACE.....	XVIII
1.0 INTRODUCTION.....	1
1.1 TRIOSEPHOSPHATE ISOMERASE.....	2
1.1.1 Protein structure and catalysis.....	2
1.1.2 TPI and its metabolic pathways	5
1.1.3 Important catabolic products	7
1.2 TRIOSEPHOSPHATE ISOMERASE DEFICIENCY	9
1.2.1 A historical perspective on TPI deficiency and its evolutionary maintenance	9
1.2.2 Known TPI deficiency mutants and investigative studies	11
1.3 TPI DEFICIENCY IN MODEL ORGANISMS	13
1.3.1 Studies in mice and yeast	13
1.3.2 Studies in <i>Drosophila</i>	14
1.3.2.1 <i>Drosophila</i> neurobiology	14
1.3.2.2 <i>Drosophila</i> reveal mechanisms of pathologic protein regulation ...	16
1.3.2.3 <i>Drosophila</i> and TPI deficiency redox changes	17
1.4 DROSOPHILA GENOMIC ENGINEERING.....	19

2.0	EVIDENCE OF A NON-CATALYTIC FUNCTION OF TRIOSEPHOSPHATE ISOMERASE CRUCIAL TO BEHAVIOR AND LONGEVITY	22
2.1	ABSTRACT.....	22
2.2	INTRODUCTION	23
2.3	RESULTS	25
2.3.1	Recombinant TPI enzyme activity	25
2.3.2	Generation of the founder knock-out line by homologous recombination	
	28	
2.3.3	Animal behavior and longevity	30
2.3.4	TPI^{sgk} animal bioenergetics and lysate enzyme activity.....	32
2.3.5	TPI^{sgk} and TPI^{Δcat} protein levels.....	34
2.4	DISCUSSION.....	36
2.5	MATERIALS AND METHODS.....	39
2.5.1	Animal Strains	39
2.5.2	Genomic Engineering.....	40
2.5.3	Mutagenesis.....	40
2.5.4	Drosophila TPI purification	41
2.5.5	Enzyme Assays.....	42
2.5.6	Behavioral Testing and Lifespan Analysis	43
2.5.7	HPLC Phosphoarginine Assay	43
2.5.8	Immunoblots	44

3.0	CHANGES IN TRIOSEPHOSPHATE ISOMERASE DIMER INTERFACE MORPHOLOGY ELICIT BEHAVIORAL DYSFUNCTION BY INHIBITING SYNAPTIC VESICLE RECYCLING	46
3.1	ABSTRACT.....	46
3.2	INTRODUCTION	47
3.3	RESULTS	49
3.3.1	RNAi knockdown of WT TPI.....	49
3.3.2	<i>In vitro</i> physical characterization of M80T	50
3.3.3	TPI dimer interface mutants	54
3.3.4	Complementation with a catalytically inactive TPI allele	58
3.3.5	Vesicle recycling at the synapse.....	62
3.4	DISCUSSION.....	65
3.4.1	Triosephosphate isomerase dimerization	66
3.4.2	TPI mutations reduce vesicle recycling at the synapse	70
3.5	MATERIALS AND METHODS	73
3.5.1	Animal Strains	73
3.5.2	Mutagenesis and Genomic Engineering	74
3.5.3	Human TPI enzyme purification.....	74
3.5.4	Dynamic Light Scattering.....	75
3.5.5	Gel Filtration Chromatography	75
3.5.6	TPI Enzyme Assays	76
3.5.7	Behavioral testing and lifespan analysis.....	77
3.5.8	Immunoblots	77

3.5.9	Filter-trap Dot Blot.....	78
3.5.10	Coimmunoprecipitations	78
3.5.11	FM1-43 Imaging Experiments	79
3.5.12	NMJ morphological analyses	80
4.0	HUMAN TRIOSEPHOSPHATE ISOMERASE I170V ALTERS CATALYTIC SITE, ENHANCES DIMERIZATION AND INDUCES PATHOLOGY IN A <i>DROSOPHILA</i> MODEL OF TPI DEFICIENCY	82
4.1	ABSTRACT.....	82
4.2	INTRODUCTION	83
4.3	RESULTS	85
4.3.1	I170V induces behavioral dysfunction in <i>Drosophila</i>	85
4.3.2	<i>in vivo</i> TPI protein levels and enzyme activity	87
4.3.3	I170V enhances substrate affinity, stability, and dimerization <i>in vitro</i>	88
4.3.4	The crystal structure of I170V supports a preferentially closed catalytic pocket	91
4.4	DISCUSSION.....	93
4.5	MATERIALS AND METHODS	98
4.5.1	Mutagenesis and Genomic Engineering	98
4.5.2	Human TPI enzyme purification.....	98
4.5.3	Gel Filtration Chromatography	99
4.5.4	TPI Enzyme Assays	100
4.5.5	Circular dichroism and thermal stability.....	101
4.5.6	Behavioral testing and lifespan analysis.....	101

4.5.7	Immunoblots	102
4.5.8	Protein crystallization and structural determination.....	102
5.0	DISCUSSION	104
5.1	TPI PROTEIN CONFORMATION AND DISEASE	106
5.2	DIMERIC COOPERATION AT THE CATALYTIC SITE.....	109
5.3	SYNAPTIC TPI DEFICIENCY AND BEHAVIOR	112
5.4	EVOLUTIONARY MAINTENANCE OF <i>TPI</i> DYSFUNCTION	118
5.5	NEW FRONTIERS IN GENOMIC ENGINEERING	119
5.6	MUTAGENESIS: FORWARD, REVERSE, AND EVERYTHING IN BETWEEN.....	122
	BIBLIOGRAPHY	126

LIST OF TABLES

Table 1. Summary of genomically engineered triosephosphate isomerase alleles.	xx
Table 2. Kinetic parameters of <i>Drosophila</i> wild type (dWT) and sugarkill (dM80T) triosephosphate isomerase enzymes.	26
Table 3. hTPI ^{WT} and hTPI ^{I170V} kinetic parameters.	88

LIST OF FIGURES

- Figure 1. Triosephosphate isomerase and its related metabolic pathways. A) The de novo glycerol synthesis pathway, B) glycolysis, and C) the pentose phosphate pathway. Only critical substrates are indicated. 5
- Figure 2. Structure of triosephosphate isomerase highlighting residues affected by human disease-associated missense mutations. TPI dimer is shown as a cartoon, with one monomer colored blue and the other gold. Known human mutations are plotted structurally and shown as white with colored elements in sticks. The active site is labeled with DHAP, shown in spheres. Labels indicate the residues and their changes. Structure shown is WT from yeast, crystallized with DHAP bound in the active site. PDB accession code: 1NEY (46)..... 10
- Figure 3. Both *Drosophila* wild type (dWT) and sugarkill (dM80T) enzymes follow traditional Michaelis-Menten kinetics. Michaelis-Menten nonlinear regression fits are shown, and all enzyme concentrations are indicated. 25
- Figure 4. Positioning of the third loop forms an interaction network connecting the dimerization interface to the catalytic pocket. A) The crystal structure of TPI dimer from *Gallus gallus* (PDB ID, 1TPH). Monomer A of the dimer is rendered as a surface and colored white, while Monomer B (blue) is shown as a cartoon with the third loop highlighted in orange. The position of the transition state analog phosphoglycolohydroxamic acid (PGH, green) is indicated within the

catalytic pocket. B) Local environment of the third loop. Colored as before, with residues making important contributions to the dimerization interface indicated as sticks. Van der Waals interactions between M81 and residues M13 and N14 are indicated as black dotted lines. Hydrogen bonds between residues on the distal end of the third loop and connecting to the catalytic core are given as green dotted lines. Residues are numbered based on Gallus gallus sequence, and for clarity we are using the TPI numbering standard that accounts for the removal of the initiator methionine. C) An alignment of TPI protein sequences from H. sapien, G. gallus, and D. melanogaster. Protein alignment was performed using the Clustal W method, with H. sapien and G. gallus showing 63.5% and 67.3% identity to D. melanogaster. Residues that mediate TPI dimerization are indicated by grey circles. Residues within the hydrogen-bonding network critical for catalysis are indicated (Cyan). The position of the sugarkill mutant (M81, red) and its positions within the third loop (orange box) are indicated. 27

Figure 5. Genomic engineering of the TPI locus. A) The target gene is replaced by the *attP* phiC31 integration site and a white minigene flanked by two *loxP* sites. B) The white minigene is removed by a CRE recombinase, leaving only the *attP* phiC31 integration site and a *loxP* site. C) *TPI* is cloned into the *pGE-attB* vector and modified, as desired. The construct is then injected into founder line embryos expressing the phiC31 integrase, which initiates specific and directional integration of the construct into the *TPI* locus. D) The *white* minigene and plasmid construct are removed through the expression of CRE recombinase, leaving only an *attR* and a *loxP* site. E) Molecular analysis reveals the addition of an *attR* site 5' of the reconstituted *TPI* gene. 29

Figure 6. Genomically engineered TPI^{sgk} displays aberrant behavior and reduced longevity. A) Genomically engineered TPI^+ (*GE-WT*) displays normal behavior, while the genomically

engineered TPI^{sgk} ($GE-sgk$) displays marked mechanical stress sensitivity. B) $GE-sgk$ exhibits reduced longevity compared to $GE-WT$. $n > 20$ for all lifespans and behavior. A Student's t test was used to assess behavioral differences between genotypes, and a Log-rank (Mantel-Cox) Test was used to assess lifespans. *** indicates $p < 0.0001$ compared to $GE-WT$. Error bars indicate \pm s.e.m. Both genomically engineered alleles were assessed over TPI^{null} 30

Figure 7. The catalytically inactive $TPI^{\Delta cat}$ rescues behavioral and longevity phenotypes in TPI^{sgk} . A) $TPI^{\Delta cat}$ complements TPI^{sgk} mechanical stress sensitivity at both day 3 and day 20. B) $TPI^{\Delta cat}$ expression complements TPI^{sgk} thermal stress sensitivity, again at both day 3 and day 20. † indicates TPI^{sgk}/TPI^+ and $TPI^{sgk}/TPI^{\Delta cat}$ animals did not paralyze. C) $TPI^{\Delta cat}$ complements the longevity defect of TPI^{sgk} . ** indicates $p < 0.01$ and *** $p < 0.001$ relative to TPI^+/TPI^+ . $n > 15$ per genotype for all behavioral assays, and $n > 150$ per genotype for all lifespans. Error bars indicate \pm s.e.m..... 31

Figure 8. $TPI^{\Delta cat}$ fails to rescue animal bioenergetics and TPI enzyme activity. A) TPI^{sgk} exhibits little activity in animal lysates. Additionally, complementing TPI^{sgk} with $TPI^{\Delta cat}$ does not rescue its activity in vivo. Inset: A between TPI^{sgk}/TPI^{null} and $TPI^{sgk}/TPI^{\Delta cat}$ lysate kinetics reveals low activity levels in both lysates. Note the axes are maintained but units have been changed. B) TPI^{sgk}/TPI^{null} animals and $TPI^{sgk}/TPI^{\Delta cat}$ animals both showed reduced ratios of P-arg/arginine indicating bioenergetic stress. *** indicates $p < 0.001$ relative to WT. Error bars indicate \pm s.e.m. 32

Figure 9. $TPI^{\Delta cat}$ expression does not prevent the degradation of TPI^{sgk} . A) Shown is a quantification of the levels of untagged TPI. TPI^{sgk} complemented with $TPI^{\Delta cat}$ shows elevated levels of total TPI similar to WT. Additionally, TPI^{sgk}/TPI^{null} have similar levels of TPI compared to $TPI^{sgk}/TPI^{\Delta cat} -CFP$. ** indicates $p < 0.01$ and *** $p < 0.001$ compared to WT.

Further, ns indicates no significant change compared to TPI^{sgk}/TPI^{null} . n = 4. B) TPI^{sgk} does not induce the degradation of $TPI^{\Delta cat-CFP}$. Shown is a quantification and comparison of the levels of $TPI^{\Delta cat-CFP}$ (C). Student's T test was used to compare the two groups and found no significant difference (ns). n = 4. C) Shown is a representative blot from which Figures 9A and 9B were quantified. The loading control used was ATPalpha (Na,K-ATPase). Error bars indicate \pm s.e.m. 35

Figure 10. The addition of the C-terminal CFP to $TPI^{\Delta cat}$ does not affect its capacity to genetically complement TPI^{sgk} . A) mechanical stress sensitivity or B) thermal stress sensitivity. Mechanical stress sensitivity was assessed on Day 1 and thermal stress sensitivity was assessed on Day 5. n > 15. † indicates animals did not paralyze. A One-way ANOVA was performed to assess variance and data sets were compared using Tukey's post-hoc analysis. *** indicates that $p < 0.001$ and ns indicates no significant difference, both compared to WT. Error bars indicate \pm s.e.m. 35

Figure 11. RNAi knockdown of TPI^+ fails to recapitulate TPI^{M80T} phenotypes. TPI transcript levels were knocked down ubiquitously and confirmed in thorax (A) and head (B) tissues (n \geq 3). Knockdown animals failed to display typical mechanical-stress dependent paralysis (C) at Day 5 aged at 25°C (n \geq 15). ns indicates no significance, ** $p < 0.01$, and *** $p < 0.001$ relative to +/+. 49

Figure 12. $hTPI^{M80T}$ phenocopies the behavioral and longevity effects of $dTPI^{M80T}$. $hTPI^{M80T}$ elicits a significant delay in time to recovery from mechanical stress (A) at Day 3, time to paralysis after thermal stress (B) at Day 4, and longevity (C) compared to $hTPI^+$, all reared at 25°C. n \geq 20 for behavior and n \geq 70 for lifespans. * indicates $p < 0.05$ and *** $p < 0.001$ 51

Figure 13. M80T elicits a conformational change in TPI resulting in reduced dimerization. The M80T mutations confers a reduction in mean protein hydrodynamic radius as measured by

dynamic light scattering (A). Intensity correlation plots reveal a largely monodisperse WT population and polydisperse M80T population (B). Gel filtration indicates a change in monomer:dimer ratios elicited by M80T (C) with relative quantification (inset). *** indicates $p < 0.001$ 53

Figure 14. Mutations affecting the TPI dimer interface recapitulate M80T phenotypes. TPI^{T74R} and TPI^{G75E} exhibit severe mechanical stress (A) and thermal stress (B) sensitivity, $n > 30$. Dimer interface mutations display severely reduced lifespans (C), $n > 150$. Both TPI^{T74R} and TPI^{G75E} display reduced protein levels (D,E) and reduced lysate isomerase activity (F). ** indicated $p < 0.01$, *** $p < 0.001$. # indicates animals did not paralyze in 360sec. 56

Figure 15. TPI dimer interface mutations do not cause aggregation. Increasing amounts of lysate were loaded and show no differences in trapped TPI across all genotypes (A) whereas huntingtin exon1-GFP displayed robust retention on the filter (B). $n = 2$ 57

Figure 16. A catalytically inactive allele is not sufficient for normal behavior and longevity. $TPI^{\Delta cat}$ complements TPI^{T74R} mechanical (A) and thermal stress (B) sensitivity and longevity (C), yet moderately attenuates behavior (D,E) and longevity (F) defects of TPI^{G75E} . It should be noted that mean thermal stress paralysis times near 360sec represent near-wild type behavior. $n \geq 30$ for behavior, and $n \geq 90$ for lifespans. ns indicates no significant, and *** $p < 0.001$. # indicates the animals did not paralyze (a score of 360 sec.). 59

Figure 17. Lysate isomerase activity does not predict disease presence or severity. Lysate activity is indicated (A) and expanded (B) as per the dashed box. ns indicates no significant differences and *** $p < 0.001$. Biological replicates are indicated. 60

Figure 18. Heterodimerization of inactive TPI and dimer interface mutations. $TPI^{\Delta cat-CFP}$ interacts modestly with TPI^{M80T} , TPI^{T74R} , and $TPI^{T74R,G75E}$, yet robustly with TPI^{G75E} .

Representative immunoprecipitation and input blots are shown (A) with IP: anti-GFP quantification (B) n=3. ns indicates no significance, ** p<0.01, and *** p<0.001. 62

Figure 19. TPIT74R,G75E behavioral dysfunction and longevity. $TPI^{T74R,G75E}$ is characterized by severe mechanical (A) and thermal (B) stress sensitivity, which responds positively to complementation by $TPI^{\Delta cat}$. $TPI^{T74R,G75E}$ exhibits reduced lysate catalytic activity compared to WT (C). $TPI^{\Delta cat}$ fails to complement $TPI^{T74R,G75E}$ longevity (D). n≥30 for all behavior, n≥80 for all lifespans. ns indicates no significance, ** p<0.01, *** p<0.001. # indicates animals did not paralyze within 360sec..... 65

Figure 20. TPI^{T74R} inhibits vesicle recycling at 38°C. An FM1-43 timecourse at the NMJ with loading times of 15, 30, and 60sec (A), with quantification of 60sec at 38C (B) and 60sec at room temperature (RT) (C). Representative images of TPI^+ , TPI^{T74R} , $TPI^{T74R/\Delta cat}$ and Shi^{ts1} (D). n=6, ***p<0.001..... 67

Figure 22. $TPI^{\Delta cat}$ rescues viability in strong TPI stability mutants, though not behavior. TPI salt bridge mutants were crossed to $TPI^{\Delta cat}$ and assessed for complementation. Complementation with the inactive enzyme restores viability in two of three salt bridge mutants, yet all exhibit similar mechanical stress sensitivity as TPI^{M80T}/TPI^{null} (A), n≥18. Salt bridge mutants were complemented with TPI^{WT-CFP} and exhibit dramatic reductions in lysate protein levels (D) with quantification (B). No significant differences were noted in TPI^{WT-CFP} levels (D), quantified in (C), though blots of TPI^{WT-CFP}/TPI^{R188L} exhibited a trend toward a reduction in the tagged protein, n=3. *** indicates p<0.001. 69

PREFACE

The findings detailed in this document are the result of my thesis work in the laboratory of Dr. Michael Palladino, and together we designed the research. With the exception of the enzyme structures, I performed all the experiments detailed, with modest assistance by a number of undergraduates working under my direction. The protein purification, crystallization, data collection, and refinement of the enzyme structures were performed by Dr. Andrew VanDemark and Christopher Amrich. Dr. VanDemark and Mr. Amrich provided the structures, and together we performed the analyses. I have analyzed the data with the assistance of Dr. Palladino and Dr. VanDemark, and the conclusions and discussion are my own. Chapter 2 was adapted with permission from the Journal of Cell Science (1).

It should be noted that triosephosphate isomerase has different amino acid numbering conventions when it is being discussed in the context of disease and normal function. Also, I will be detailing work with both the human and *Drosophila* proteins, which also have different amino acid numbering. All of these conventions have been merged into one strategy for the purposes of this document to avoid confusion, and will be altered to suit the most appropriate strategy for each presentable/publishable unit. Please see the alignment in Figure 4 for any confusion regarding numbering or conservation.

Finally, I would like to acknowledge the contributions of several individuals and institutes; without their support this research would not have been possible. In no particular order, I would like to thank the Pittsburgh Institute for Neurodegenerative Disease, the Molecular Pharmacology graduate training program, and the Department of Pharmacology & Chemical Biology; my parents, sisters, and family; my laboratory coworkers, Atif, Robert, Stacy, John, Kim, and Alicia; my friends in the graduate program, Rakesh, Harshad, Grant, Yao, Kelly, David, Cassie, Shelley, Yu, Anny, Prince, Arvind, Melanie, Abi; the ARCS society of Pittsburgh, specifically Millie and Gary Ryan, and Barbara Granito; institutional friends, Eric, Maxx, the coffee pot, Victor, Steve, Annabel, and Marsha; department members Dr. Romero, Dr. Pagano, Dr. Freeman, Pat, Lynda, Melanie, Holly, Jim, Lisa; collaborators Dr. VanDemark, Chris, Irene, Kar, Dr. Shakiryanova, Dr. Wetzel; and Dr. Ivan Tarkin for putting me back on my feet.

Table 1. Summary of genomically engineered triosephosphate isomerase alleles.

Allele name	Homozygous viability	Protein levels	Lysate isomerase activity	Mechanical stress sensitivity	Thermal stress sensitivity	Longevity	Known or Hypothesized affect
<i>dTPI</i> ⁺	Viable	+++	+++	None	None	+++	WT
<i>dTPI</i> ^{<i>Δcat(K12M)</i>}	Lethal	+++	n.d.	n.d.	n.d.	n.d.	Prevents catalysis
<i>dTPI</i> ^{<i>I74R</i>}	Reduced	+	++	+++	+++	+	Alters dimer interface
<i>dTPI</i> ^{<i>G75E</i>}	Reduced	+	++	+++	++	+	Alters dimer interface
<i>dTPI</i> ^{<i>I74R,G75E</i>}	Reduced	+	++	+++	+++	+	Alters dimer interface
<i>dTPI</i> ^{<i>M80T</i>}	Viable	++	+	++	+	++	Alters dimer interface
<i>dTPI</i> ^{<i>R188A</i>}	Lethal	+	n.d.	n.d.	n.d.	n.d.	Breaks salt bridge
<i>dTPI</i> ^{<i>R188L</i>}	Lethal	+	n.d.	n.d.	n.d.	n.d.	Breaks salt bridge
<i>dTPI</i> ^{<i>R188S</i>}	Lethal	+	n.d.	n.d.	n.d.	n.d.	Breaks salt bridge
<i>dTPI</i> ^{<i>R188K</i>}	Viable	+++	n.d.	None	None	n.d.	Maintains salt bridge
<i>hTPI</i> ⁺	Viable	+++	+++	None	None	+++	WT
<i>hTPI</i> ^{<i>I74R</i>}	Lethal	n.d.	n.d.	n.d.	n.d.	n.d.	Alters dimer interface
<i>hTPI</i> ^{<i>G75E</i>}	Lethal	n.d.	n.d.	n.d.	n.d.	n.d.	Alters dimer interface
<i>hTPI</i> ^{<i>I74R,G75E</i>}	Lethal	n.d.	n.d.	n.d.	n.d.	n.d.	Alters dimer interface
<i>hTPI</i> ^{<i>M80T</i>}	Viable	++	+	+	+	++	Alters dimer interface
<i>hTPI</i> ^{<i>I170V</i>}	Viable	+++	+	+	+	+++	Alters lid conformation

1.0 INTRODUCTION

Over the course of evolution, biology has frequently recycled and repurposed protein conformations for roles other than their original function. One of the greatest examples of this repurposing of protein structure has been the tertiary structure known as the triose isomerase (TIM) barrel. The TIM barrel was first described in triosephosphate isomerase (TPI), but has since been found to be shared by over one hundred functionally diverse enzymes (2). From endonucleases (3), to subunits of the K^+ channels (4), to phospholipase signaling enzymes (5), this diversity clearly demonstrates the versatility of this structure. Further, the concept of multifunctional protein structures has similarly been supported by work over the last few decades, revealing the oversimplification of the one protein–one function idea, similar to that of the one gene–one enzyme hypothesis. These additional functions are often regulated by post-translational modifications, subcellular localization, secretion, differential expression, and oligomerization (6). Many enzymes, such as pyruvate kinase (PK), have been demonstrated to perform additional activities upon changes in their oligomerization. As a monomer, PK is able to bind and inhibit the signaling of thyroid hormone receptors in the cytosol (7); yet upon oligomerization, PK loses its ability to sequester thyroid hormone receptors and becomes a full participant in glycolysis (8). Other examples of novel functions are based on subcellular localization; hemoglobin is a well-described molecule capable of binding gases, and used to transfer oxygen throughout an organism. However, recent studies in the vasculature have

identified it as a regulator of nitric oxide signaling (9,10), due to its ability to bind and sequester NO in a spatial and temporal manner (11). These examples are beautiful illustrations of how evolution has recycled and reused elements of biochemistry to arrive at our current biological complexities, and emphasize the ability of proteins to function in numerous capacities.

In my dissertation work I have utilized the *Drosophila* model system to examine the complexities of the glycolytic enzyme, TPI. I have established a genomic engineering approach to examine the functional properties of TPI and the pathogenesis of its associated disease, triosephosphate isomerase deficiency. Collectively, my work examines the structure of TPI, and how changes in this structure may induce pathophysiology. I believe my work supports a role for localized TPI catalysis at the synapse, though the precise mechanism is still unclear. In this introduction I will briefly review the literature surrounding the known biochemistry of TPI, the pathology associated with TPI deficiency, and the utility of *Drosophila* and the genomic engineering methodology.

1.1 TRIOSEPHOSPHATE ISOMERASE

1.1.1 Protein structure and catalysis

Triosephosphate isomerase (TPI) is a non-linear enzyme of the glycolytic pathway. Within glycolysis, TPI is located immediately downstream of aldolase and parallels glyceraldehyde 3-phosphate dehydrogenase (GAPDH) [Figure 1]. TPI catalyzes the isomerization of dihydroxyacetone phosphate (DHAP) into glyceraldehyde 3-phosphate (GAP), as GAP is the necessary 3-carbon substrate capable of producing pyruvate. This isomerization reaction

requires a catalytic base to initiate deprotonation of the DHAP substrate (12). If allowed to proceed non-enzymatically using a chemical base, the slow deprotonation of DHAP would result in equivalent levels of GAP and an enediolate intermediate, whose kinetics would deviate thermodynamically toward the production of a reactive Schiff base, methylglyoxal (13). Methylglyoxal contains a highly reactive aldehyde group that will readily adduct to proteins and DNA, thereby causing cellular damage (14). The positioning of the catalytic residues in TPI facilitates an extremely rapid deprotonation of DHAP, yet if left unguided this reaction would also generate methylglyoxal. To inhibit the formation of this toxic byproduct and bias the formation of GAP, TPI utilizes a “lid” mechanism which gates the diffusion of any reaction intermediates, thereby directing nearly all of the substrate to the appropriately isomerized product (13).

To understand the catalysis of TPI, you must understand its structure. TPI utilizes a TIM barrel base, upon which its catalytic properties have been built (15). The TIM barrel is a commonly used enzymatic tertiary structure which involves alternating beta sheets and alpha helices for the production of a stable barrel. This stable foundation coordinates the positioning of looped segments between the beta sheet/alpha helix stretches, and these loops are what give each TIM barrel enzyme their respective functional properties. In TPI, several loops contain elements which assist with enzyme dimerization as well as the formation and support of the catalytic site (16).

TPI has traditionally been thought of as an obligatory homodimer, as monomeric versions of the protein have yet to be identified *in vivo* and the catalysis of the enzyme is greatly influenced by dimerization. Indeed, targeted modifications to the TPI dimer interface have been generated and characterized *in vitro*, with all iterations displaying a significant reduction in

catalysis (17-19). These catalytic changes are in stark contrast to the diffusion-limited rates achieved upon appropriate dimerization (20). Structural analyses have revealed that the dimerization of TPI helps support the formation of a rigid catalytic pocket (18). In particular, several critical catalytic residues, such as N10 and K12, are supported by hydrophobic interactions at the dimer interface (18,19). Without appropriate positioning in monomeric forms of the enzyme, these residues and the catalytic lid appear flexible. Similarly, molecular simulation experiments have concluded that the catalytic residue H95 is coordinated by a hydroxyl group extending from a threonine as part of the partner dimer (21). This hydroxyl group is part of the critical loop 3 of the enzyme, which forms a majority of the dimer interface surface area. The tip of TPI loop 3, of which T74 is a key component, reaches into and stabilizes the catalytic site of its dimer partner (18,22). Mutations in T74 and its neighbor G75 have been shown to be sufficient to disrupt dimer formation (19). These residues and their pathogenic propensities will be analyzed in Chapter 3.

Although dimerization has been well-established as a means to regulate the catalytic capacity of TPI, little has been done to study how catalysis may convey changes back to the dimer interface. One hint of this type of bidirectional relationship was revealed by (23) wherein the authors studied the capacity of thiol-targeted reagents to adduct dimer interface cysteines. It was established that occupation of the enzyme protected the buried dimer interface cysteines from modification. Conversely, enzyme without substrate – a more dynamic open conformation – exhibited substantial susceptibility for modification by the chemical agents methylmethane thiosulfonate (MMTS) and 5,5-dithiobis(2-nitrobenzoate) (DTNB) (23). These data would suggest the capacity for the catalytic site to modulate accessibility of buried dimer interface residues. If occupancy of the enzyme were truly to influence dimerization and stability, it is

tempting to think that this may be a self-regulatory mechanism for sensing its necessity and regulating turnover. Through structural and biochemical analyses, I have established that changes in lid conformation are capable of influencing dimerization through the reinforcement of a trans-monomeric hydrogen bond network. This bidirectional relationship between the dimer interface and catalytic site will be explored and discussed in Chapter 4.

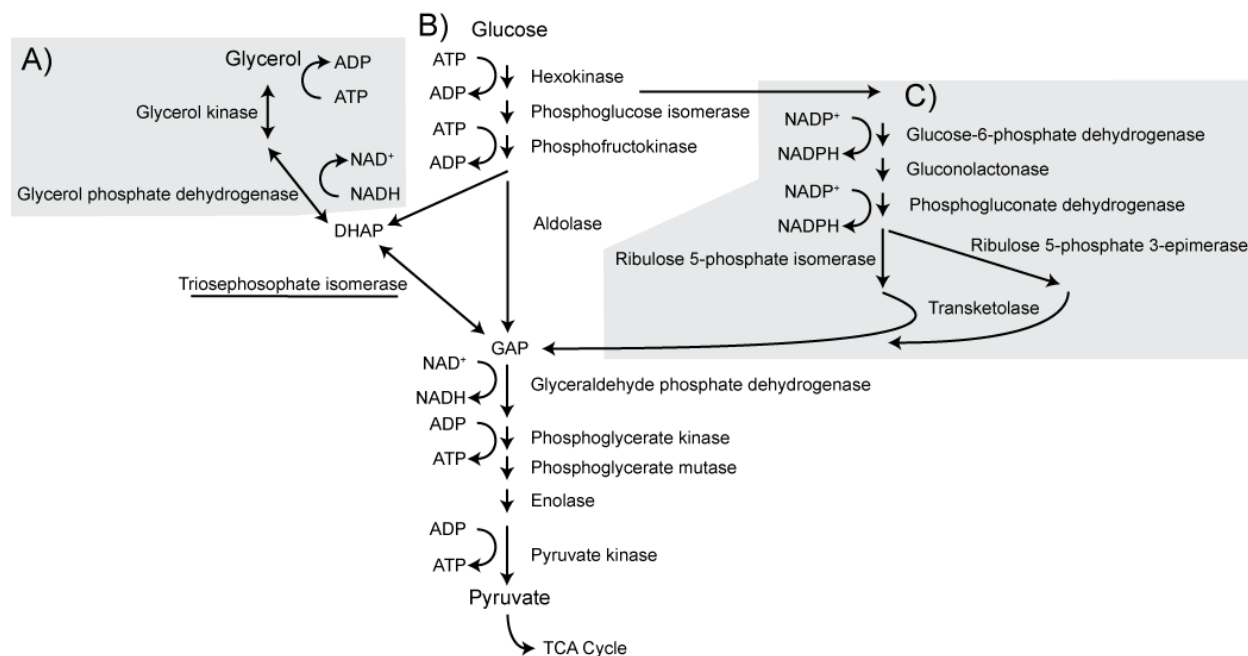


Figure 1. Triosephosphate isomerase and its related metabolic pathways. A) The de novo glycerol synthesis pathway, B) glycolysis, and C) the pentose phosphate pathway. Only critical substrates are indicated.

1.1.2 TPI and its metabolic pathways

TPI sits at the crux of glycolysis and enhances its bioenergetic capacity [Figure 1]. The additional GAP molecule generated through the isomerization of DHAP contributes a second three-carbon substrate for the production of adenosine triphosphate (ATP), the reduced form of

nicotinamide adenine dinucleotide (NADH), and pyruvate (24). The two molecules of ATP generated through this molecule of GAP result in a net gain in ATP for the entire glycolytic process. GAPDH, the next enzyme in glycolysis following TPI, generates NADH from the oxidation of GAP (24).

The relationship between TPI and NADH however does not stop at its ability to help generate GAP simply for glycolysis; TPI is also involved in the glycerol 3-phosphate (G3P) proton shuttle (25). Cytosolic and mitochondrial pools of NADH are discrete, with the exceptions of the malate-aspartate and glycerol 3-phosphate shuttles (25). NADH generated in cytosol is oxidized by glycerol 3-phosphate dehydrogenase (GPDH) with DHAP to form glycerol 3-phosphate (24). This glycerol is the backbone of most phospholipids and triglycerides, but can also pass through the inner mitochondrial membrane where mitochondrial GPDH oxidizes G3P and FAD^+ is reduced to $FADH_2$ and DHAP (24). If TPI were inactive, one would predict that this irreversible transfer mechanism would be enhanced through the accumulation of DHAP, possibly leading to a depletion of cytosolic NADH. Again, although TPI's role in this process is peripheral, its inhibition through catalysis or mislocalization could result in a selective depletion of cytosolic NADH pools, potentially influencing pyridine effectors.

In addition to its intimate relationship to glycolysis, TPI peripherally participates in the pentose phosphate pathway (PPP) through its relationship with GAP (24). GAP is a product of the PPP, which generates reducing cofactors (nicotinamide adenine dinucleotide phosphate – NADPH) and precursors of nucleotides and aromatic amino acids (24). In this way, the PPP could be a means to bypass initial inefficiencies in glycolysis, and inhibition of TPI is predicted to increase glucose 6-phosphate flux from the glycolytic pathway to the PPP (26). Within the

PPP, this 6 carbon molecule will be broken down, yielding NADPH, ribose 5-phosphate, and erythrose 4-phosphate (24). NADPH is a key electron donor for the regeneration and maintenance of glutathione and the cellular redox environment as well as signaling enzymes such as NADPH oxidases. Ribose 5-phosphate can be shunted to help generate nucleotides, while erythrose 4-phosphate can be diverted for the production of aromatic amino acids (24). However, the progression toward the production of nucleotides or amino acids is regulated by their respective anabolic enzymes; in the absence of a need for either of these constituents, the ribose 5-phosphate and erythrose 4-phosphate would be further catabolized through the PPP to generate fructose 6-phosphate and GAP. GAP can be handed back to the glycolytic pathway through GAPDH while fructose 6-phosphate can be reused by the PPP to generate more GAP, or fed directly back into glycolysis (24).

1.1.3 Important catabolic products

Through directly- or indirectly-linked pathways, TPI yields three molecules of biochemical importance: ATP, NADH, and NADPH. The function of ATP as a phosphate donor has been well-established in the literature as a central molecule in biochemistry, yet NADH and NADPH are still gaining appreciation for their biological activities. Previously, NADH was largely thought to feed the electron transport chain (ETC) of mitochondria simply for the production of ATP, yet biochemists are finding increasingly influential roles for this type of electron donor species in signal transduction events. One well-established pathway through which this molecule can modulate biology has been control over the Sirtuin family (27,28). The Sirtuins bind the unreduced form of NAD^+ to induce the deacetylation of other transcription factors and histones (29). Through these means, local NAD^+ gradients can regulate gene

transcription, and enhancement of this capacity has been shown to phenocopy the longevity enhancement seen in caloric restriction models of aging (30-34). Indeed, we see a progressive increase in NAD^+ relative to NADH in our TPI^{M80T} animals (35), and if recapitulated in our dimer mutants, a putative increase in NAD^+ is possibly the means through which we see a substantial increase in the longevity of our heterozygotes animals (Chapter 3), though such hypotheses are as of yet untested.

Additionally, both NAD^+ and NADP^+ have been shown to modulate K^+ channel activity (36). NAD^+ has been demonstrated to bind the cytoplasmic domain of Slo2 K^+ channels (BKCa) (37), leading to a 2-fold increase in open probability. Additionally, the beta subunit of voltage-gated potassium channels ($\text{Kv}\beta$) binds both NAD^+ and NADP^+ , but not their reduced counterparts (38). As mentioned previously, the $\text{Kv}\beta$ proteins are members of the aldo-keto reductase family of proteins and in an extremely interesting coincidence, utilize a TIM barrel structure to bind pyridine nucleotides (4). This binding event removes their inactivating influence on the alpha units of the channel, thereby facilitating K^+ flux (39,40). Finally, the transient receptor potential M2 channel (TRPM2) has been shown to be redox sensitive (41), with applications of NAD^+ increasing permeability (42). Direct binding experiments have been performed (41), though some contend these results are controversial (43). Regardless, it is clear that there is an increasing appreciation for the cytosolic activities of these molecules, and further work detailing the importance of local changes in redox pyridines will be extremely interesting.

1.2 TRIOSEPHOSPHATE ISOMERASE DEFICIENCY

1.2.1 A historical perspective on TPI deficiency and its evolutionary maintenance

Schneider and colleagues first identified a disease associated with triosephosphate isomerase back in the 1960s (44). In this seminal article, a small cohort of individuals was examined in an isolated area of Louisiana wherein a number of children were identified with a curious collection of symptoms. The affected infants/children often displayed signs of hemolytic anemia, weakened immune responses, and progressive neuromuscular impairments. The children would exhibit an odd collection of periodic dystonia, episodic seizures, and progressive weakness and flaccidity in their extremities. These behaviors often would continue to progress until the point of early death, though the cause of death was often ascribed to the persistent infections the patients experienced. Pedigree analyses suggested an autosomal recessive disease, and although no consanguinity was initially described, the children's parents admitted to being 'almost certain that they were related in some way' (26). Through metabolic experiments it was revealed that the hemolytic anemia experienced by these patients was likely derived from reduced TPI activity. Later, molecular studies of these and similar patients revealed that the disease was caused by a collection of mutations within the promoter and coding regions of the *TPI* gene (45).

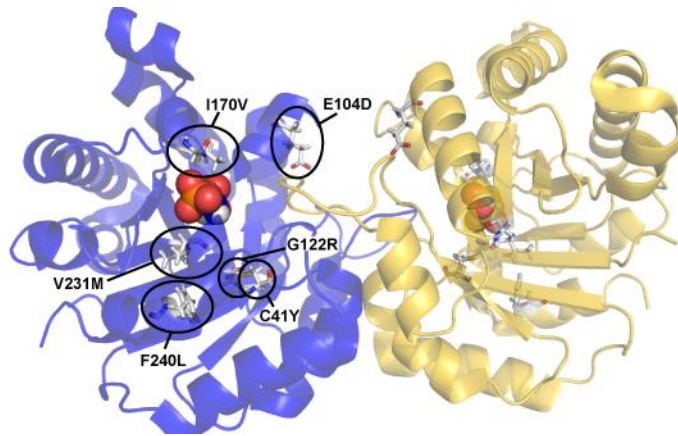


Figure 2. Structure of triosephosphate isomerase highlighting residues affected by human disease-associated missense mutations. TPI dimer is shown as a cartoon, with one monomer colored blue and the other gold. Known human mutations are plotted structurally and shown as white with colored elements in sticks. The active site is labeled with DHAP, shown in spheres. Labels indicate the residues and their changes. Structure shown is WT from yeast, crystallized with DHAP bound in the active site. PDB accession code: 1NEY (46).

Typically, patients are genetically characterized as transheterozygotes, with a point mutation paired with one of several null alleles. These null alleles are most often elicited through the introduction of a premature stop codon, with the resulting transcript left untranslated due to nonsense-mediated decay (45,47,48). Indeed, hypomorphic alleles have been widely described in the general population, though no individuals have yet been identified with homozygous null mutations. A population screen of infant mortality suggested that a homozygous null condition is embryonic lethal, and these data are supported by similar observations in rodents and *Drosophila* (49-52). Therefore to achieve viability, some degree of activity must be retained – these observations are supported by the homozygous lethality found in our catalytically inactive mutants described in Chapter 2.

Of particular interest to population geneticists has been the wide geographic prevalence of the toxic E104D allele. Flanking polymorphisms were used to establish that the *E104D* allele likely arose roughly 1000 years ago (53,54). The genetic maintenance of this mutation has been curious, and many suggested could likely be indicative of an advantageous hypomorphic loss-of-function. Indeed, population surveys of hemocyte TPI activity and gene integrity revealed a substantial rate of promoter mutations in African American populations (41%) (55). It is still unclear exactly what advantageous properties are conveyed through a hypomorphic condition, though the simplest explanation would be one of mild metabolic restriction, and again could be related to the genomic signaling properties of NAD⁺ accumulation. A human population analysis of the activity rates of 11 metabolic enzymes identified TPI as enriched in functional deficiencies, second only to pyruvate kinase, the second most prevalent glycolytic enzymopathy (56). Caloric restriction has emerged in the field of aging as one of the most reliable means of extending lifespans. Our results in Chapter 3 detail the dramatically increased longevity in *Drosophila* heterozygous for dimer interface mutations. These data are the first to demonstrate a definitive advantage conveyed by heterozygous loss-of-function *TPI* alleles in a uniform genetic background, and support the conclusions of decades of population genetics.

1.2.2 Known TPI deficiency mutants and investigative studies

Disease-associated mutations have been described in several functionally relevant, yet diverse structural locations. Residues affected by disease mutations are plotted on an image of the enzyme in Figure 2. To date, the only mutations that have been identified as homozygotes are those resulting in E104D and V231M (45,48). Further, only E104D, V231M, and F240L have been demonstrated to be sufficient to elicit TPI deficiency in human patients; C41Y, I170V

and G122R have never been identified in patients without accompanying the E104D allele (45,48). Due to the rarity of this disease it is unclear whether these mutations are viable, lethal, pathogenic, or simply lack sufficient consanguinity; this topic will be addressed in Chapter 4. The most widely identified mutation to date has been a Glu-to-Asp change at position 104 (E104D) (26). This mutation occurs at the dimer interface of the enzyme and has been associated with disease in a multitude of different allelic contexts; homozygous and trans-heterozygous in combination with null alleles as well as other point mutations.

One such trans-heterozygote case provided a unique opportunity within the TPI deficiency field – in 1993 a group of clinical researchers identified two genotypically similar brothers, one with neurological dysfunction and another healthy and normal (57). The brothers each had an allele bearing the F240L point mutation and the other a null. These phenotypically-contrasting patients spurred a number of investigations into possible biological explanations for the neurological symptoms. Using primary tissue samples, (erythrocytes taken from patients) the research group identified an increase in plasma membrane calcium ATPase levels (PMCA: 2-3 fold increase) and acetylcholinesterase activity (~30%) in the affected compared to the symptom-free brother (58). Later experiments working with the same F240L mutation identified enhanced association of the mutant variant of the enzyme to the plasma membrane of erythrocytes as well as microtubules, though this enhancement was admittedly modest (59). To explain these observations, the authors proposed a gain-of-function model; wherein mutations in TPI caused enhanced binding to microtubules and PM. The authors also demonstrated a reduction in TPI activity upon the addition of microtubules, which they proposed would further exacerbate the deficiencies found in patients (59). These hypotheses have largely gone unexplored in the last decade, though data discussed in Chapters 2,3 and 4 strongly suggest a loss-of-function disease

mechanism rather than a gain-of-function. Indeed, the recessive nature of this disease would support such a conclusion, and no published or unpublished results have indicated a toxic gain-of-function in any *TPI* alleles.

1.3 TPI DEFICIENCY IN MODEL ORGANISMS

1.3.1 Studies in mice and yeast

Given the rarity of this disorder, pathogenic studies of TPI deficiency have been difficult. The majority of research surrounding the disease has thus far focused on primary tissue samples derived from a select few patients. These studies are inherently limited to descriptive analyses, precluding hypothesis-driven research. The dearth of available patient tissues has severely limited the ability to study the basis of the neurological phenotypes associated with TPI deficiency. To this end, the development of a tractable model system would significantly impact the field, yet the genetics of such a system have proven difficult to manage. The homozygous lethality, and dose-dependent loss-of-function nature of TPI deficiency necessitates gene replacement or mutagenesis of the endogenous locus. As a result, few model organisms exist with which to examine TPI deficiency. Murine and *Drosophila* *TPI* knockouts and null alleles have been generated, but proven lethal (50,60). One mouse point mutant of *TPI*, D49G, has recently been identified in a biased screen for erythrocyte enzyme mutations (61), though this study focused on hematological parameters of the animals, and no behavioral defects were noted.

Work in the yeast species *S. cerevisiae* has proven informative for the *in vivo* biochemical characterization of the various human mutations (62). Indeed, Ralser and

colleagues were the first to establish that the most prevalent mutation, E104D, exhibited an odd dimerization phenotype using the yeast-two-hybrid approach (62). These data were later corroborated by a more focused structural analysis which deduced that the dimerization phenotype was due to a miscoordination of dimer interface water molecules via the shortening of the glutamic acid residue (63). This evidence set precedent that TPI pathology could be due to a reduction in dimerization, though a pathophysiological mechanism was still unclear.

1.3.2 Studies in *Drosophila*

1.3.2.1 *Drosophila* neurobiology

Around the same time as the Ralser publication, two independent groups of *Drosophila* biologists identified the same Met-to-Thr substitution at position 80 (M80T) in *TPI* (50,64). This M80T mutation led to neuropathology and behavioral dysfunction. These mutants were identified in a chemical mutagenesis screen for aberrant behavior, and were characterized with two typically distinct behaviors: thermal stress and mechanical stress sensitivity. The former behavior was pioneered by Ganetzky and colleagues as a phenotype enriched for neurological dysfunction. This behavioral test uses elevated temperature to stress the animals to a non-permissive level, and the subjects are monitored for seizures or paralysis relative to appropriate genetic controls. The basis for this stress-dependency include a trio of factors which are believed to lead to the aberrant behavior: i) elevated temperature increases basal *Drosophila* neural activity, ii) increased temperature enhances sensory inputs to the central nervous system, and iii) elevated temperature could negatively influence thermolabile proteins (65-69). This thermal stress methodology has been used in conjunction with forward genetic screens to reveal mechanisms of neurological function, such as voltage-gated ion channels and their associated

transcriptional regulators (69,70), vesicle fusion/recycling proteins (71), and regulators of synapse development (72,73), among others. Of particular interest is the nature of the aberrant behavior and the time of onset; the faster the time of onset the more germane the mutant is likely to be to neurological function (72).

Comparatively, the latter phenotype, mechanical stress sensitivity, has been thoroughly examined by Tanouye and colleagues as an insect analog of mammalian seizures (74,75). Supporting this assertion, recent work in our laboratory has established that strobe light stimulation is sufficient to phenocopy mechanical stress-dependant phenotypes, suggesting that overstimulation of sensory inputs is both necessary and sufficient to elicit these behaviors (76). Indeed, targeted electrophysiology experiments with mechanical stress-sensitive mutants have demonstrated fundamental characteristics of seizures: electrically-inducible uncontrolled activity followed by refractory periods (77-79). These “seizures” are threshold events, capable of being achieved in even wild type animals with enough stimulation. Using a modified *Drosophila* giant fiber preparation, Tanouye and colleagues established that many anti-epileptic drugs were capable of increasing the threshold to seizure activity in wild type and several mechanically stress sensitive mutant alleles (80-84). These results were leveraged further to identify novel putative therapeutic targets for treating epileptic patients, a forward genetic approach badly needed in the epileptic community. These experiments have been extremely fruitful for basic research into the causes of epilepsy and potential therapeutic strategies, often revealing an intimate link between metabolism and seizure activity.

Collectively, characterization of a *Drosophila TPI* allele with both of these behaviors corroborated the diverse spectrum of abnormal neuro- and neuromuscular symptoms seen in human patients. The *TPI*^{MSOT} phenotypes suggested the potential for underlying neuropathology,

and indeed evidence was found of both peripheral and central neuropathy in this *Drosophila* model of TPI deficiency (50), again, much like in the human patients. To date, *Drosophila* are the only model organism to effectively recapitulate the neurological dysfunction seen in human patients (48).

1.3.2.2 *Drosophila* reveal mechanisms of pathologic protein regulation

Yet the similarities do not end with the neurological phenotypes displayed by the animals; the *TPI*^{M80T} allele shares many biochemical similarities with the mutant human proteins. Importantly, all of the severely pathological human *TPI* mutations exhibit thermolability (26,45,48). Thermolability of a protein establishes a susceptibility to inactivation due to heat stress, and this could be indicative of stability/conformational defects within the protein. Previous studies in our laboratory have established that *TPI*^{M80T} is found at reduced protein levels, while transcript levels actually increase (85); collectively these data suggest a defect in translation or stability of the protein which causes cellular depletion. Later examinations revealed that molecular chaperones, heat shock protein 70 and 90 (Hsp70, Hsp90), were preferentially bound to the *TPI*^{M80T} protein (86). The pathologic relationship between this *Drosophila* mutant and these chaperones was established through pharmacologic and genetic inhibition, which both moderately attenuated *TPI*^{M80T} levels and also helped ameliorate some of the behavioral phenotypes seen in the mutants. Experiments seeking to examine the possible relationship between the chaperones and protein levels established that proteosomal inhibition, genetic or pharmacologic, was sufficient to increase *TPI*^{M80T} protein levels (86). These results concluded that reduced TPI levels in *TPI*^{M80T} were in part attributable due to increased protein degradation. Importantly, reduced TPI levels have been detected in primary human tissue from

patients. These observations set the stage for us to question whether the activity of the enzyme or its presence was most critical to the disease phenotypes in our animals (Chapter 2).

1.3.2.3 *Drosophila* and TPI deficiency redox changes

The *Drosophila* system also recapitulates the lack of ATP depletion found in patient tissues (87-89), and these data have led us to question the pathogenic importance of general metabolism in TPI deficiency (Chapter 2,3). Reduced glycolytic flux is known to be compensated by rerouting substrates from glycolysis to the PPP (90), and this detour is likely controlled by two possible mechanisms; i) a buildup of DHAP substrate to inhibit aldolase, and/or ii) oxidative stress-induced redirection of metabolites (90-92). We find it likely that both mechanisms are influencing metabolic rerouting, as DHAP has been shown to accumulate in patient tissues with reduced TPI activity (57), and oxidative stress has been demonstrated to target redox-sensitive glycolytic enzymes to reroute glycolytic intermediates through the PPP (91). Further, the *TPI*^{M80T} allele has been characterized as exhibiting mitochondrial oxidative stress (35).

Previous work by our lab and others suggested that mitochondrial redox changes could be due to an accumulation of a toxic byproduct of DHAP (35,64,93). If allowed to accumulate, DHAP can be non-enzymatically converted into the reactive Schiff base, methylglyoxal (MG). Hrizo and colleagues suggest that the accumulation of this advanced glycation end-product (AGE) could be responsible for inducing the mitochondrial stress exhibited in the *TPI*^{M80T} animals (94,95). To address this possibility, we have generated knockouts (KOs) of the initial glyoxylase enzyme responsible for detoxifying the organism of MG. These glyoxylase KO animals failed to recapitulate our mutant *TPI* phenotypes [data not shown]. Further, gross measurements of AGEs have not revealed an obvious contribution to the pathology of the

animals, as changes in genetic background have a more dramatic effect on AGE accumulation than the inhibition of TPI or the glyoxylase enzyme [data not shown]. This work is still ongoing in the laboratory, yet the initial experiments suggest that MG is not a primary contributor to TPI deficiency pathology.

Still, TPI deficiency-associated changes in redox status provide a platform to ask a number of intriguing questions surrounding the relationship between glycolysis, the PPP, and mitochondrial redox changes. It has been demonstrated that inhibition of TPI increases PPP flux (90,91), yet this increase in PPP and production of NADPH protects the cells from redox changes in only certain human disease-associated *TPI* mutants (62). Further, the simple conclusion that mitochondrial reactive oxygen species (ROS) increases as a function of glycolytic flux inhibition is also unclear. Is the cell compensating for reduced glycolytic ATP production by upregulating oxidative phosphorylation, or are changes in ROS elicited by a non-metabolic mechanism? Why can activation of the PPP in certain *TPI* mutants counter this putative increase in mitoROS; does this suggest differences in pathogenesis? Are changes in redox status in the cell a toxic byproduct of reduced glycolytic flux, or a purposeful signal from the mitochondria to reroute glycolytic metabolites through the PPP? Noting the modest changes in TPI pathology elicited through redox modulation (35), I propose that mitochondrial ROS in the *TPI*^{M80T} animals is likely signaling a purposeful rerouting of metabolic substrates toward the PPP. However, it is not clear whether these observed redox changes in pyridines are derived from mitochondrial or cytosolic sources. Later discussions will focus on the putative impact of changing cytosolic redox status, with a focus on local changes in pyridine oxidation at the plasma membrane [Chapter 3,5].

1.4 DROSOPHILA GENOMIC ENGINEERING

Work spanning the last decade has outlined *Drosophila* as a model organism capable of recapitulating the neurological dysfunction seen in human TPI deficient patients (1,35,50,64,85,86). This observation provided a unique opportunity to perform hypothesis-driven experiments aimed at delineating the pathogenic mechanism through which this neurological dysfunction occurs. Given that TPI deficiency is a dose-dependent loss-of-function disorder, traditional transgenic modulations – often considered the strength of the *Drosophila* system – were deemed inadequate. Fortunately, recent advances in *Drosophila* homologous recombination and genomic engineering technology provided a unique opportunity to study this disorder.

For several years *Drosophila* homologous recombination (HR) technology lagged behind that of yeast and murine systems. This was fortunately changed roughly 13 years ago by the work of Rong and Golic (96). In this seminal study, the authors first outlined an efficient methodology for performing ends-out and ends-in targeting in *Drosophila*. The HR system was designed to utilize elements encoded entirely by the genome, requiring no injections of pre-linearized DNA. Shortly thereafter, a number of groups within the *Drosophila* community began pursuing phiC31-mediated integration as a means to overcome positional variability in transgene expression (97,98). These studies stemmed from an older challenge with random transposon-mediated transgenesis, wherein genomic changes in transgene positioning could influence expression of the construct. These expression/position based complications made comparisons between two constructs difficult, necessitating numerous replicates and control experiments. To anticipate this problem, geneticists conscripted a viral integrase technology known as the phiC31 integrase system. The complementary integrase sites, attP and attB, were used in conjunction to

ensure site-specific and directional transgenesis. First, an *attP* site was placed on a traditional transposon and integrated into the genome through standard p-element transgenesis. Once placed, this site became an anchor for future phiC31-mediated transgenesis with the *attP* directing uniform localization of all transgenic permutations. Constructs containing the complementary *attB* site were generated and injected into the embryos expressing germ-line phiC31 integrase to mediate inheritance.

A major advance in *Drosophila* genetics was ushered in by uniting the HR and phiC31 genomic techniques. A few years ago Huang and colleagues (99,100) utilized the knock-in technology pioneered in HR to replace endogenous genes with *attP* engineering sites. The directed placement of these phiC31 landing sites opened a window into the originally targeted gene, making it amenable to future modifications [Schematic shown in Figure 5]. This genomic engineering (GE) strategy has been an extremely valuable tool for the meticulous evaluation of a specific gene. Yet the technology's true utility was in studying highly dose-dependent loci, where traditional transgenic expression could introduce over/under-expression and misexpression complications. The importance of using the endogenous regulatory machinery was illustrated as the Hong group was able to tag developmentally critical proteins of interest, revealing novel functions due to the lack of typical untoward effects associated with transgenic manipulations (101). To this end, the two gene loci I have worked on in my graduate career have both been characterized as dose-dependent. In collaboration with the Hong group we have targeted the *ATPa* gene encoding the major catalytic subunit of the Na,K-ATPase [unpublished], and *TPI* (1). The work I will describe in this document will be primarily composed of alleles generated using GE of the *TPI* locus. It is critical to note the beauty of this genetic approach, as all of these alleles were generated in a uniform background. Therefore the key differences

between the animals will be the subtle allelic changes made through our targeted modifications. This genetic approach is unparalleled, allowing me with confidence to say that my thesis work truly is a structure-function analysis within the context of a whole organism.

2.0 EVIDENCE OF A NON-CATALYTIC FUNCTION OF TRIOSEPHOSPHATE ISOMERASE CRUCIAL TO BEHAVIOR AND LONGEVITY

2.1 ABSTRACT

Triosephosphate isomerase (TPI) is a glycolytic enzyme that converts dihydroxyacetone phosphate (DHAP) into glyceraldehyde-3-phosphate (GAP). Glycolytic enzyme dysfunction leads to metabolic diseases collectively known as glycolytic enzymopathies. Of these enzymopathies, TPI deficiency is unique in the severity of neurological symptoms. The *Drosophila sugarkill* mutant closely models TPI deficiency and encodes a protein prematurely degraded by the proteasome. This result caused us to question whether enzyme catalytic activity was critical to pathogenesis of *TPI sugarkill* neurological phenotypes. To study TPI deficiency *in vivo* we developed a genomic engineering system for the *TPI* locus that enables the efficient generation of novel *TPI* genetic variants. Using this system we demonstrate that *TPI sugarkill* can be genetically complemented by *TPI* encoding a catalytically inactive enzyme. Further, our results demonstrate a nonmetabolic function for TPI, the loss of which contributes significantly to the neurological dysfunction in this animal model.

2.2 INTRODUCTION

Triosephosphate isomerase (TPI) is a homodimeric enzyme that functions in a non-linear step of glycolysis, converting dihydroxyacetone phosphate (DHAP) into glyceraldehyde 3-phosphate (GAP). Both DHAP and GAP are produced from the catabolism of fructose 1,6-bisphosphate by the enzyme aldolase; however, only GAP can be utilized by the remaining steps in glycolysis. Therefore, TPI is responsible for the net gain of glycolysis-derived ATP as well as the production of an extra molecule of pyruvate per molecule of glucose. This enhancement of glycolysis plays an important role in the bioenergetics of both aerobic and anaerobic metabolism.

Mutations in *TPI* have been identified in humans that result in a disease known as TPI deficiency. TPI deficiency is a recessive loss-of-function disease resulting from missense mutations in the gene. The disease is clinically characterized by symptoms such as hemolytic anemia, cardiomyopathy, neurological dysfunction and degeneration, and premature death (26,45). Pathogenic mutations can be found in various regions of *TPI* affecting either the promoter or coding sequence, and all patients suffering from TPI deficiency have been reported as having dramatically reduced TPI activity *in vivo* owing to changes in catalysis and/or enzyme stability (57,102,103). Patients suffering from TPI deficiency may present with one or more of the previously described symptoms with no reliably predictive biochemical or structural characteristics ascribed to each phenotype or degree of severity.

Drosophila are the only model system identified to date in which mutants have been shown to recapitulate the neurological phenotypes seen in human patients (50,64). We have previously isolated an animal model of TPI deficiency known as *TPI^{sugarkill} (sgk)*. *TPI^{sgk}* is characterized by shortened lifespan, neurodegeneration, and conditional behavioral abnormalities (50) resulting from a missense mutation causing a methionine to threonine substitution (M80T).

The affected methionine is present near the dimer interface yet does not seem to result in a shift in monomer-dimer populations *in vivo* (85). However, the TPI^{sgk} mutation has been shown to induce abnormal proteasomal degradation of TPI resulting in reduced total TPI protein (85,86). Interestingly, we have previously shown that this loss-of-function mutation can be attenuated by overexpressing mutant TPI^{sgk} (50). This result caused us to question whether the presence of the enzyme or its catalytic activity was most important to the pathogenesis of TPI^{sgk} . Here we demonstrate that the M80T substitution in TPI^{sgk} reduces its isomerase activity and, based on the proximity to one of the TPI catalytic sites, we predict that the reduced catalytic efficiency is a result of the mutation's influence on dimeric catalytic activity.

To address whether the presence of the enzyme or its catalysis were most important to the TPI^{sgk} disease phenotypes *in vivo*, we developed genomic engineering (GE) of the *Drosophila* TPI locus. This process establishes an *attP* ΔTPI founder line, which can be used to modify the gene locus using highly efficient *attP/attB* transgenesis. We hypothesized that if the presence of the enzyme was critical to pathogenesis independent of catalytic activity, then we would be able to rescue the disease phenotypes with a catalytically inactive variant of the protein. Lys12 of TPI is a fully conserved catalytic residue previously shown to be required for substrate binding, and a mutation to Met completely abrogates catalysis (16,104). We have generated the *attP* ΔTPI founder line and have used GE to create *Drosophila* $TPI^{\Delta cat}$ encoding a catalytically-inactive TPI. Here we demonstrate that $TPI^{\Delta cat}$ genetically complements the longevity and behavior of the TPI^{sgk} animal model of TPI deficiency. Furthermore, catalytically inactive TPI complements TPI^{sgk} phenotypes without enhancing its stability or catalysis or reducing the associated metabolic stress.

2.3 RESULTS

2.3.1 Recombinant TPI enzyme activity

Previous studies established that TPI^{sgk} is a recessive loss-of-function mutation characterized by reduced TPI levels (85). Further, it was suggested that TPI^{sgk} retained sufficient activity to rescue mutant survival and behavioral phenotypes if overexpressed (85). Based on these data we hypothesized that reduced TPI catalysis was critical to the pathogenesis of TPI deficiency. To investigate this hypothesis further we generated recombinant *Drosophila* WT (dWT) and TPI^{sgk} (dM80T) and examined the kinetics of isomerase activity for each (Table 1). These data demonstrate that TPI^{sgk} (dM80T) exhibits a substantial reduction in isomerase activity. The dM80T protein does not significantly change substrate affinity, yet elicits an ~11-fold reduction in catalytic activity compared to WT enzyme. This ultimately resulted in a ~15-fold reduction in enzyme efficiency. Both enzymes displayed typical Michaelis-Menten kinetics (Figure 3).

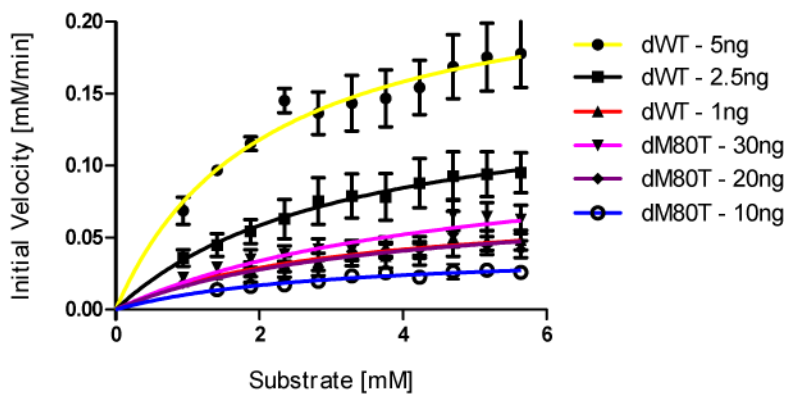


Figure 3. Both *Drosophila* wild type (dWT) and sugarkill (dM80T) enzymes follow traditional Michaelis-Menten kinetics. Michaelis-Menten nonlinear regression fits are shown, and all enzyme concentrations are indicated.

Table 2. Kinetic parameters of *Drosophila* wild type (dWT) and sugarkill (dM80T) triosephosphate isomerase enzymes.

	dWT	dM80T
k_{cat} (GAP) (s^{-1})	1454 ± 163.6	129.6 ± 1.5
K_m (GAP) (mM)	2.8 ± 0.4	3.7 ± 0.5
k_{cat}/K_m (GAP) ($\text{s}^{-1} \text{M}^{-1}$)	5.2×10^5	3.5×10^4

* \pm SEM

To assess the role of the M80 position within TPI function, we analyzed the crystal structure of TPI from *G. gallus* (105) – *Drosophila* TPI shows 67% identity and 80% functional conservation with *G. gallus*. This structure was determined in the presence of the transition-state analog phosphoglycolohydroxamic acid (PGH), and the homologous methionine (M81) is located within TPI’s third loop (residues 63 to 86) (Figure 4A). This loop coordinates numerous interactions within the dimerization interface of TPI including important contacts between M81 and M13 and N14 of the neighboring subunit (Figure 4B). These hydrophobic interactions help position the third loop, and are aided by hydrogen bonding between residues T74 and E76 (also on the third loop), which interact with H95 and R98, respectively. The sum of these interactions is a coordinated network using conserved residues to mediate both hydrophobic and hydrogen-bonding interactions that ultimately positions both K12 and H95 properly within the active site of the enzyme (Figure 4B & 4C). These residues are critical for enzymatic function in TPI (106,107) and establish a connection between M80 in *Drosophila* TPI and reduced catalysis for TPI^{sgk}.

Biochemically establishing that TPI^{sgk} still retains catalytic activity supported a catalytic explanation of our phenotypic attenuation via TPI^{sgk} transgenic overexpression. However, a rigorous assessment of this hypothesis *in vivo* would require supplementation of TPI levels without modifying its activity.

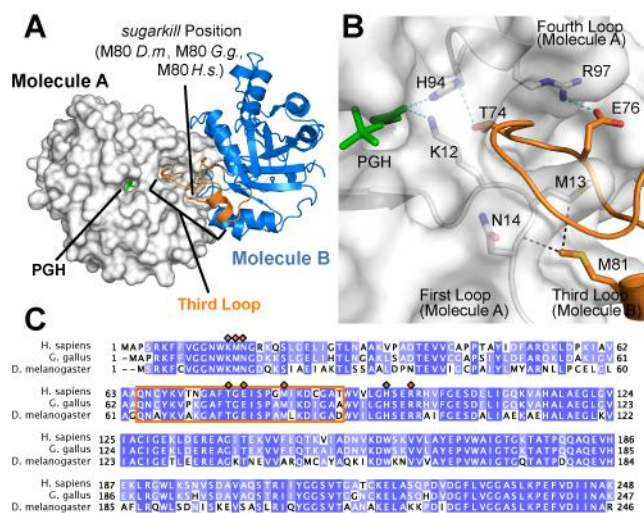


Figure 4. Positioning of the third loop forms an interaction network connecting the dimerization interface to the catalytic pocket. A) The crystal structure of TPI dimer from *Gallus gallus* (PDB ID, 1TPH). Monomer A of the dimer is rendered as a surface and colored white, while Monomer B (blue) is shown as a cartoon with the third loop highlighted in orange. The position of the transition state analog phosphoglycolohydroxamic acid (PGH, green) is indicated within the catalytic pocket. B) Local environment of the third loop. Colored as before, with residues making important contributions to the dimerization interface indicated as sticks. Van der Waals interactions between M81 and residues M13 and N14 are indicated as black dotted lines. Hydrogen bonds between residues on the distal end of the third loop and connecting to the catalytic core are given as green dotted lines. Residues are numbered based on *Gallus gallus* sequence, and for clarity we are using the TPI numbering standard that accounts for the removal of the initiator methionine. C) An alignment of TPI protein sequences from *H. sapien*, *G. gallus*, and *D. melanogaster*. Protein alignment was performed using the Clustal W method, with *H. sapien* and *G. gallus* showing 63.5% and 67.3% identity to *D. melanogaster*. Residues that mediate TPI dimerization are indicated by grey circles. Residues within the hydrogen-bonding network critical for catalysis are indicated (Cyan). The position of the sugarkill mutant (M81, red) and its positions within the third loop (orange box) are indicated.

2.3.2 Generation of the founder knock-out line by homologous recombination

To create a catalytically inactive allele of *TPI* we developed a GE approach for the *TPI* locus. Homologous recombination (HR) in *Drosophila* had previously been developed (96,108) but recent advances in GE technology have made the process considerably more efficient (99,100). The GE founder line was generated through replacement of the endogenous *TPI* locus using ends-out homologous recombination with a functional *attP* element (Figure 5A). *TPI* is located on the third chromosome between *CG31029* (centromeric) and *AdoR* (telomeric). Homology arms directing the deletion of the entire *TPI* locus were PCR amplified from the *w*¹¹¹⁸ wild type genomic DNA and cloned into the *pGX-attP* targeting vector. Traditional P-element transgenesis was used to obtain *pGX-attP* insertion on the second chromosome. HR was induced as previously outlined (99). Approximately four hundred putative positive HR events were identified after screening ~ sixty thousand (60,000) animals. Among the putative positives, three positive HR lines were identified and verified using genetic and molecular methods.

Genetic validation included failure to complement a previously identified *TPI* null allele, *TPI*^{JS10} (50), and homozygous lethality. Molecular validation included PCR analyses to confirm proper targeting of left and right homology arms using primers directed outside the homology arms and within construct elements. The confirmed founder line was reduced to remove *w*^{mc+} using a CRE recombinase and is designated *attP ΔTPI* (Figure 5B). The entire *attP ΔTPI* region was sequenced to confirm the correct placement of the GE elements and the integrity of the homology arms.

GE was performed to create *TPI*⁺ (*attR*), *TPI*⁺-CFP (*attR*), *TPI*^{M80T} (*attR*), *TPI*^{Δcat} (*attR*), and *TPI*^{Δcat}-CFP (*attR*) animals using standard phiC31 site-directed integration followed by CRE-mediated reduction to remove *w*^{mc+} (Figure S2). These animals were molecularly verified

using PCR analyses of the *attR* construct element (Figure 5E) and the locus was sequenced. Importantly, GE *TPI*⁺ (*attR*) animals are homozygous viable and behave normally while animals bearing the M80T substitution are substantially stress sensitive and exhibit reduced longevity (Figure 6). Animals homozygous for *TPI*^{Δ*cat*} (*attR*) are lethal, indicating a necessity for TPI catalysis during development.

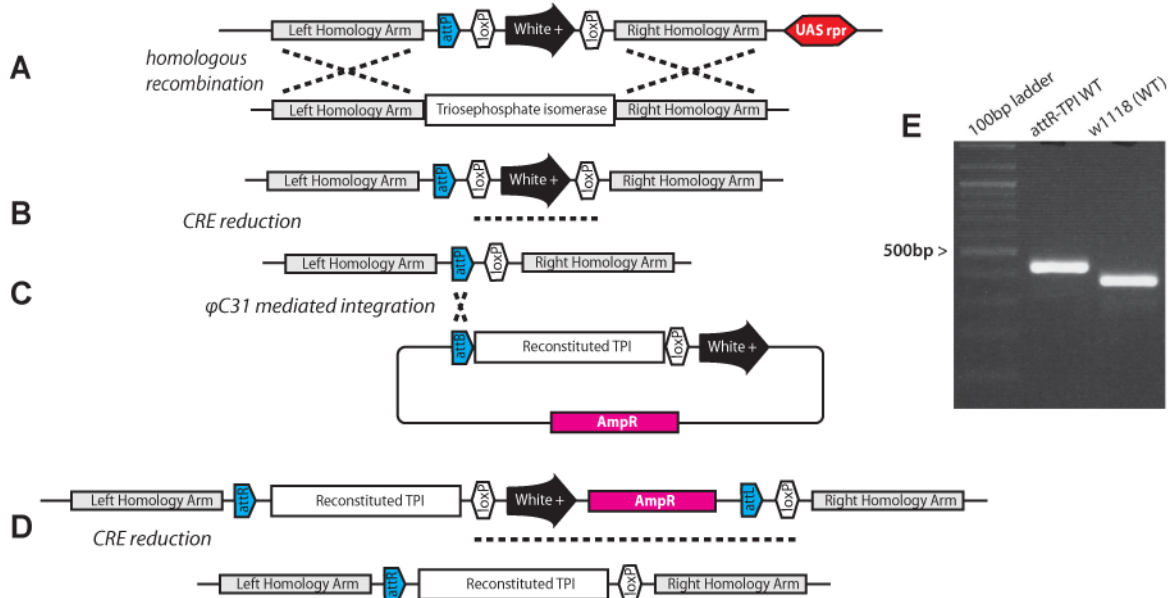


Figure 5. Genomic engineering of the TPI locus. A) The target gene is replaced by the *attP* phiC31 integration site and a *white* minigene flanked by two *loxP* sites. B) The *white* minigene is removed by a CRE recombinase, leaving only the *attP* phiC31 integration site and a *loxP* site. C) *TPI* is cloned into the *pGE-attB* vector and modified, as desired. The construct is then injected into founder line embryos expressing the phiC31 integrase, which initiates specific and directional integration of the construct into the *TPI* locus. D) The *white* minigene and plasmid construct are removed through the expression of CRE recombinase, leaving only an *attR* and a *loxP* site. E) Molecular analysis reveals the addition of an *attR* site 5' of the reconstituted *TPI* gene.

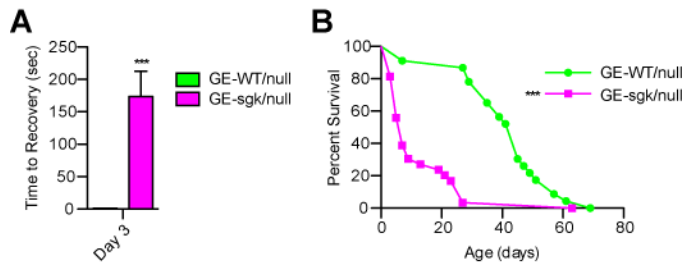


Figure 6. Genomically engineered TPI^{sgk} displays aberrant behavior and reduced longevity. A) Genomically engineered TPI^+ (*GE-WT*) displays normal behavior, while the genomically engineered TPI^{sgk} (*GE-sgk*) displays marked mechanical stress sensitivity. **B)** *GE-sgk* exhibits reduced longevity compared to *GE-WT*. $n > 20$ for all lifespans and behavior. A Student's t test was used to assess behavioral differences between genotypes, and a Log-rank (Mantel-Cox) Test was used to assess lifespans. *** indicates $p < 0.0001$ compared to *GE-WT*. Error bars indicate \pm s.e.m. Both genomically engineered alleles were assessed over TPI^{null} .

2.3.3 Animal behavior and longevity

To test whether TPI – independent of catalytic activity – is crucial to disease pathogenesis, TPI^{sgk}/TPI^+ , TPI^{sgk}/TPI^{sgk} , TPI^{sgk}/TPI^{null} , and $TPI^{sgk}/TPI^{\Delta cat}$ animals were collected and aged at 25°C. TPI^{null} is a null allele owing to a 1.6 kb deletion, therefore TPI^{sgk}/TPI^{null} animals represent approximately the amount of TPI produced by one allele of TPI^{sgk} . For the purposes of this study, contrasting TPI^{sgk}/TPI^{null} with $TPI^{sgk}/TPI^{\Delta cat}$ provides the most informative comparison, as each animal population contains one catalytically active *TPI* allele.

Male and female animals were housed in vials of 10-20 individuals and examined for mechanical- and temperature-dependent locomotor defects on day three and twenty. Time to recovery and time to paralysis were measured in each assay. While TPI^{sgk}/TPI^+ shows no sign of paralysis or seizures upon mechanical stress, TPI^{sgk}/TPI^{sgk} and TPI^{sgk}/TPI^{null} exhibit a clear delay in recovery (Figure 7A). In contrast, $TPI^{sgk}/TPI^{\Delta cat}$ animals display no signs of stress sensitivity

(Figure 7A). Previously, we have shown that TPI^{sgk} phenotypes are progressive in nature (50,85). We measured these behaviors at two time points, day 3 and day 20 to reveal whether $TPI^{\Delta cat}$ fully complements the TPI^{sgk} phenotypes or simply delays their onset. The catalytically inactive enzyme was shown to rescue mechanical stress sensitivity at both time points indicating that the $TPI^{\Delta cat}$ allele does not simply delay the progression of the disease phenotype (Figure 7A).

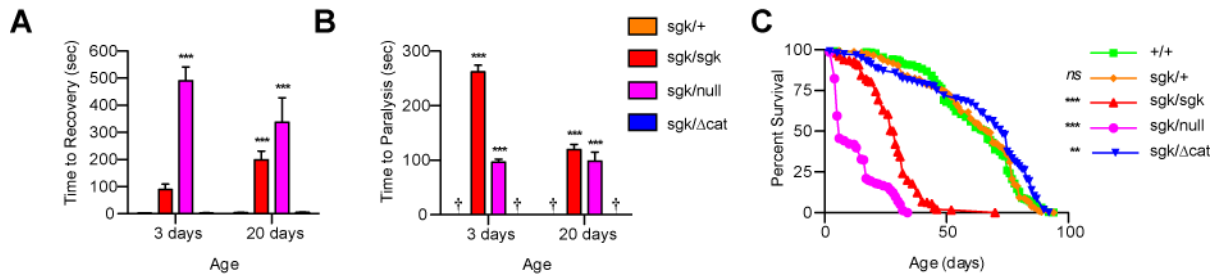


Figure 7. The catalytically inactive $TPI^{\Delta cat}$ rescues behavioral and longevity phenotypes in TPI^{sgk} . A) $TPI^{\Delta cat}$ complements TPI^{sgk} mechanical stress sensitivity at both day 3 and day 20. B) $TPI^{\Delta cat}$ expression complements TPI^{sgk} thermal stress sensitivity, again at both day 3 and day 20. † indicates TPI^{sgk}/TPI^+ and $TPI^{sgk}/TPI^{\Delta cat}$ animals did not paralyze. C) $TPI^{\Delta cat}$ complements the longevity defect of TPI^{sgk} . ** indicates $p < 0.01$ and *** $p < 0.001$ relative to TPI^+/TPI^+ . $n > 15$ per genotype for all behavioral assays, and $n > 150$ per genotype for all lifespans. Error bars indicate \pm s.e.m.

Thermal stress sensitivity of the animals was also evaluated to test the possibility of pathogenic divergence (Figure 7B). Here, TPI^{sgk}/TPI^+ shows no signs of paralysis or seizures upon thermal stress, while TPI^{sgk}/TPI^{sgk} and TPI^{sgk}/TPI^{null} animals show distinct paralytic phenotypes initiated at ~240 sec. and ~90 sec. respectively (Figure 7B). In contrast, animals expressing the catalytically inactive allele $TPI^{sgk}/TPI^{\Delta cat}$ displayed no signs of paralysis after thermal stress induction (Figure 7B). Again, we measured these behaviors at two time points, day 3 and day 20, and expression of the catalytically inactive enzyme was shown to rescue thermal stress sensitivity at both time points (Figure 7B).

To test whether genetic complementation extended to longevity we assessed lifespans as previously described (109). TPI^{sgk} animals exhibit a marked reduction in median longevity that was also complemented with the catalytically inactive $TPI^{\Delta cat}$ allele (Figure 7C). Finally, all genotypes eclosed at Mendelian rates suggesting the absence of developmental deficits and that the behavior of the adult population is representative of the genotype as a whole.

2.3.4 TPI^{sgk} animal bioenergetics and lysate enzyme activity

Genetic complementation with $TPI^{\Delta cat}$ could indicate a previously unidentified non-isomerase function of the enzyme or it could result from a restoration of isomerase activity by a number of possible mechanisms. Thus, we examined whether $TPI^{\Delta cat}$ provided genetic complementation through a restoration of enzyme isomerase activity. TPI enzyme activity was robust in both TPI^+/TPI^+ and TPI^{sgk}/TPI^+ lysates yet markedly reduced in TPI^{sgk}/TPI^{sgk} and TPI^{sgk}/TPI^{null} animals (Figure 8A). Most importantly, $TPI^{sgk}/TPI^{\Delta cat}$ animals exhibit levels of isomerase activity similar to TPI^{sgk}/TPI^{sgk} and TPI^{sgk}/TPI^{null} animals demonstrating that the genetic complementation is independent of isomerase activity (Figure 8A).

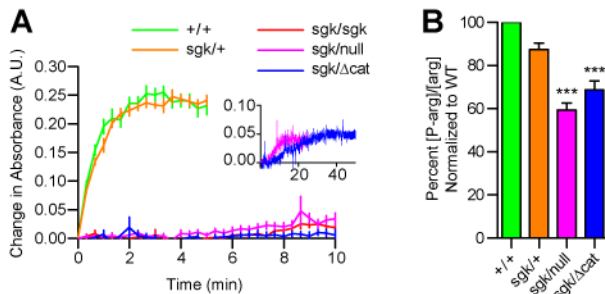


Figure 8. $TPI^{\Delta cat}$ fails to rescue animal bioenergetics and TPI enzyme activity. A) TPI^{sgk} exhibits little activity in animal lysates. Additionally, complementing TPI^{sgk} with $TPI^{\Delta cat}$ does not rescue its activity in vivo. Inset: A between TPI^{sgk}/TPI^{null} and $TPI^{sgk}/TPI^{\Delta cat}$ lysate kinetics reveals low activity levels in both

lysates. Note the axes are maintained but units have been changed. B) TPI^{sgk}/TPI^{null} animals and $TPI^{sgk}/TPI^{\Delta cat}$ animals both showed reduced ratios of P-arg/arginine indicating bioenergetic stress. *** indicates $p < 0.001$ relative to WT. Error bars indicate \pm s.e.m.

The dramatic reduction in lysate isomerase activity suggested that pathogenesis of TPI^{sgk} neurological phenotypes could be unrelated to animal metabolic stress. Previous studies measuring ATP levels in this same mutant have failed to detect a significant change (64). To further evaluate the relationship between metabolism and TPI deficiency behavioral and longevity phenotypes we measured phospho-arginine [P-arg] to arginine [arg] ratios as previously described (110), as this is an extremely sensitive assay of *Drosophila* bioenergetic status (76). [P-arg]/[arg] ratios in TPI^{sgk} mutant animals were depressed compared to wild type, consistent with a strong loss-of-function mutation in glycolysis (Figure 8B). This represents a reduction in the available pool of [P-arg] normalized to the total [arg] available, and suggests that the animals are utilizing this pool at a higher rate to buffer their ATP levels, similar to how mammals utilize phosphocreatine (76). Importantly, $TPI^{sgk}/TPI^{\Delta cat}$ animals exhibiting low levels of catalytic activity also showed a similar depression in their [P-arg]/[arg] ratios compared to wild type animals (Figure 8B). These data indicate that $TPI^{\Delta cat}$ rescues TPI^{sgk} phenotypes by a mechanism independent of TPI's well-established role in cellular bioenergetics, and may provide an explanation as to the absence of an association between enzyme catalysis and neurological complications in human patients.

2.3.5 TPI^{sgk} and $TPI^{\Delta cat}$ protein levels

The capacity of a catalytically inactive allele of *TPI* to genetically complement all behavioral and longevity phenotypes independent of isomerase activity and animal metabolism strongly supports the conclusion that TPI^{sgk} phenotypes are due to a change in total TPI protein levels, not a reduction in TPI catalytic capacity. To determine whether the catalytically inactive TPI rescues total TPI levels, we immunoblotted for the presence of TPI with or without a cyan fluorescent protein (CFP) tag; the use of the tag allowed us to discriminate between protein isoforms. Figure 10 shows that the addition of this C-terminal CFP does not influence the capacity of $TPI^{\Delta cat}$ to rescue the TPI^{sgk} phenotypes. TPI^{sgk} display reduced TPI protein levels in vivo (85,86), and TPI levels were further reduced when TPI^{sgk} was paired with the null allele, TPI^{null} (Figure 9A,C). Interestingly, complementing TPI^{sgk} with the catalytically inactive allele $TPI^{\Delta cat}$ rescues the total TPI protein levels to that seen in the aphenotypic TPI^+/TPI^+ wild type homozygotes. Observing $TPI^{\Delta cat -CFP}$ and TPI^{sgk} independently, it can be seen that $TPI^{\Delta cat -CFP}$ fails to rescue TPI^{sgk} levels (Figures 9A,C) and, conversely, mutant TPI^{sgk} protein does not induce the degradation of $TPI^{\Delta cat -CFP}$ (Figures 9B,C).

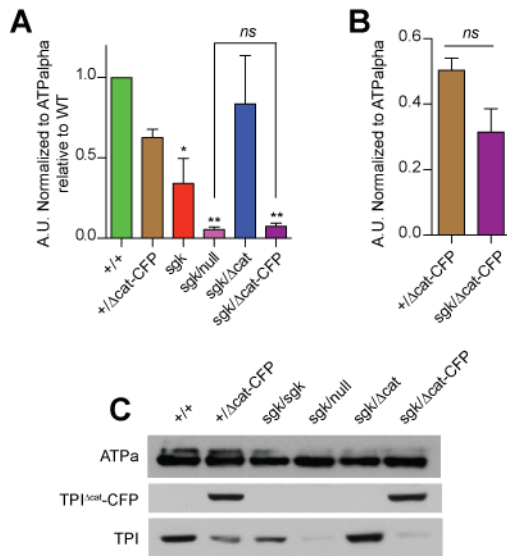


Figure 9. $TPI^{\Delta cat}$ expression does not prevent the degradation of TPI^{sgk} . **A)** Shown is a quantification of the levels of untagged TPI. TPI^{sgk} complemented with $TPI^{\Delta cat}$ shows elevated levels of total TPI similar to WT. Additionally, TPI^{sgk}/TPI^{null} have similar levels of TPI compared to $TPI^{sgk}/TPI^{\Delta cat-CFP}$. ** indicates $p < 0.01$ and *** $p < 0.001$ compared to WT. Further, ns indicates no significant change compared to TPI^{sgk}/TPI^{null} . $n = 4$. **B)** TPI^{sgk} does not induce the degradation of $TPI^{\Delta cat-CFP}$. Shown is a quantification and comparison of the levels of $TPI^{\Delta cat-CFP}$ (**C**). Student's T test was used to compare the two groups and found no significant difference (ns). $n = 4$. **C)** Shown is a representative blot from which Figures 9A and 9B were quantified. The loading control used was ATPalpha (Na,K-ATPase). Error bars indicate \pm s.e.m.

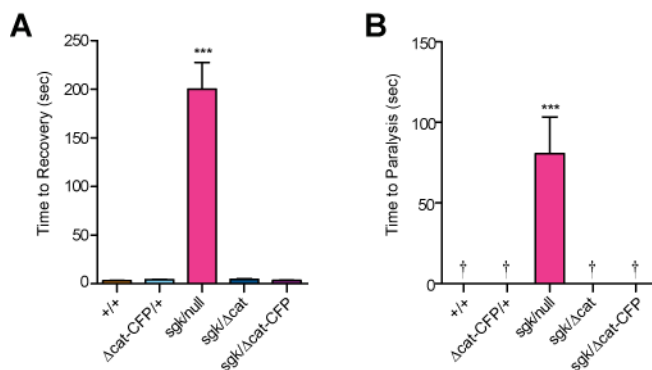


Figure 10. The addition of the C-terminal CFP to $TPI^{\Delta cat}$ does not affect its capacity to genetically complement TPI^{sgk} . **A)** mechanical stress sensitivity or **B)** thermal stress sensitivity. Mechanical stress sensitivity was assessed on Day 1 and thermal stress sensitivity was assessed on Day 5. $n > 15$. † indicates animals did not paralyze. A One-way ANOVA was performed to assess variance and data sets were

compared using Tukey's post-hoc analysis. *** indicates that $p < 0.001$ and ns indicates no significant difference, both compared to WT. Error bars indicate \pm s.e.m.

The inability of $TPI^{\Delta cat -CFP}$ to modulate TPI^{sgk} levels suggests that any phenotypic rescue is likely being performed by the catalytically inactive isoform, and not merely increasing the presence of a still catalytically active TPI^{sgk} . Secondly, it is of particular interest that TPI^{sgk} does not significantly influence the levels of $TPI^{\Delta cat -CFP}$. These results suggest three possible interpretations: i) TPI^{sgk} is degraded prior to but stable upon heterodimerization, ii) TPI^{sgk} monomers are selectively degraded from heterodimer complexes, or iii) that TPI^{sgk} and $TPI^{\Delta cat}$ never exist as a heterodimer. Taken together, these results confirm that $TPI^{\Delta cat}$ complements the TPI^{sgk} phenotypes independent of isomerase activity demonstrating a non-catalytic function of TPI critical to the pathogenesis and severity of TPI deficiency.

2.4 DISCUSSION

The *sugarkill* model of TPI deficiency used in these experiments is characterized by reduced catalysis and protein stability, characteristics found in several of the more toxic human *TPI* alleles (57,102,111). Similarly, the M80T mutation recapitulates the neurological dysfunction and toxicity exhibited in many of the human patients. Using the *Drosophila* model we have genomically engineered (GE) the *TPI* locus to make targeted in vivo modifications to the endogenous gene. GE allows us to study *TPI* manipulations under endogenous regulatory control, allowing rigorous experiments that would not be feasible with traditional transgenic approaches (101,112,113). The power of GE is born in its capacity to study a gene's function in

vivo while reducing artifacts due to transgenic over expression and miss expression. Previous studies analyzing TPI deficiency have primarily utilized human patient erythrocytes, yeast and mammalian cellular expression systems. Although these experimental paradigms are valuable, they do not provide the elegant endogenous genetic control of GE and preclude the examination of *in vivo* phenotypes such as behavior and longevity.

We initiated this study asking whether the presence of the enzyme or its catalytic activity was most important to the pathogenesis of our mutant. Our experiments assessing enzyme activity identified that the M80T substitution in TPI^{sgk} resulted in a ~15-fold reduction in enzyme efficiency (Table 1). This reduction in catalytic activity was more severe than those reported in two human mutations (63,114), but was not nearly as severe as those modifying critical catalytic components (115-118). An analysis of the TPI enzyme structure taken from *G. gallus* suggested that this mutation might affect isomerase activity through its proximity to several catalytic residues (Figure 4). These results initially supported a catalytic source of disease pathogenesis, but further experimentation revealed the capacity for an isomerase-inactive isoform of TPI to genetically complement all behavioral and longevity phenotypes of TPI^{sgk}. The capacity of a catalytically inactive TPI to rescue a severe variant of TPI deficiency independent of any changes in isomerase activity was striking. Thus far most research on TPI deficiency has focused on two core principles: i) Inhibited TPI activity would slow glycolysis, and ii) Inhibition of TPI would lead to a buildup of excess DHAP and henceforth toxic advanced glycation end-products (AGEs) (48). Here we have shown that the addition of an isomerase-dead isoform of TPI rescues all behavior independent of catalysis, making it unlikely that AGEs are playing a significant role in the genesis of our behavioral or longevity phenotypes. Our findings of genetic

complementation independent of an effect on *TPI^{sgk}* isomerase activity or animal bioenergetics suggest a non-metabolic source of TPI deficiency pathogenesis.

Although glycolytic enzymes are not often thought of as important players in non-metabolic cellular mechanisms, work spanning the past two decades has clearly outlined vital non-metabolic roles for some of these ancient proteins. Glycolytic enzymes have been described in a multitude of different non-catalytic roles, including assistance in assembly and function of the vacuolar-type proton-ATPase by aldolase (119,120), inhibition of apoptosis through the modulation of Bax, Bak and Bad by hexokinase (121,122), transcriptional regulation of the histone H2B gene during cell cycle progression by glyceraldehyde 3-phosphate dehydrogenase (123), and the induction of cell motility and invasion through the secretion and binding of glucose-6-phosphate isomerase to the autocrine motility factor receptor gp78 (124). Based on this diversity of functions, it is clear that there is the potential for glycolytic enzymes to perform functions dramatically independent from their roles in glycolysis. Our findings are particularly relevant as TPI is one of the primary targets of nitrotyrosination in Alzheimer's disease and is sequestered in the neurofibrillary tangles in patient brains (125,126). Sequestration such as this could inhibit a critical non-catalytic function of TPI, further contributing to the neurological dysfunction known to be associated with tau aggregation and toxic amyloid beta.

Recently TPI has been identified as a target of cyclin dependant kinase 2 (cdk2) (127) and arginine methyltransferase 5 (PRMT5) (128). Together, these studies conclude that TPI is more highly regulated than previously appreciated. Furthermore, it was noted that TPI protein levels could be modulated via methylation (128). These results portend the enticing possibility that TPI protein levels are regulated in a cell-cycle dependent manner, and that its relationship to the cell cycle could be perturbed in TPI deficient patients experiencing neurological symptoms.

Indeed, a relationship has already been well-established between cell cycle misregulation and neurodegeneration (reviewed in 129), and inappropriate regulation of the cell cycle has been described in Alzheimer's Disease (130). It is clear that further work is needed to define the biological role of post-translational modifications of TPI, and the role of TPI as either a direct or indirect component of the cell cycle.

In conclusion, our data demonstrate the capacity of a catalytically inactive TPI enzyme to genetically complement TPI deficiency behavioral phenotypes independent of changes in bioenergetics or enzyme catalysis. The identification of an isomerase-independent function for this critical protein opens up new avenues of investigation that will prove critical to understanding TPI's role in maintaining normal neural function and TPI deficiency pathogenesis.

2.5 MATERIALS AND METHODS

2.5.1 Animal Strains

The w^* ; $P[GawB] 477w^-$; $TM2/TM6B$, Tb^1 and $y,w/Y$, $hs-hid$; $hs-FLP$, $hs-I-SceI/CyO$, $hs-hid$; stocks were obtained from Dr. Yang Hong. TPI^{sgk} is a missense mutation resulting in a Met-to-Thr change at position 80, while TPI^{null} is a null allele owing to a 1.6 kb deletion of two of the three constitutively expressed exons of the TPI locus (50). This numbering uses the established nomenclature for TPI mutations, assuming the start methionine is removed following translation (45); and for consistency all residue numbering in this study uses the same convention. The Cre recombinase stock was used to reduce the locus following homologous recombination and phiC31 integration. The strain used, $y^1 w^{67c23} P[y[+mDint2]=Cre]1b$; $D^*/TM3$, Sb^1 , was

obtained from the Bloomington *Drosophila* Stock Center (Bloomington, IN, USA). Care was taken to ensure all animal populations assessed were approximately equivalent mixtures of males and females, with the exception of the TPI^{sgk}/TPI^{null} day 20 behavioral tests – in this genotype males died noticeably faster than females and as a result this small population of survivors consisted mostly of female animals.

2.5.2 Genomic Engineering

We performed the *TPI* GE similar to previously published methods (99,100). Briefly, ~ 2.6 kb homology arms were generated by PCR amplification to areas 5' and 3' of the *TPI* locus. These homology arms were inserted into the *pGX-attB* vector (99) and transferred onto the second chromosome of w^{1118} animals using traditional P-element transgenesis. Ends-out homologous recombination was performed and founder lines were molecularly verified. The wild type *TPI* locus was cloned into the *pGE-attB* vector via PCR and verified by sequencing. Founder lines were mated to *vasa-phiC31^{ZH-2A}* animals expressing the integrase on the X chromosome and their progeny injected with *pGE-attBTPI⁺*, *pGE-attBTPI⁺-CFP*, *pGE-attBTPI^{M80T}*, *pGE-attBTPI^{Δcat}*, or *pGE-attBTPI^{Δcat}-CFP* constructs. Integration events between *attP* and *attB* elements produce an *attL* and *attR* and reconstitute the target locus. Such events were identified based on the presence of the w^+ phenotype and verified molecularly.

2.5.3 Mutagenesis

Site directed mutagenesis was performed using the QuikChange Lightning Site-Directed Mutagenesis Kit (Agilent Technologies, Santa Clara, CA, USA). Mutagenesis primers were

generated (Integrated DNA Technologies, Coralville, IA, USA) to introduce a Lys-to-Met codon change affecting position 11 and a Met-to-Thr codon change affecting position 80 of the protein. Mutagenesis was performed on the *pGE-attBTPI*⁺ plasmid and confirmed by sequencing.

2.5.4 *Drosophila* TPI purification

The coding sequence for *Drosophila* TPI was cloned into the bacterial expression vector pLC3 using standard techniques. The resulting plasmid directs expression of TPI containing N-terminal His₆- and MBP-tags, both of which can be removed with TEV protease. TPI protein was expressed in BL21(DE3) Codon-Plus (RILP) *E. coli* (Agilent Technologies) grown in ZY auto-induction media (131) at room temperature for 24-30 hours. Cells were harvested by centrifugation, lysed via homogenization in 25 mM Tris pH 8.0, 500 mM NaCl, 10% glycerol, 5 mM Imidazole, 1 mM β-mercaptoethanol and cleared by centrifugation at 30,000 x *g*. TPI was purified by nickel affinity chromatography followed by overnight TEV protease treatment to cleave the His₆-MBP tag from TPI. A second round of nickel affinity purification was performed to separate the His₆-MBP and TEV protease. TPI protein was further purified using cation-exchange chromatography (HiTrap-QP) followed by gel filtration (Sephacryl S-200, GE Healthcare, Little Chalfont, England, UK). Peak fractions were concentrated to 4-8 mg/ml in 20 mM Tris pH 8.8, 25 mM NaCl, 2.0% glycerol and 1 mM β-mercaptoethanol using a Vivaspin concentrator (GE Healthcare). The purity was >99% as verified by SDS-PAGE. Expression and purification of the *Drosophila* TPI M80T *sgk* mutant was performed as described above.

2.5.5 Enzyme Assays

Isomerase activity was determined using an NADH-linked assay as previously detailed (132). TPI activity was measured with three different enzyme concentrations of both purified *Drosophila* WT and M80T enzyme. Initial velocity of the enzyme was calculated over a GAP (Sigma-Aldrich, St. Louis, MO, USA) range of 0.94-5.64 mM. All kinetic measurements were performed three times in triplicate by monitoring the absorbance of NADH at 340 nm in a SpectraMax Plus 384 microplate reader (Molecular Devices, Sunnyvale, CA, USA). The assay was performed using 80 μ l mixtures containing varied GAP and enzyme concentrations, 0.42 mM NADH (Sigma-Aldrich), and 1 unit glycerol-3-phosphate dehydrogenase (Sigma-Aldrich) in 100 mM triethanolamine (TEA), pH 7.6. Enzyme activity curves were normalized to reactions performed without GAP. Enzyme kinetics were determined by assessing initial velocities taken during the linear phase of each reaction, and the data were fit to the Michaelis-Menten equation using nonlinear regression in Graphpad Prism 5.0b (GraphPad Software, La Jolla, CA, USA).

For lysate assays, animals were collected and aged to day 3 at 25°C and frozen in liquid nitrogen. Bodies lacking the head and appendages (abdomen and thorax) were isolated after vigorous mechanical shaking of the frozen animals. Tissues lacking eye pigments were used to reduce background absorbance. The bodies were homogenized in 0.75 ml of 1X PBS (2.7 mM KCl, 137 mM NaCl, 2 mM NaH₂PO₄, 10 mM Na₂HPO₄ pH 7.4) with protease inhibitors Leupeptin 1:1000 (Acros Organics, Geel, Belgium), Pepstatin 1:1000 (Sigma-Aldrich), PMSF 1:100 (Pierce, Rockford, IL, USA). The homogenates were ice bath-sonicated for 10 min. then centrifuged at 4°C for 5 min. at 5,000 x g to remove exoskeletal debris. Lysates were diluted to 1 μ g/ μ l in 100 mM TEA, pH 7.6 + inhibitors and TPI enzyme activity was assessed using a

linked-enzyme assay, similar to that outlined above. The assay was performed using 80 μ l mixtures containing 0.47 mM GAP, 0.42 mM NADH, 1 unit glycerol-3-phosphate dehydrogenase and 30 μ g of lysate protein in 100 mM TEA, pH 7.6. Enzyme activity curves were performed three times in triplicate and normalized to reactions performed without GAP. A One-way ANOVA was performed to assess variance and data sets were compared using Tukey's post-hoc analysis.

2.5.6 Behavioral Testing and Lifespan Analysis

Mechanical stress sensitivity was determined by vortexing the animals in a standard media vial for 20 seconds and measuring time to recovery, similar to (133). Thermal stress sensitivity was assessed by acutely shifting animals to 38°C and measuring time to paralysis, as previously described (65,109). All behavioral responses were capped at 600 seconds. Testing days were selected based on previous experience with TPI deficiency progression in *Drosophila* (50). Animal lifespans were performed at 25°C as previously described (109). Two-way ANOVAs were performed with Bonferroni's post test to compare genotype behavior over time, and lifespans were compared with Log-rank (Mantel-Cox) survival tests.

2.5.7 HPLC Phosphoarginine Assay

Three sets of 25 animals per genotype were collected and aged to day 3 at 25°C and frozen in liquid nitrogen. The animals were homogenized in 200 μ l 0.6 M perchloric acid and neutralized with 25 μ l of 2 M potassium carbonate. The lysates were then centrifuged at 12,000 x *g* for 10 min. at 4°C and the supernatant filtered through a PVDF 0.45 μ m spin column (National

Scientific, Rockwood, TN, USA) at 12,000 x *g* for 5 min. at 4°C as previously described (76). These extracts were injected onto a Phenomenex Luna 5µm NH₂ 250 x 4.6 mm column (Torrance, CA, USA) using a Shimadzu high performance liquid chromatography (HPLC) system (Kyoto, Japan) and separated with a 95:5 20 mM KH₂PO₄ pH 2.6: acetonitrile linear mobile phase at a flow rate of 0.6 ml/min. Arginine (Acros Organics) and phospho-arginine (P-arg) standards were detected at 205 nm, and all samples were measured in triplicate (76). Phosphoarginine standards were generated as previously described (134). Peak analysis was performed using EZStart 7.3 software (Shimadzu), and P-arg levels were normalized to total arginine and compared across genotypes. Retention times for arginine and phospho-arginine were 3.7min and 5.4min respectively. A One-way ANOVA was performed to assess variance and data sets were compared using Tukey's post-hoc analysis.

2.5.8 Immunoblots

Animals were collected and aged at 29°C. After 24hrs., ten fly heads were collected in triplicate from each genotype and processed as outlined previously (86). Briefly, the fly heads were ground by pestle in 80µl 2× SDS-PAGE sample buffer (4% SDS, 4% β-mercaptoethanol, 130mM Tris-HCl pH 6.8, 20% glycerol) and spun for 5min. at 5,000 x *g* to pellet the exoskeleton. Proteins were resolved by SDS-PAGE and transferred onto PVDF membrane. Following treatment in 1% milk PBST, the blots were incubated with anti-TPI (1:5000; rabbit polyclonal FL-249; Santa Cruz Biotechnology, Santa Cruz, CA, USA) or anti-ATPalpha (1:10,000; mouse monoclonal alpha5; Developmental Studies Hybridoma Bank, Iowa City, IA, USA). The blots were washed in PBST, incubated in the appropriate HRP-conjugated secondary antibody, and developed using ECL (Pierce). Densitometric analyses of the scanned films were

performed digitally using ImageJ software available from the National Institutes of Health. A One-way ANOVA was performed to assess variance of TPI levels and data sets were compared using Tukey's post-hoc analysis.

3.0 CHANGES IN TRIOSEPHOSPHATE ISOMERASE DIMER INTERFACE MORPHOLOGY ELICIT BEHAVIORAL DYSFUNCTION BY INHIBITING SYNAPTIC VESICLE RECYCLING

3.1 ABSTRACT

Triosephosphate isomerase (TPI) is a homodimeric non-linear glycolytic enzyme, which enhances glycolytic efficiency yet is not required for the production of pyruvate. Dysfunction within TPI elicits a disease called TPI deficiency, and this pathology currently lacks any treatments. TPI Deficiency is unique among other glycolytic enzymopathies for its severe patient neurological dysfunction and early death. Previous studies have detailed structural and catalytic changes elicited by disease-associated TPI substitutions, but the pathophysiology of this disease has never been examined. In this study, *in vitro* experiments demonstrate that a previously identified toxic *Drosophila* *TPI*^{M80T} allele is characterized by a defect in enzyme dimerization. Using the *Drosophila* genomic engineering system we generated several novel *TPI* alleles which further support the conclusion that changes at the dimer interface are sufficient to elicit TPI deficiency. Genetic complementation and behavioral rescue conclusively establish that TPI activity is not predictive of disease presence or severity. However, examination of a severe TPI allele demonstrated that the neurological phenotypes associated with TPI Deficiency are caused by impaired vesicle recycling at the synapse. It is not currently understood why TPI

Deficiency is unique among other glycolytic enzymopathies in these patient symptoms, though our findings suggest a critical subcellular locale deficient in glycolytic ATP. Clinically, these findings are the first to inform targeted therapeutic strategies for patients suffering from TPI Deficiency.

3.2 INTRODUCTION

Triosephosphate isomerase (TPI) is a glycolytic enzyme that converts dihydroxyacetone phosphate (DHAP) into glyceraldehyde-3 phosphate (GAP). TPI is a non-linear member of the glycolytic pathway, enhancing the efficiency of the catabolic process, and mutations within coding region of *TPI* lead to a disease known as TPI deficiency (26). TPI deficiency is one of the few glycolytic diseases associated with neurological dysfunction, and by far the most severe (48). Previously, a M80T substitution in *Drosophila TPI* (*TPI*^{M80T}) was identified which elicited mechanical- and thermal-stress dependent paralysis (50,64). Both of these behavioral phenotypes have been independently established as hallmarks of neurological dysfunction, and each has been used in forward genetic screens to identify novel components of neuronal transmission (66,68,69). To this end, the *TPI*^{M80T} allele was identified in such a screen (65), and the protein was found to be prematurely degraded with reduced catalytic activity (1,85). This reduction in catalytic activity was shown to inhibit glycolytic flux as well as induce metabolic stress (1,50). Subsequent studies demonstrated that the M80T point mutation could be complemented by the addition of a catalytically inactive *TPI* without increasing lysate isomerase activity or alleviating metabolic stress (1). These results were in agreement with observations made from patient tissue samples, wherein no changes in ATP were identified (57) and

concluded that the behavioral dysfunction associated with *Drosophila* TPI deficiency was not a function of metabolic stress, but instead a result of either a depletion of cellular TPI or a change in its protein conformation.

The results of the present study extend this work and suggest that conformational changes of the TPI dimer interface are sufficient to cause *Drosophila* TPI deficiency. Indeed, an alteration of the dimer interface was previously identified in the most prevalent human disease-associated TPI mutation (63). We purified and assessed the physical characteristics of TPI^{M80T}, identifying a change in protein dimerization. These results were further supported when independent mutations at the TPI dimer interface phenocopied the behavioral dysfunction seen in the TPI^{M80T} allele. A previous study established that TPI^{M80T} could be complemented with a catalytically inactive TPI allele, and complementation analyses with the new dimer mutant alleles support the conclusion that an improperly formed dimer interface is a far greater determinant of behavioral dysfunction than enzyme catalysis. Further, our experiments establish that *Drosophila* TPI deficiency results in an impairment of synaptic vesicle recycling, which we believe are the source of neurological dysfunction in both our *Drosophila* model and the human condition. A recent study quantifying the ATP production and consumption at the synapse established that activity-driven glycolysis was the most critical source of ATP in the synapse (135). Additional analyses of activity-dependant ATP consumption demonstrated that vesicle recycling was the largest consumer of ATP in the synapse (135). These observations suggest that our TPI dimer mutations may elicit a local depletion of ATP due to impaired synaptic glycolytic flux. Collectively, these data conclude that *Drosophila* TPI deficiency is not elicited through a general metabolic defect, and suggests that the neurological dysfunction is elicited by changes in the dimer interface likely coordinating localization of synaptic isomerase activity.

3.3 RESULTS

3.3.1 RNAi knockdown of WT TPI

Our previous results suggested that TPI deficiency neurological and longevity phenotypes were not a result of metabolic stress. We found that the severe longevity and behavioral phenotypes elicited through the M80T mutation could be complemented through the addition of a stable, catalytically inactive isoform of TPI. These results suggested one of two possibilities through which M80T elicited its disease phenotypes: i) that the depletion of cellular TPI was sufficient to elicit disease phenotypes, or that ii) M80T generated a conformational change in TPI which could be rescued through the addition of a properly folded yet catalytically inactive isoform. To assess the first possibility, we employed the GAL4-UAS expression system to knock down wild type (WT) TPI using a UAS-RNAi line directed toward *dTPI* (*Drosophila* TPI) messenger RNA (mRNA) (136). These lines were driven by an actin-GAL4, UAS-GAL4 superexpressor to obtain a dramatic reduction of TPI in all tissues.

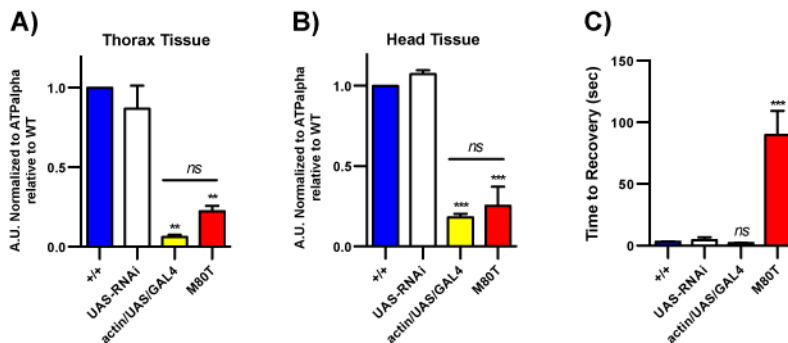


Figure 11. RNAi knockdown of TPI^+ fails to recapitulate TPI^{M80T} phenotypes. TPI transcript levels were knocked down ubiquitously and confirmed in thorax (A) and head (B) tissues ($n \geq 3$). Knockdown

animals failed to display typical mechanical-stress dependent paralysis (C) at Day 5 aged at 25°C (n≥15). ns indicates no significance, ** p<0.01, and *** p<0.001 relative to +/-.

Using UAS-RNAi in conjunction with the superexpressor GAL4, we found that *w;actin-GAL4,UAS-GAL4/+;UAS-RNAi^{TPI}/+* animals exhibited a dramatic reduction in TPI protein levels similar to that seen in head and thorax tissue from *w;;TPI^{M80T}* homozygotes [Figure 11A,B]. Head and body tissues were assessed separately to ensure equivalent knockdown in both tissues. Next, we examined animal behavior in these knockdown populations to determine whether depletion of cellular TPI was sufficient to elicit TPI deficiency pathology. Mechanical stress responses were used to measure behavioral dysfunction. Behavioral characterization of these knockdown animals demonstrated no abnormal mechanical- or thermal-stress dependent responses akin to those seen in the *TPI^{M80T}* model [Figure 11C]. The only behavioral abnormality noted was an observation of hypoactivity at elevated temperatures, with the knockdown animals consistently dwelling near the bottom of the vial relative to their *TPI⁺* and undriven UAS controls [data not shown].

3.3.2 *In vitro* physical characterization of M80T

These knockdown data suggested a significant depletion of cellular TPI is not sufficient to elicit TPI deficiency neurological dysfunction. This left us to explore the possibility that M80T elicited a conformational change in TPI leading to a loss-of-function unrelated to general metabolism. Numerous misfolding events could be hypothesized to occur as a function of the M80T substitution, among them alterations of dimerization (62,63) and aggregation (126). To examine the structure of M80T *in vitro* we attempted to purify *Drosophila* TPI^{M80T} (dM80T).

Previous purification experiments had yielded small amounts of pure *Drosophila* TPI enzyme, but these samples proved unstable, necessitating rapid usage of fresh aliquots of purified enzyme for the characterization of kinetic properties (1). Indeed, even *Drosophila* TPI⁺ (dWT) was aggregation prone at high concentrations, making it difficult to conduct physical characterization of the protein *in vitro*. Conversely, purified human TPI (hTPI) was well-behaved. Therefore, in order to physically characterize TPI we were forced to work with human protein *in vitro*. To validate this approach we generated human WT (*hTPI*⁺) and human M80T (*hTPI*^{M80T}) TPI alleles in the *Drosophila* gene locus using our genomic engineering (GE) system (1). We found that *hTPI*^{M80T} was able to recapitulate the disease phenotypes observed in *Drosophila* protein (dTPI) [Figure 12]. It was noted that the phenotypes of *hTPI*^{M80T} were less severe than *dTPI*^{M80T}, possibly due to subtle organism-specific changes in the dimer interface (137). However, to prevent xenogenic complications of our behavioral results, we decided to work exclusively with the *Drosophila* protein *in vivo* for the remainder of our genetic experiments. Confirmation that *hTPI*^{M80T} pathologically phenocopied *dTPI*^{M80T} indicated that any conformational change elicited by M80T was likely retained in the human protein, making us confident that evaluating hTPI *in vitro* would yield informative results.

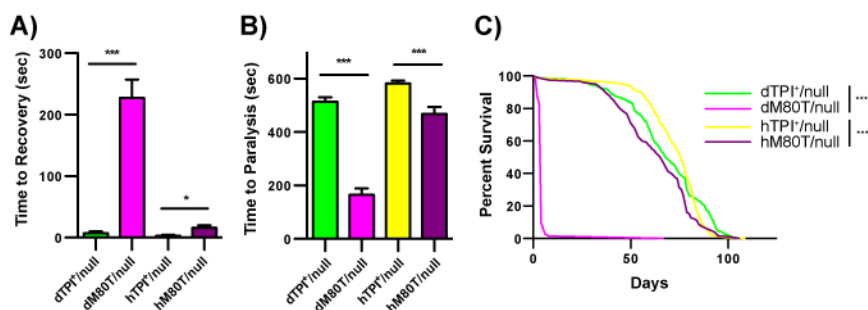


Figure 12. *hTPI*^{M80T} phenocopies the behavioral and longevity effects of *dTPI*^{M80T}. *hTPI*^{M80T} elicits a significant delay in time to recovery from mechanical stress (A) at Day 3, time to paralysis after thermal

stress (B) at Day 4, and longevity (C) compared to *hTPI*⁺, all reared at 25°C. n≥20 for behavior and n≥70 for lifespans. * indicates p<0.05 and *** p<0.001.

To generally assess potential conformational differences elicited by the M80T substitution, we utilized dynamic light scattering (DLS) to examine hWT and hM80T. We hypothesized that any significant conformational changes would likely be reflected by the protein's hydrodynamic radius. Analyses of 15μM solutions of hWT revealed a hydrodynamic radius of 4.3±0.08nm, while hM80T exhibited a significant reduction to 3.3±0.06nm [Figure 13A]. The linear slope generated by plotting the intensity correlation data suggested the hWT sample was largely monodispersed, much like that of the 15μM sample of bovine serum albumin [Figure 13B]. This result was contrasted by the non-linear slope generated upon analysis of hM80T [Figure 13B], suggesting the possibility of a polydisperse protein population. Polydisperse protein populations would qualify the mean hydrodynamic radius, and indicate that it may represent a mixed population of proteins in solution. Polydisperse populations often represent sample aggregation, but sample aggregation would be correlated by an increase in the predicted mean hydrodynamic radius. The observed reduction in TPI mean hydrodynamic radius could most simply be interpreted as a disruption of the dimer interface resulting in a mixed population of monomer and dimer TPI species.

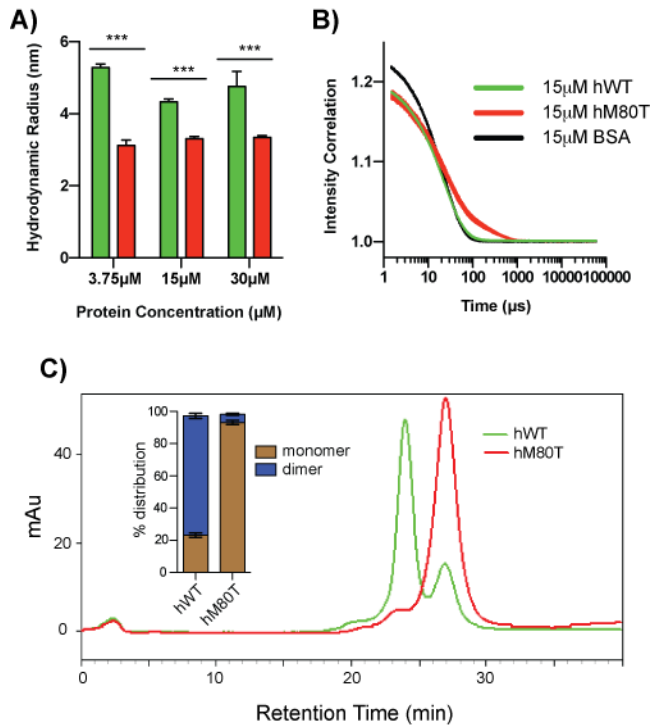


Figure 13. M80T elicits a conformational change in TPI resulting in reduced dimerization. The M80T mutations confers a reduction in mean protein hydrodynamic radius as measured by dynamic light scattering (A). Intensity correlation plots reveal a largely monodisperse WT population and polydisperse M80T population (B). Gel filtration indicates a change in monomer:dimer ratios elicited by M80T (C) with relative quantification (inset). * indicates $p < 0.001$**

We examined the possibility of a dimerization defect by assessing protein size using gel filtration chromatography. We predicted that if the protein was failing to dimerize appropriately we would be able to resolve these species independently and quantify their distribution. A standard curve was used to establish column resolution and 15 μM samples of hWT and hM80T were injected onto the gel filtration column and their migration monitored by UV light at 280nm. As shown in Figure 13C, hWT separated into two distinct peaks – one at 24 min. and another at 27 min. The elution times indicate that the 24 min. elution correlated with species around 50kDa, while 27 min. was predicted to be approximately 28kDa; these sizes corroborate with the

predicted molecular weight of both monomeric (27kDa) and dimeric (54kDa) hTPI. Integrating the peak areas revealed an 80:20 split in dimer:monomer ratio of hWT [Figure 13C inset]. Conversely, it is clear to see that the majority of the hM80T sample eluted at 27 min., resulting in a 5:95 dimer:monomer split [Figure 13C inset]. These data conclude that the M80T mutation elicits a dramatic conformational change in TPI, resulting in a disruption of dimerization. Interestingly, the gel filtration results contradict the monodisperse vs. polydisperse observations of the DLS experiments; we believe this could be due to dilution effects as the proteins migrated over the large gel filtration column.

3.3.3 TPI dimer interface mutants

Having established that the M80T mutation alters enzyme dimerization *in vitro*, we sought to assess whether other independent mutations at the dimer interface of TPI were sufficient to elicit neuropathology. Two novel *TPI* alleles were generated using GE based on previous studies of TPI (19): *TPI*^{T74R}, *TPI*^{G75E}. Upon generating and balancing the new alleles, it was clear that the dimer interface mutants were far more toxic than *TPI*^{M80T}. Test crosses of balanced stocks yielded significantly fewer homozygous animals than the 33% predicted by Mendelian rates, and unlike *TPI*^{M80T}, these new stocks required maintenance over balancer chromosomes due to their poor viability. These homozygous animals were extremely short-lived [Figure 14C], with median lifespans of 2 and 5 days for *TPI*^{T74R} and *TPI*^{G75E} respectively.

To obtain a fair sample size, the poor health of these stocks necessitated the examination of behavior on Day 1 and Day 2 while reared at room temperature. Mechanical- and thermal stress-dependent behavioral defects were assessed. *TPI*^{M80T} was previously described to exhibit a modest phenotype at these time points (50), and these data corroborate our analysis of the GE

TPI^{M80T} allele [Figure 14A,B]. In contrast, the dimer interface mutants displayed a more severe degree of behavioral dysfunction than that seen in *TPI*^{M80T} [Figure 14A,B]. These data supported our hypothesis that mutations at the dimer interface were sufficient to induce neurological dysfunction.

Lysate isomerase activity was then compared between samples taken from animals homozygous for the dimer interface mutants. First, it was noted that all dimer interface mutants exhibited reductions in TPI activity [Figure 14F]. However, a comparison of the *TPI*^{M80T}, *TPI*^{T74R}, and *TPI*^{G75E} lysates revealed a striking observation – the least phenotypically severe mutation (*TPI*^{M80T}) was characterized by the lowest isomerase activity. In comparison, the most toxic allele, *TPI*^{T74R}, retained robust activity [Figure 14F]. These data strongly support previous observations that TPI activity does not predict the severity or presence of TPI deficiency (1), and underlined the conclusion that TPI deficiency is not due to general metabolic stress, but likely a change in protein conformation.

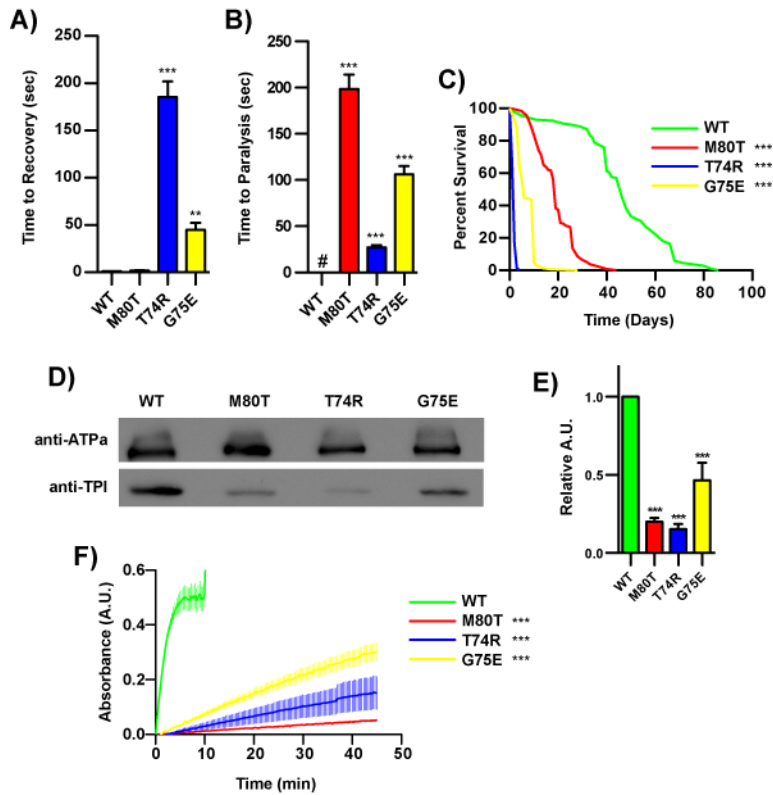


Figure 14. Mutations affecting the TPI dimer interface recapitulate M80T phenotypes. *TPI*^{T74R} and *TPI*^{G75E} exhibit severe mechanical stress (A) and thermal stress (B) sensitivity, n>30. Dimer interface mutations display severely reduced lifespans (C), n>150. Both *TPI*^{T74R} and *TPI*^{G75E} display reduced protein levels (D,E) and reduced lysate isomerase activity (F). ** indicated p<0.01, *** p<0.001. # indicates animals did not paralyze in 360sec.

Many conformational diseases are elicited through changes in protein structure and stability leading to misfolding, then either sequestration and degradation, or aggregation (138). First, we examined whether these new dimer interface alleles produced robust levels of TPI protein. We determined TPI levels in our dimer interface mutants as previously (86), and found that both *TPI*^{T74R} and *TPI*^{G75E} exhibited reduced protein levels in homozygotes [Figure 14D,E].

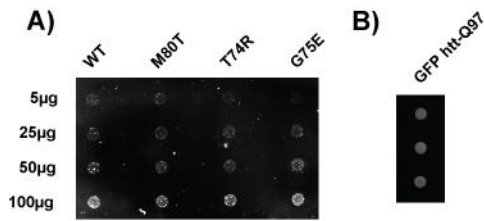


Figure 15. TPI dimer interface mutations do not cause aggregation. Increasing amounts of lysate were loaded and show no differences in trapped TPI across all genotypes (A) whereas huntingtin exon1-GFP displayed robust retention on the filter (B). n=2

It has previously been shown that TPI has the capacity to aggregate, and thereby seed the aggregation of other proteins such as tau (126). When measuring protein levels via SDS-PAGE, it is important to note that not all aggregate species are SDS soluble, and a reduction in protein levels can often be an indication that the aggregates are not passing through the gel matrix. To determine whether the T74R and G75E mutations resulted in protein aggregation we used a dot-blot filter trap assay to assess retention differences between TPI mutant isoforms, as outlined previously (139). Lysates were collected from homozygous mutants, and from PC12 cells expressing GFP-huntingtin-Q97 (GFP htt-Q97) as a positive control. The results indicate that little TPI was trapped on the 200nm filter, yet each sample showed a concentration-dependent increase in signal [Figure 15A]. Importantly, no differences were observed in TPI signal between any of the dimer interface alleles [Figure 15A]. These data support similar findings suggested by sedimentation assays performed on *TPI*^{M80T} (86). These experiments lead us to conclude that although these dimer interface mutants display reduced protein levels via SDS-PAGE, this is not due to the insolubility of large aggregates.

3.3.4 Complementation with a catalytically inactive TPI allele

Our previous work suggested that TPI deficiency is a loss-of-function disease caused by either i) the depletion of cellular TPI, or ii) a conformational change which could be rescued through the addition of a properly folded yet catalytically open/inactive isoform (1). Having utilized knockdown strategies to examine the necessity of total TPI levels, we sought to confirm the capacity of TPI^{Acat} (Lys-to-Met, position 12) to complement disease-associated TPI alleles. To evaluate whether TPI^{Acat} is sufficient to support normal behavior and longevity, TPI^+/TPI^+ , TPI^+/TPI^{T74R} , TPI^{T74R}/TPI^{T74R} , TPI^{T74R}/TPI^{Acat} , TPI^+/TPI^{G75E} , TPI^{G75E}/TPI^{G75E} , and TPI^{G75E}/TPI^{Acat} animals were collected and tested as outlined above. These experiments demonstrated that TPI^{T74R} was robustly complemented by TPI^{Acat} [Figure 16A,B,C], similar to the results found with TPI^{M80T} (1). It should be noted however that this complementation was not fully penetrant in that 5 out of the 30 TPI^{T74R}/TPI^{Acat} animals did cease moving near the end of the thermal stress assay period [Figure 16B]. Conversely, TPI^{G75E} displayed modest behavioral complementation and attenuation of its toxicity, decreasing the penetrance of the thermal stress sensitivity to 20 out of 30 animals and extending the median lifespan of the TPI^{G75E} mutants from 5 to 21 days [Figure 16D,E,F]. It should be noted that neither of these dimer interface mutants elicited dominant negative effects within the TPI^+ heterozygotes; to the contrary, TPI^{T74R} and TPI^{G75E} promoted a significant increase in animal health, extending the median 48 day TPI^+/TPI^+ lifespans to 77 and 71 days respectively [Figure 16C,F]. Experiments assessing TPI activity in these animal lysates revealed no link between isomerase activity and disease presence or severity. Although TPI^{T74R} , TPI^{G75E} , and TPI^{M80T} exhibit reduced isomerase activity, complementation with TPI^{Acat} occurred without increasing lysate TPI activity, and in all but one case significantly reduced it [Figure 17A,B]. The best illustration of this isomerase-

phenotype disparity can be seen when comparing the activity of TPI^{G75E} with $TPI^{M80T}/TPI^{\Delta cat}$. The $TPI^{M80T}/TPI^{\Delta cat}$ animals exhibit normal behavior and longevity (1) yet display substantially less isomerase activity than the severely toxic allele, TPI^{G75E} [Figure 17B].

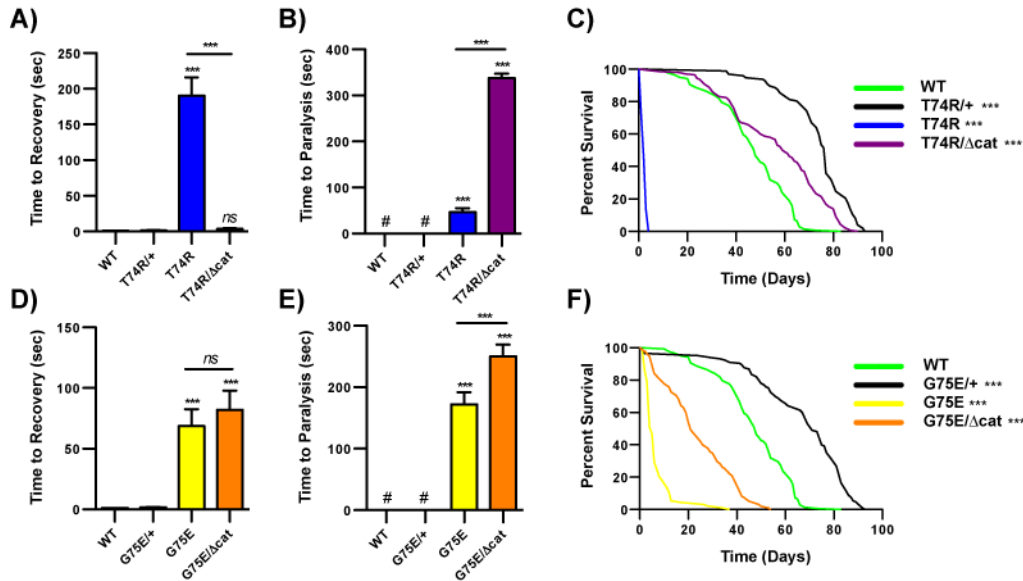


Figure 16. A catalytically inactive allele is not sufficient for normal behavior and longevity. $TPI^{\Delta cat}$ complements TPI^{T74R} mechanical (A) and thermal stress (B) sensitivity and longevity (C), yet moderately attenuates behavior (D,E) and longevity (F) defects of TPI^{G75E} . It should be noted that mean thermal stress paralysis times near 360sec represent near-wild type behavior. $n \geq 30$ for behavior, and $n \geq 90$ for lifespans. ns indicates no significant, and * $p < 0.001$. # indicates the animals did not paralyze (a score of 360 sec.).**

The incomplete complementation of TPI^{G75E} was unexpected; our previous experiments suggested that $TPI^{\Delta cat}$ was sufficient to support normal behavior and longevity. This observation alluded that $TPI^{\Delta cat}$ alone was not sufficient for normal behavior and longevity, and could depend on productive interactions with the active isoform. To examine this possibility, we measured the capacity of these TPI isoforms to co-precipitate using a cyan fluorescent protein (CFP) tagged variant of $TPI^{\Delta cat-CFP}$. The CFP tag was immunoprecipitated in $TPI^+/TPI^{\Delta cat-CFP}$, $TPI^{M80T}/TPI^{\Delta cat-CFP}$, $TPI^{T74R}/TPI^{\Delta cat-CFP}$, and $TPI^{G75E}/TPI^{\Delta cat-CFP}$ animal lysates and probed. Protein size was used

to discriminate between the two isoforms, as the CFP tag roughly doubled the weight of TPI. Robust levels of TPI⁺ precipitated with TPI^{Δcat-CFP}, establishing substantial heterodimerization between the two species [Figure 18A,B]. Conversely, TPI^{M80T} and TPI^{T74R} displayed markedly reduced associations with TPI^{Δcat-CFP}, reflecting their overall prevalence in the lysate [Figure 18A] and corroborating their previously established dimerization deficiencies. Finally, it was surprising to see that TPI^{G75E} produced heterodimerization similar to that seen in TPI⁺; it was predicted that the rotational flexibility of G75 was necessary for the appropriate positioning of loop 3 and establishment/rigidification of the dimer interface. Further, our genetic data suggested that complementation required a productive interaction between TPI^{Δcat} and its partner, and based on these observations we predicted that TPI^{G75E} would lack such interactions, not maintain them. This observation led us to generate a double mutant which contained both T74R and G75E, predicting that the T74R mutation would reduce enzyme heterodimerization as previously published (19).

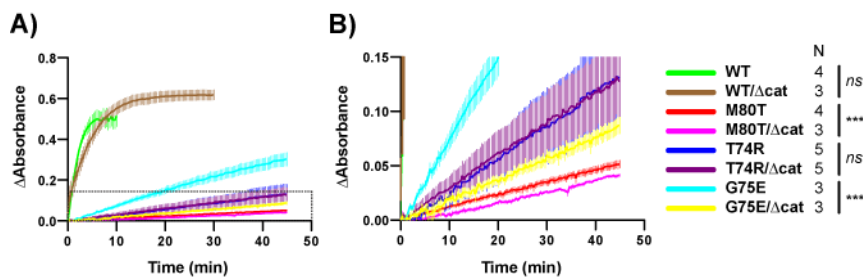


Figure 17. Lysate isomerase activity does not predict disease presence of severity. Lysate activity is indicated (A) and expanded (B) as per the dashed box. ns indicates no significant differences and * p<0.001. Biological replicates are indicated.**

We generated a double mutant, $TPI^{T74R,G75E}$, and discovered that combining the two mutations resulted in an allele that closely resembled TPI^{T74R} with respect to animal toxicity, behavior, protein levels, and isomerase activity [Figure 19A,B,C]. Additionally, precipitation

experiments confirmed the addition of the T74R mutation to TPI^{G75E} also reduced its capacity to interact with $TPI^{\Delta cat-CFP}$ [Figure 18A,B]. We repeated our complementation studies, generating TPI^+/TPI^+ , $TPI^+/TPI^{T74R,G75E}$, $TPI^{T74R,G75E}/TPI^{T74R,G75E}$ and $TPI^{T74R,G75E}/TPI^{\Delta cat}$ animals. Characterization of these animals revealed the addition of the T74R point mutation to TPI^{G75E} enhanced the behavioral attenuation of this dimer interface mutant by $TPI^{\Delta cat}$; the mean time to recovery after mechanical stress was reduced from 204 sec. to 50 sec., with approximately 60% of the animals no longer responding to the stressor (defined as a recovery time ≤ 5 sec.). This stood in contrast to TPI^{G75E} , whose time to recovery after mechanical stress changed from 69 sec. to 82 sec. with approximately 30% of the animals no longer stress sensitive upon $TPI^{\Delta cat}$ complementation; thermal stress-sensitive phenotypes exhibited a similar trend. Observing $TPI^{T74R,G75E}$ lysate isomerase activity did not suggest a role for gross catalysis: $TPI^{\Delta cat}$ complementation resulted in a marked reduction in activity [Figure 19C] with positive behavioral affects. Measuring animal longevity however yielded disparate results, as both $TPI^{T74R,G75E}$ homozygotes and $TPI^{T74R,G75E}/TPI^{\Delta cat}$ survived a median of 2 days. It is important to note that this is the first example in which TPI deficiency behavior and longevity phenotypes have not been in congruence, and suggests the possibility that these effects are derived from different pathogenic sources. We conclude that the allelic context-dependence of $TPI^{\Delta cat}$ complementation suggests a requirement for intermolecular interactions. Further, it is clear that these interaction requirements differ for the purposes of longevity and behavior.

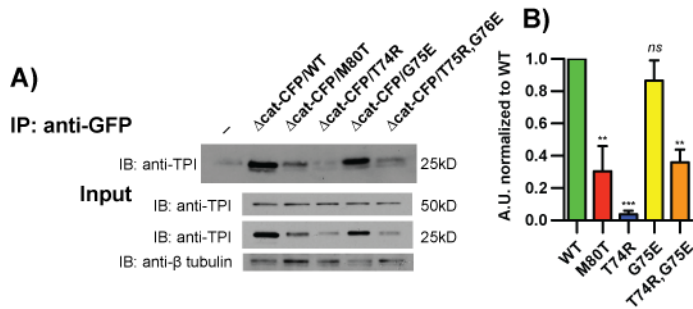


Figure 18. Heterodimerization of inactive TPI and dimer interface mutations. $TPI^{\Delta cat-CFP}$ interacts modestly with TPI^{M80T} , TPI^{T74R} , and $TPI^{T74R,G75E}$, yet robustly with TPI^{G75E} . Representative immunoprecipitation and input blots are shown (A) with IP: anti-GFP quantification (B) $n=3$. ns indicates no significance, ** $p<0.01$, and *** $p<0.001$.

3.3.5 Vesicle recycling at the synapse

Seeing no obvious mechanistic trend from our genetic or biochemistry experiments, we turned to the phenotype to direct our next experiments. In this regard, the TPI^{T74R} temperature-dependent paralysis was particularly striking, with a mean time to paralysis of 27 sec. Acute (<60 sec.) temperature-dependent phenotypes have only been identified in a handful of mutants in all of *Drosophila* biology and result from neural conductance or synaptic defects (72).

To determine whether TPI was playing a role in neural transmission, we first examined vesicle recycling efficiency at the synapse using the lipophilic dye, FM1-43FX. Measuring recycling in this context allowed us to assess two possibilities; i) a primary recycling defect, or ii) a secondary recycling defect due to aberrant excitation or fusion. We dissected larvae homozygous for TPI^+ , TPI^{T74R} , and Shi^{ts1} as previously detailed (140). The neuromuscular junction (NMJ) preparations were heated to 38°C over 3 min. and a loading curve was generated from a series of three different high $[K^+]$ loading times – 15 sec., 30 sec., and 60 sec. as previously detailed (141). TPI^+ displays a progressive increase in dye loading from 15 sec. to 60

sec. [Figure 20A], while the temperature sensitive dynamin mutant control *Shi^{ts1}* showed no signs of vesicle recycling at any heated time points [Figure 20D, data not shown]. Conversely, although *TPI^{T74R}* displayed similar loading to *TPI⁺* at 15 and 30 sec., *TPI^{T74R}* exhibited a striking 50% decrease in loading at 60sec. [Figure 20A,B,D]. This precipitous decrease in loading is temperature dependent [Figure 20C] and corroborated roughly with the mean time to paralysis in these animals (27sec). To examine the relationship between vesicle recycling and animal behavior, *TPI^{T74R/Δcat}* larvae were assessed, and loading experiments demonstrated a significant increase in vesicle recycling [Figure 20B,D] corroborating the behavioral complementation [Figure 16B]. The utilization of chemical stimulation in these preparations demonstrates a synaptic defect arising from the severe *TPI^{T74R}* dimer mutation, as this methodology bypasses conductance requirements. Further, these mutations were revealed to have a purely functional impact on the synapse, as morphological characterizations of bouton number and branches revealed no significant differences relative to *TPI⁺* [Figure 21]. Collectively, these data demonstrate that TPI Deficiency thermal-stress sensitivity is elicited through inhibition of synaptic vesicle recycling.

The identification of a synaptic phenotype generated increasing interest in the possibility that these dimer interface mutations may be altering the stability of the enzymes, thereby inhibiting transport and maintenance at distal sites. To independently assess this possibility, we engineered a series of permutations of the R188 residue. This R188 residue forms a well-described and entirely conserved salt bridge with D224, helping to stabilize the overall TIM barrel structure (142). We predicted that if stability and putative localization of activity were the key elements to pathogenesis, with dimerization being a contributing determinant, we should be able to observe phenotypes in these animals as well. We engineered *TPI^{R188A}*, *TPI^{R188L}*, and

TPI^{R188S} mutants to examine different biochemical exploitations of this salt bridge, as previously assessed (142). Additionally, we included a TPI^{R188K} control to maintain the charged interactions in this region, again as previously established (142). Upon generating these animals, it was noted that TPI^{R188A} , TPI^{R188L} , and TPI^{R188S} proved homozygous lethal. Conversely, TPI^{R188K} was homozygous viable, easily maintained as a homozygous stock, and exhibited no mechanical or thermal stress sensitivities as a homozygote or trans-heterozygote over TPI^{null} [data not shown].

Establishing these initial viability phenotypes, we sought to confirm their levels *in vivo*, and to do so required mating these alleles with those encoding CFP-tagged TPI⁺ for animal viability and to discriminate between species (TPI^{WT-CFP}) (1). Immunoblot results corroborated our viability data, with all the lethal TPI^{R188} alleles exhibiting dramatic reductions in protein levels [Figure 22B,D]. The low levels of these proteins necessitated an overexposure of the blot to even see evidence of these species [Figure 22D]. Next, we sought to examine the ability of $TPI^{\Delta cat}$ to complement these stability mutants. We found that the inactive allele restored viability in $TPI^{R188A}/TPI^{\Delta cat}$, and $TPI^{R188S}/TPI^{\Delta cat}$, but oddly not $TPI^{R188L}/TPI^{\Delta cat}$. Observing the tagged protein levels of TPI^{WT-CFP}, however, suggested that TPI^{R188L} may have a dominant capacity to induce degradation of its partner [Figure 22C,D].

To examine behavior, we aged the animals at 25°C and tested them on day 3, as this has been shown to be an optimal time to discriminate behavioral effect in *Drosophila* TPI deficiency (1). Importantly, even though $TPI^{\Delta cat}$ was capable of complementing the lethality in these animals, they still displayed signs of behavioral dysfunction [Figure 22A]; and although no formal longevity assays were performed, we noted reduced longevity. These data suggest that even with the addition of a stable, inactive isoform of TPI, these animals likely experienced a

similar deprivation of TPI at critical locales much like the trans-heterozygote TPI^{M80T}/TPI^{null} . These data support a role for TPI stability in the pathogenesis of TPI deficiency.

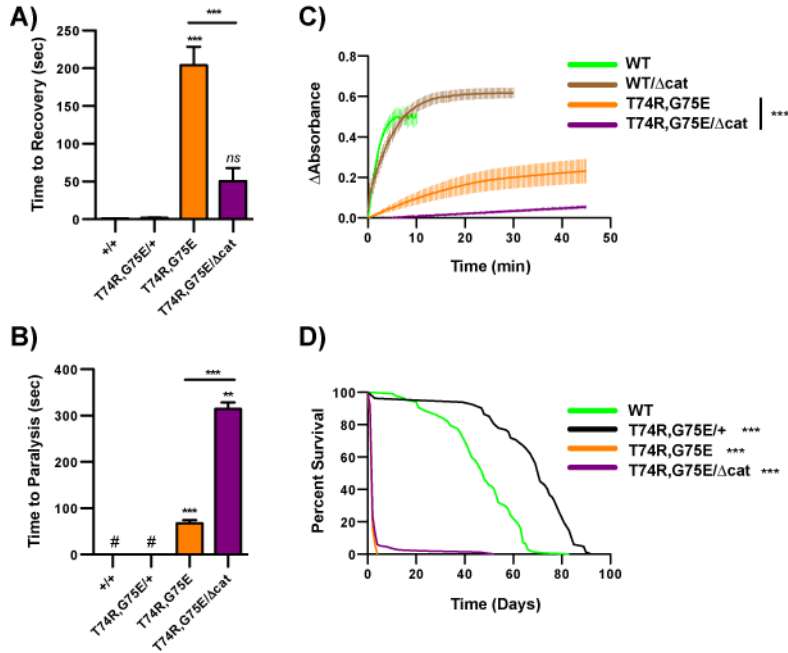


Figure 19. TPIT74R,G75E behavioral dysfunction and longevity. $TPI^{T74R,G75E}$ is characterized by severe mechanical (A) and thermal (B) stress sensitivity, which responds positively to complementation by $TPI^{\Delta cat}$. $TPI^{T74R,G75E}$ exhibits reduced lysate catalytic activity compared to WT (C). $TPI^{\Delta cat}$ fails to complement $TPI^{T74R,G75E}$ longevity (D). $n \geq 30$ for all behavior, $n \geq 80$ for all lifespans. ns indicates no significance, ** $p < 0.01$, *** $p < 0.001$. # indicates animals did not paralyze within 360sec.

3.4 DISCUSSION

TPI deficiency is a disease caused by insufficiencies in subcellular catalytic activity. This disruption of localized activity can be achieved through mutations that directly affect enzyme catalysis, transport, or stability. Previous studies of TPI Deficiency have focused largely on molecular and cellular analyses of the disease-associated substitutions. These structural studies

have revealed the importance of the dimer interface for maintaining protein stability. Conversely, cellular studies in yeast have revealed complex redox changes which occur as a function of inhibiting glycolytic flux. This study builds upon previous structural work, but examines TPI Deficiency neuropathogenesis. Using a *Drosophila* GE strategy, we have conclusively shown that neurological phenotypes seen in TPI Deficiency are attributable to impaired vesicle recycling at the synapse.

3.4.1 Triosephosphate isomerase dimerization

In this report we describe the M80T substitution as impairing TPI dimerization. These results were obtained from purified proteins and do not corroborate those from non-denaturing gel filtration experiments from animal lysates. However, several *in vitro* studies have found that mutations which render TPI a monomer severely destabilize the protein (17,19,143-145). *In vivo*, unstable proteins are bound by chaperones and either refolded, targeted to the proteasome, or aggregate (146). The results presented here suggest that M80T does not cause TPI to aggregate [Figure 15], while previous work (86) extensively details the recruitment of Hsp70 and Hsp90 to TPI^{M80T} and its degradation through the proteasome. Therefore, we hypothesize that TPI monomer was not previously detected in animal lysates due to its rapid sequestration and degradation. Further, the TPI levels from each mutant closely correlate with their propensity to coprecipitate with TPI^{Δcat-CFP} [Figure 18A]. We believe these data, along with the previous inability to identify monomer *in vivo*, collectively suggest that TPI does not stably exist *in vivo* as a soluble monomer.

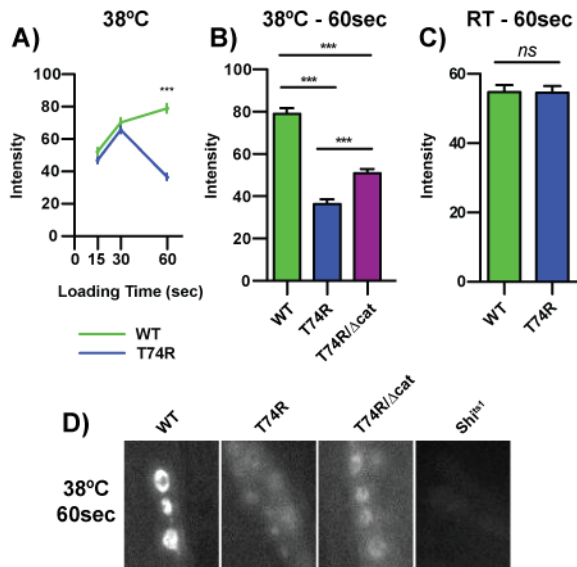


Figure 20. *TPI*^{T74R} inhibits vesicle recycling at 38°C. An FM1-43 timecourse at the NMJ with loading times of 15, 30, and 60sec (A), with quantification of 60sec at 38C (B) and 60sec at room temperature (RT) (C). Representative images of *TPI*⁺, *TPI*^{T74R}, *TPI*^{T74R/Δcat} and *Shi*^{ts1} (D). n=6, ***p<0.001.

Once M80T was identified as having elicited a dimer defect, we used our GE system to generate two *TPI* alleles with point mutations at the dimer interface which had previously been described to impair homodimerization. These mutations were located at the tip of the 3rd loop of TPI which extends into its dimer partner and stabilizes/rigidifies a network of hydrophobic interactions and hydrogen bonds which form the dimer interface (18,19,147). The substitution of these dimer interface residues resulted in extremely toxic *TPI* alleles, eliciting greater behavioral dysfunction and shorter lifespans than M80T [Figure 14]. The new mutant animal phenotypes were in contrast to our measurements of enzyme activity, which revealed that the dimer interface mutants exhibited reduced, yet substantial isomerase activity. These data firmly establish a disjunction between toxicity/neurological dysfunction and gross isomerase activity. However, the allelic differences in *TPI*^{Δcat} complementation suggested a role for the still-catalytically active mutant alleles as a determinant of animal survival and behavior [Figure 16].

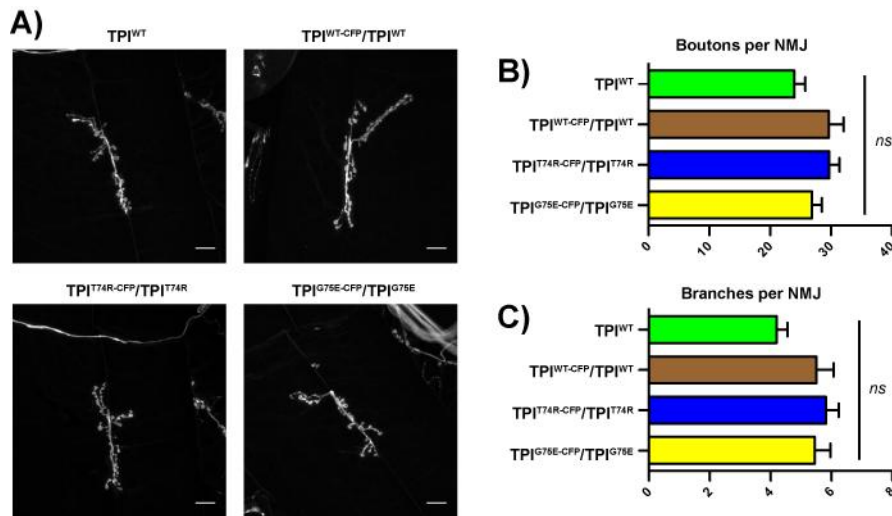


Figure 21. TPI dimer interface substitutions do not alter NMJ development and morphology. NMJ morphology of segment A2 muscle 6/7 was characterized for bouton number (B) and branching (C). Neither parameter showed significant differences elicited by the mutations, relative to either TPI^{WT} or TPI^{WT-CFP}/TPI^{WT} . Representative images shown in (A). $n=10$. Scale bar = $10\mu m$.

Our previous work indicated that a properly folded, stable, inactive isoform of TPI fully complemented the loss-of-function dimer mutant, TPI^{M80T} . We sought to confirm this result by crossing that same catalytically inactive TPI allele with our new, more toxic dimer interface mutants. We hypothesized that the inactive enzyme would be able to complement the TPI^{T74R} and TPI^{G75E} alleles as it did TPI^{M80T} . We found that although $TPI^{\Delta cat}$ complemented TPI^{T74R} , it only moderately attenuated the behavioral dysfunction and longevity defects of TPI^{G75E} [Figure 16]. From these data we concluded that $TPI^{\Delta cat}$ was not sufficient to maintain normal animal health and behavior and may require productive intermolecular interactions. It was curious that measurements of heterodimerization demonstrated that the extremely toxic and complemented TPI^{T74R} interacted very poorly with $TPI^{\Delta cat-CFP}$, while the incompletely complemented TPI^{G75E} maintained a robust capacity to bind $TPI^{\Delta cat-CFP}$, similar to that of TPI^+ [Figure 18]. Though these results reflected the proteins' overall presence in the lysate, these observations were

unexpected; based on the genetic data we had predicted that TPI^{T74R} and TPI^{M80T} would have interacted more amiably while TPI^{G75E} less so.

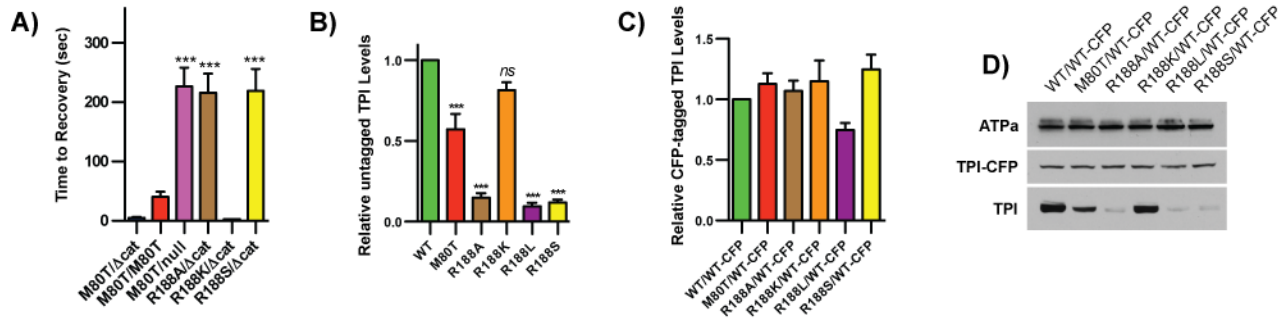


Figure 21. $TPI^{\Delta cat}$ rescues viability in strong TPI stability mutants, though not behavior. TPI salt bridge mutants were crossed to $TPI^{\Delta cat}$ and assessed for complementation. Complementation with the inactive enzyme restores viability in two of three salt bridge mutants, yet all exhibit similar mechanical stress sensitivity as TPI^{M80T}/TPI^{null} (A), $n \geq 18$. Salt bridge mutants were complemented with TPI^{WT-CFP} and exhibit dramatic reductions in lysate protein levels (D) with quantification (B). No significant differences were noted in TPI^{WT-CFP} levels (D), quantified in (C), though blots of TPI^{WT-CFP}/TPI^{R188L} exhibited a trend toward a reduction in the tagged protein, $n=3$. *** indicates $p < 0.001$.

To explore the role of heterodimerization on TPI deficiency complementation we generated a double mutant allele bearing both T74R and G75E mutations. The addition of T74R to the TPI^{G75E} allele indeed reduced its ability to physically interact with $TPI^{\Delta cat-CFP}$ [Figure 18]. Further, this lack of heterodimerization improved the efficacy of behavioral complementation via $TPI^{\Delta cat}$ yet failed to alter toxicity [Figure 19]. It is currently unclear precisely why the $TPI^{T74R,G75E}$ allele exhibits greater behavioral complementation compared to TPI^{G75E} . The results of these experiments suggest that either TPI^{G75E} is capable of interfering with the behavior-relevant functions of $TPI^{\Delta cat}$, or that T74R facilitates these interactions. Yet the dominant negative hypothesis is contradicted by TPI^{G75E} 's inability to negatively modulate behavior or longevity when paired with a wild type allele. This leaves us to hypothesize that T74R facilitates

a productive effect when paired with $TPI^{\Delta cat}$, even though their heterodimerization is extremely limited.

3.4.2 TPI mutations reduce vesicle recycling at the synapse

The severity of the newly generated TPI dimer interface mutants provided insight regarding the anatomical source of pathology. It was intriguing that the TPI^{T74R} allele exhibited temperature-dependant paralysis at a mean time of approximately 27 sec. As mentioned previously, this type of behavior is rare and highly enriched for synaptic or conductance defects. Only a handful of mutant alleles have been identified with this type of behavior, including voltage-gated Na^+ , K^+ , and Ca^{2+} channels (*para*, *sei*, *cac*) (70,148,149), the sodium-potassium exchanging ATPase (*ATPa*) (109), and components of vesicle fusion and recycling (N-ethylmaleimide sensitive fusion protein – *dNSF1*, dynamin – *Shi*) (71,150). Noting these phenotypic similarities we broadly examined synaptic function. We found that the TPI^{T74R} mutant inhibited FM1-43 loading at the synapse in a temperature dependant manner [Figure 20]. The TPI^{T74R} mutants were characterized by normal loading during acute exposures (15 and 30 sec.) but exhibited a dramatic reduction at 60sec. [Figure 20A], suggesting a time/excitation dependant phenotype. Further, complementation with the $TPI^{\Delta cat}$ allele significantly increased the temperature-dependent FM1-43 loading at these terminals, much like the allele complements the adult thermal stress behavioral phenotype. Collectively, these data establish that impaired vesicle recycling is the pathophysiologic mechanism underlying the thermal stress dependent paralysis.

It has previously been demonstrated that functional as well as developmental changes at the synapse can influence vesicle recycling. Of note, *trans*-synaptic signaling components of the Glass bottom boat (*Gbb* – a bone morphogenic protein)/Wingless (*Wnt*)/Transforming growth

factor beta (TGF- β) pathways have been shown to modulate synaptic growth and activity (151-155). Given the reduced developmental viability of the *TPI*^{T74R} and *TPI*^{G75E} alleles, we examined whether these substitutions may be altering functional properties of the synapse through a primary change in development. To assess development, we quantified neuromuscular junction (NMJ) 6/7 morphology at segment A2 [Figure 21], the same NMJs used for the functional FM1-43 dye uptake assays. Our analyses revealed no morphological changes in this NMJ as a function of our dimer mutations, supporting a primary functional defect of TPI Deficiency on vesicle recycling at the synapse [Figure 21].

The observed synaptic defect also provided insight into to why the majority of human disease-associated TPI mutations occur at the dimer interface. First, all substitutions which disrupt the dimer interface have been shown to destabilize the enzyme *in vitro* (18,19,147). This destabilization is likely responsible for the reduced cellular TPI found in patient samples, and our work with the *TPI*^{M80T}, *TPI*^{T74R}, and *TPI*^{G75E} mutants support a reduction in TPI levels *in vivo* as a function of dimer interface substitutions [Figure 14D,E]. Secondly, the cellular depletion of *TPI*^{M80T} has been shown to be mediated by heat shock protein sequestration and proteasomal degradation (86). If chaperones sequestered and degraded these misfolded or unstable proteins, this would likely prevent the distribution and maintenance of TPI activity at specific subcellular locales. Finally, recent work has shown that the anterograde transport of globular/soluble proteins to the terminals is a slow process, moving at a rate of approximately 0.008-0.01 μ m/sec (156). To put this in the context of the *Drosophila* nervous system, the length of the relatively short larval motor axon innervating muscle 4 of segment A3 has been measured to be ~220 μ m (157). Based on these approximations, one could estimate that it would take ~6hrs for TPI translated in the soma to be transported to the terminal. In this way, substitutions which affect

protein stability likely result in improper localization or sequestration of TPI during distal transport.

To examine the potential for stability mutations independent of the dimer interface to elicit pathology, we generated mutants of the entirely conserved R188-D224 salt bridge, previously shown to be critical to enzyme stability (142). The TPI^{R188A} , TPI^{R188L} , and TPI^{R188L} substitutions proved lethal, while the conservative TPI^{R188K} substitution behaved like wild type. Previous data establishing changes in stability, and our lethality observations, corroborated the dramatic reductions of these proteins in animal lysates [Figure 21B,D]. It was intriguing that the $TPI^{\Delta cat}$ allele was capable of complementing two of the three lethal alleles to viability, yet these trans-heterozygotes ($TPI^{R188A}/TPI^{\Delta cat}$ and $TPI^{R188S}/TPI^{\Delta cat}$) exhibited behavioral dysfunction, much like the partially complemented TPI^{G75E} and $TPI^{T74R,G75E}$. These data support the hypothesis that dimer mutations elicit pathology by changing the stability of TPI.

The biochemical mechanism through which TPI regulates synaptic function is not yet known, but our work and that of others strongly suggests the importance of catalytic microdomains at the synapse. These conclusions are based on the genetic indications of allelic interdependence for complementation, TPI Deficiency impaired vesicle recycling, and work by others detailing the importance of glycolysis-derived ATP for synaptic vesicular endocytosis (135,158). Indeed, recent work quantifying the ATP consumption in the synapse demonstrated that the vesicle cycle represents the greatest ATP burden at the terminals, and this was further supported by the cessation in vesicle endocytosis during the inhibition of glycolysis and oxidative phosphorylation (OXPHOS) (135). Of particular note was that inhibition of glycolysis had a more dramatic effect on the vesicle cycle compared to that of OXPHOS. Inhibition of glycolysis was also noted to have a more dramatic effect on overall ATP production in the

terminal relative to OXPHOS. These observations suggested that glycolysis, rather than OXPHOS, is the primary means through which neural activity drives ATP production. Further, mutations in *Drosophila* phosphoglycerate kinase, an ATP-producing step of glycolysis, have previously been demonstrated to reduce vesicle recycling (158). Our data and the work of others strongly suggests that TPI facilitates the local production of glycolytic ATP, and the subcellular localization of this deficiency is the ultimate determinant of neurological dysfunction.

3.5 MATERIALS AND METHODS

3.5.1 Animal Strains

The Vienna *Drosophila* RNAi Center (VDRC) line used for knockdown experiments was stock #25644 (136). The w;*actin-GAL4,UAS-GAL4*; animals were generated by recombining the second chromosomes of the *Drosophila* Genetic Resource Center (DGRC) stock #108492 and Bloomington Stock Center stock #4414; recombinants were screened molecularly and balanced. All TPI alleles used in this study were generated using the GE system: *TPI*⁺, *TPI*^{M80T}, *TPI*^{T74R}, *TPI*^{G75E}, *TPI*^{T74R,G75E}, *TPI*^{Acat}, *TPI*^{R188A}, *TPI*^{R188K}, *TPI*^{R188L}, *TPI*^{R188S}, and *TPI*^{Acat-CFP}. The development of the GE system and the production of the *TPI*⁺, *TPI*^{M80T}, *TPI*^{Acat}, and *TPI*^{Acat-CFP} alleles were initially described elsewhere (1). It is important to note that the numbering used in this study utilizes the established nomenclature for TPI mutations, assuming the start methionine is removed following translation (45); and for consistency all residue numbering in this study uses the same convention. Care was taken to ensure all animal populations assessed were approximately equivalent mixtures of males and females.

3.5.2 Mutagenesis and Genomic Engineering

Site directed mutagenesis was performed using the QuikChange Lightning Site-Directed Mutagenesis Kit (Agilent Technologies). Mutagenesis primers were generated (Integrated DNA Technologies) to introduce a Thr-to-Arg codon change at position 74, and a Gly-to-Glu change at position 75 – both separately and together for the purpose of creating the double-mutant. Additionally, primers were generated to create Arg-to-Ala, Arg-to-Lys, Arg-to-Leu, and Arg-to-Ser mutations at position 188. Mutagenesis was performed on the previously published *pGE-attBTPI*⁺ plasmid and confirmed by sequencing. Once the constructs were generated, *TPI* GE was performed using previously published methods (1,99,100). Briefly, the *PGX-TPI* founder animals were mated to *vasa-phiC31*^{ZH-2A} animals expressing the integrase on the X chromosome and their progeny injected with *pGE-attBTPI* constructs. Integration events were identified via the *w*⁺ phenotype and verified molecularly.

3.5.3 Human TPI enzyme purification

Human TPI enzyme was purified as outlined previously (1). Briefly, the coding sequence for *H.sapien* TPI was cloned into the bacterial expression vector pLC3 using standard techniques. The resulting plasmid directs expression of TPI containing N-terminal His₆- and MBP tags, both of which can be removed with TEV protease. TPI protein was expressed in BL21(DE3) Codon-Plus (RILP) *E. coli* (Agilent Technologies) grown in ZY auto-induction media (131) at room temperature for 24–30 hours. Cells were harvested by centrifugation, lysed via homogenization in 25 mM Tris pH 8.0, 500 mM NaCl, 10% glycerol, 5 mM imidazole, 1 mM β-mercaptoethanol and cleared by centrifugation at 30,000 **g**. TPI was purified by nickel affinity chromatography

followed by overnight TEV protease treatment to cleave the His₆-MBP tag from TPI. A second round of nickel affinity purification was performed to separate the His₆-MBP and TEV protease. TPI protein was further purified using cation-exchange chromatography (HiTrap-QP) followed by gel filtration (Sephacryl S-200, GE Healthcare). Peak fractions were concentrated to 4–8 mg/ml in 20 mM Tris pH 8.8, 25 mM NaCl, 2.0% glycerol and 1 mM β-mercaptoethanol using a Vivaspin concentrator (GE Healthcare). The purity was >99% as verified by SDS-PAGE.

3.5.4 Dynamic Light Scattering

DLS measurements were taken using a DynaPro Plate reader (Wyatt Technology) equipped with a temperature control unit. Purified BSA (Sigma Aldrich), hTPI⁺ and hTPI^{M80T} were diluted to concentrations of 5 μM, 15 μM and 30 μM in 100mM triethanolamine (TEA); pH 7.6. Aliquots of 75 μl were loaded in triplicate onto a 384-well microplate and read at 37°C. Ten measurements were taken per sample and Dyanmics V6 software (Wyatt Technology) was used to process the scattering data, generating autocorrelation functions. Autocorrelation functions were then analyzed to obtain the hydrodynamic radii. Student's T test was used to compare samples.

3.5.5 Gel Filtration Chromatography

Gel filtration was performed as outlined previously (85). Briefly, separations were performed with a Shimadzu high performance liquid chromatography (HPLC) system using a Superdex 75/300 GL column (Amersham Biosciences) set to a flow rate of 0.4 ml/min at room temperature. A non-denaturing mobile phase was selected consisting of 25mM NaH₂PO₄, 25mM Na₂HPO₄, 150mM NaCl; pH 7.0. The column was calibrated with a Low Molecular Weight Gel

Filtration Calibration Kit (GE Healthcare Life Sciences) according to the manufacturer's instructions. Calibration standards included Aprotinin (6.5kDa), RNAase A (13.7kDa), Carbonic Anhydrase (29kDa), Ovalbumin (44kDa), and Conalbumin (75kDa). Purified TPI samples were diluted to 15 μ M in mobile phase and 100 μ l were injected and measured in triplicate, and their elution monitored at 280nm. Chromatography traces were collected and analyzed using EZStart 7.3 (Shimadzu) to quantify the relative monomer and dimer populations. Curve integration data were compared using Student's T test.

3.5.6 TPI Enzyme Assays

Isomerase activity was determined using an NADH-linked assay as previously detailed (1,132). Briefly, animals aged 1-3 days were collected and frozen in liquid nitrogen. Bodies lacking heads or appendages were isolated and homogenized in 100mM TEA pH 7.6 supplemented with cComplete mini Protease Inhibitors (Roche Diagnostics). The homogenates were sonicated in an ice bath for 10min and centrifuged twice at 4°C for 5min at 5,000g to remove exoskeletal debris. Lysates were diluted to 0.1 μ g/ μ l in 100mM TEA pH 7.6 + inhibitors and enzyme activity was assessed. Reaction assays were performed using 80 μ l mixtures composed of 0.5mM NADH, 0.752mM GAP, 1 unit glycerol-3-phosphate dehydrogenase and 1 μ g of lysate protein in 100mM TEA; pH 7.6. Consumption of NADH was monitored at 340nm using a SpectraMax Plus 384 microplate reader (Molecular Devices). All reactions were performed in both experimental and biological triplicate. Reaction components were purchased from Sigma-Aldrich. Enzyme activity curves were normalized to reactions performed without GAP. A one-way ANOVA was performed to assess variance and data sets were compared using Tukey's post-hoc analysis.

3.5.7 Behavioral testing and lifespan analysis

Mechanical stress sensitivity was examined by vortexing the animals in a standard media vial for 20 seconds and measuring time to recovery, similar to (133). Thermal stress sensitivity was assessed by acutely shifting animals to 38°C and measuring time to paralysis, as previously described (65,109). Behavioral responses were capped at 360 and 600 seconds where indicated. Animal lifespans were performed at 25°C as previously described (109). One-way ANOVAs were performed with Tukey's post test to compare behavior, and lifespans were assessed with Log-rank (Mantel–Cox) survival tests.

3.5.8 Immunoblots

Animals were collected aged 1-2 days at room temperature. Ten fly heads were obtained in triplicate from each genotype and processed as outlined previously (86). Briefly, the fly heads were ground by pestle in 80 µl 2× SDS–PAGE sample buffer (4% SDS, 4% β-mercaptoethanol, 130 mM Tris–HCl pH 6.8, 20% glycerol) and centrifuged for 5 minutes at 5000 *g* to pellet the exoskeleton. Proteins were resolved by SDS–PAGE and transferred onto 0.45µm PVDF membrane. Following treatment in 1% milk PBST, the blots were incubated with anti-TPI (1 : 5000; rabbit polyclonal FL-249; Santa Cruz Biotechnology) or anti-ATPalpha (1 : 10,000; mouse monoclonal alpha5; Developmental Studies Hybridoma Bank). The blots were washed in PBST, incubated in the appropriate HRP-conjugated secondary antibody, and developed using ECL (Pierce). Densitometric analyses of the scanned films were performed digitally using ImageJ software available from the National Institutes of Health. A one-way ANOVA was

performed to assess variance of TPI levels and data sets were compared using Tukey's post-hoc analysis.

3.5.9 Filter-trap Dot Blot

The filter-trap dot blot was modified from methods published previously (139). Animals were aged 1-2 days, collected and homogenized in 1X PBS (2.7mM KCl, 137mM NaCl, 2mM NaH₂PO₄, 10mM Na₂HPO₄; pH 7.4) supplemented with cOmplete mini Protease Inhibitors, and diluted to 1µg/µl. Samples were diluted 1:2 in 1% SDS, 1X PBS, boiled for 5min, and filtered through a cellulose acetate membrane (Whatman, 0.2µm pore) using a 96-well vacuum dot blot apparatus. Positive controls were collected from PC12 cells stably expressing huntingtin exon1 with a stretch of 97 glutamines and C-terminally tagged with GFP. The membrane was washed four times with the 1% SDS-PBS and blocked with Odyssey Blocking Buffer (LiCor), and primary antibodies applied in Odyssey Blocking Buffer. Blots were incubated with anti-TPI (1:5000) and anti-GFP (1:5000) (Santa Cruz Biotechnology). The membranes were then washed and incubated with the secondary antibody IRDye 800-conjugated goat anti-rabbit (LiCor) at 1:20,000 in the same buffer used for the primary antibodies. Direct-to-scanner detection and band visualization were performed using a LiCor Odyssey scanner.

3.5.10 Coimmunoprecipitations

Coimmunoprecipitations were performed using the Pierce® Co-Immunoprecipitation Kit (Thermo Scientific) as per manufacturer's instructions. Lysates were generated by mechanically homogenizing 50 animals in 0.5ml of IP Lysis buffer (25mM Tris, 150mM NaCl, 1mM EDTA,

1% NP-40, 5% glycerol; pH 7.4) supplemented with cOmplete mini Protease Inhibitors. After homogenization, lysates were frozen and thawed in liquid nitrogen, then centrifuged twice at 5,000g to pellet exoskeletal debris. Supernatants were collected and diluted to 1µg/µl and 400µg were loaded onto 25µl of gel pre-coupled with 10µg of anti-GFP (Santa Cruz). A negative control was performed using uncoupled gel and TPI⁺/TPI^{Δcat} lysate. Samples were incubated overnight at 4°C and washed ten times with IP Lysis buffer at 4°C. Beads were eluted with 70µl of 2X SDS-PAGE sample buffer, separated via SDS-PAGE, immunoblotted, and analyzed as outlined above. Coimmunoprecipitations were performed in biological triplicate.

3.5.11 FM1-43 Imaging Experiments

Images were taken with an Olympus BX51WI fluorescence microscope with Till Photonics Polychrome V monochromater excitation, and Hamamatsu C4742-95 digital camera. Heterozygous *TPI^{T74R}* larvae were maintained over TM6B and *Tb⁺* 3rd-instar larvae selected for analysis. Dissection and preparation of larval NMJs were performed as outlined previously (140). FM1-43FX dye [Molecular Probes, Invitrogen] loading was performed as previously detailed (141). Briefly, animals were dissected in ice cold 0mM Ca²⁺ HL-3 with 0.5mM EGTA, then heated to room temperature or 38°C over the course of 3 min. Bath temperature was monitored throughout the experiments with a microthermal probe to ensure consistency [Fisher Scientific]. Loading experiments were performed with room temperature or 38°C preheated 90mM KCl 1.5mM CaCl₂ HL-3 supplemented with 4µM FM1-43FX, and preparations were washed quickly and thoroughly during the experiments to avoid Ca²⁺ chelation. After loading, preparations were washed with 15ml of 0mM Ca²⁺ HL-3 with 0.5mM EGTA at room temperature for 10 min. Preparations were immediately imaged with a water immersion 60X

objective, using 450nm excitation and a 500 nm longpass filter [Chroma Technology]. Simple PCI imaging software was used for acquisition and ImageJ for analysis. Two NMJs from muscles 6/7 were assessed per animal, one from segment A2 and A3. Six biological replicates were assessed per genotype per time point for a total of 12 NMJs per experimental condition. Boutons were defined as being greater than or equal to 2 μ m in diameter, and background intensity was subtracted from adjacent tissue. Image analysis was performed blinded, with all file names relabeled by an independent researcher. Pair-wise analyses were performed using a two-tailed Student's t test, while comparisons among multiple experimental conditions was performed using a one-way Analysis of Variance (ANOVA) with Tukey's post-hoc analysis.

3.5.12 NMJ morphological analyses

For NMJ morphological analyses, 3rd-instar larvae were collected and dissected as detailed above, without transection of the descending motor neurons. Preparations were fixed in 3.5% paraformaldehyde HL-3, permeabilized with 0.1% Triton X-100 in 1X PBS (PBST), and blocked with 0.2% BSA in PBST (PBSTB) for 2hrs. Preps were washed and incubated with goat anti-HRP [Jackson Laboratories] at 1:200 in PBSTB for 2hrs. Primary antibodies were removed, washed in PBSTB, and incubated with Cy3-labeled donkey anti-goat in PBSTB at 1:400 for 1.5hrs. Preps were washed, mounted in VectaShield [Vector Laboratories], and imaged within three days. Images were acquired with an Olympus confocal FV1000 microscope, using a 559nm excitation laser. Z stacks of segment A2 of muscle 6/7 were taken using 1 μ m steps, and the start and end of the stacks were set just outside the range of the NMJ. The Z stacks were merged using Olympus FV1000 Fluoview Viewer, and morphology determined. Ten biological replicates were assessed per genotype, one NMJ per animal, for a total of ten NMJs per

experimental condition. Boutons were defined as varicosities at least 2 μ m in diameter, and branches defined as extensions containing at least 2 boutons. Images were relabeled by an independent researcher for blinded analysis. Variance within the data set was examined using a one-way ANOVA, with comparisons made using Tukey's post hoc test.

4.0 HUMAN TRIOSEPHOSPHATE ISOMERASE I170V ALTERS CATALYTIC SITE, ENHANCES DIMERIZATION AND INDUCES PATHOLOGY IN A *DROSOPHILA* MODEL OF TPI DEFICIENCY

4.1 ABSTRACT

Oligomerization is often an important regulator of protein function. The formation of an oligomer can be simple or complex, uniting two homologous subunits, or assembling multiunit heterocomplexes. Modifying the way proteins associate can have tremendous pharmacologic and pathologic implications. Triosephosphate isomerase (TPI) is a glycolytic enzyme which homodimerizes for full catalytic activity. Mutations of the *TPI* gene elicit a disease known as TPI deficiency, a glycolytic enzymopathy noted for its unique severity of neurological symptoms. Recently, a high-resolution structure of one disease-associated *TPI* mutation revealed an alteration of the homodimer interface resulting in a reduction in enzyme stability, and not catalytic activity. This study suggested that TPI deficiency pathogenesis may be due to conformational changes of the protein, likely affecting dimerization and protein stability. In the present report, we genetically and physically characterize a previously unstudied human disease-associated TPI mutation, which confers an I170V substitution. *TPI*^{I170V} elicits behavioral abnormalities in *Drosophila*, and purified protein reveals dramatic increases in substrate affinity, enhanced enzyme dimerization, and increased thermal stability. A high-resolution crystal

structure of the homodimeric I170V mutant reveals changes in catalytic site morphology. Collectively these data reveal new insights into the structural determinants of TPI deficiency pathology, and suggest new means of disease pathogenesis.

4.2 INTRODUCTION

Protein oligomerization is a phenomenon seen in many facets of biology. The ability to create and stabilize complex quaternary structures from simple subunits is seen in the generation of glycolytic enzymes (159-161), receptor tyrosine kinases (162,163), actin filaments (164), vesicle fusion proteins (165,166), and countless other examples. One of the most commonly used protein structures in nature is the β/α TIM barrel. The TIM barrel is the structural base of over one hundred different enzymes, but was first identified in triosephosphate isomerase (TPI). TPI uses the TIM barrel to form the tertiary structure of its monomers, and like many other TIM barrel proteins, only functions as an oligomer/dimer *in vivo*. TPI monomers *in vitro* exhibit little catalytic activity (18,19), but attain diffusion-limited catalytic properties upon dimerization (20). Structural analyses of artificial monomeric TPI variants have revealed flexibility of normally rigid motifs in and around the catalytic pocket (18,19). These studies concluded that dimerization facilitates the rigidification of the catalytic pocket through a variety of *trans*-monomeric Van der Waals forces, hydrogen bonds, and salt bridges (107), but little work has been done to examine the role of the catalytic site on the formation or maintenance of the homodimer.

Functionally, TPI is a glycolytic enzyme that isomerizes dihydroxyacetone phosphate into glyceraldehyde 3-phosphate. This isomerization occurs at a non-linear step in the catabolic

process, enhancing the efficiency of glycolysis, and is not required for the production of pyruvate. Mutations within the *TPI* coding region lead to a recessive disease known as TPI Deficiency, which is characterized by hemolytic anemia, neurologic dysfunction and often early death (26). TPI Deficiency is unique among all other glycolytic enzymopathies in the presentation of severe neurological deficits and the lack of ATP depletion (45). It is not currently understood why mutations in a non-linear glycolytic enzyme elicit far greater pathology than other central glycolytic enzymes, though recent work has suggested that these neurological differentia are derived from a source other than general metabolic stress (1). To date, only one disease-associated TPI mutation has been structurally characterized (63). Additional physical analyses of disease-associated substitutions are clearly needed to more fully understand the unique pathology associated with TPI Deficiency.

In the present report, we have investigated a poorly studied human disease-associated mutation of TPI which occurs at the catalytic lid of the enzyme. Previously, patients bearing the I170V substitution had only been identified in a *trans*-heterozygous state with the more common E104D missense mutation (102). Due to the rarity of this particular point mutation, it was previously unclear whether I170V was viable as a homozygote, pathogenic, or simply lacked sufficient consanguinity for observation. Our work has revealed that I170V is homozygous viable and elicits behavioral dysfunction in a *Drosophila* model of TPI deficiency. Further, *in vitro* measurements of TPI^{I170V} dimerization indicated a more robust homodimer population than WT, an observation corroborated by increased thermal stability of the TPI^{I170V} enzyme. A crystal structure of TPI^{I170V} revealed a predominantly closed lid conformation, changes in the positioning of S96, and a water network coordinating E165 and H95. Our data establish that the disease-associated I170V substitution is sufficient to alter both catalytic and dimerization

properties. These data support and contrast the findings of the only previous structural analysis of a disease-associated TPI substitution, reaffirming the importance of enzyme dimerization in TPI deficiency pathology, but demonstrating a unique pathogenic increase in dimerization and stability. These findings are critical to the understanding of the unique pathology associated with TPI deficiency, and suggest either a physiologic role for TPI in catalytic microdomains, or the necessity of dynamic regulation of the TPI dimer.

4.3 RESULTS

4.3.1 I170V induces behavioral dysfunction in *Drosophila*

We initiated this study seeking to examine the toxic potential of the TPI^{I170V} allele. Using our *Drosophila* genomic engineering (GE) system (1), we generated novel alleles of human TPI with an I170V substitution ($hTPI^{WT}$ and $hTPI^{I170V}$). A GE approach is optimal for examining this type of dose-dependant loss-of-function disease, as it seamlessly places the modified alleles directly into the *Drosophila* TPI gene locus ensuring endogenous expression at all developmental stages and in all tissues (99,101). Due to the relative abundance of null TPI alleles, many TPI deficient patients are genetically identified as trans-heterozygotes with a point mutation over a null allele (26,45). $hTPI^{I170V}$ proved homozygous viable, and we generated *trans*-heterozygous populations and assessed two genotypes: $hTPI^{WT}/TPI^{null}$ and $hTPI^{I170V}/TPI^{null}$. The TPI^{null} allele is a deletion of two of the three exons of the TPI gene (formerly called TPI^{JS10}) (50) while $hTPI^{WT}$ is the human WT enzyme.

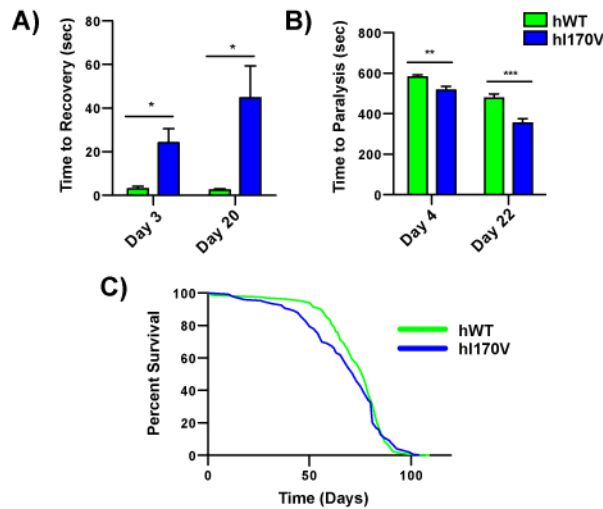


FIGURE 23. *hTPI^{170V}* is characterized by behavioral dysfunction but not reduced longevity. *hTPI^{170V}/TPI^{null}* exhibits mechanical (A) and thermal (B) stress sensitivity relative to *hTPI^{WT}/TPI^{null}*, n>20. Conversely, *hTPI^{170V}/TPI^{null}* demonstrated similar lifespans (C) as *hTPI^{WT}/TPI^{null}*, n≥120. * indicates p<0.05, ** p<0.01, and *** p<0.001.

We collected animals, aged them at 25°C, and examined their mechanical- and thermal-stress sensitivity and longevity, as these phenotypes have been shown to be hallmarks of *Drosophila* TPI Deficiency (1,50,64,85). Mechanical- and thermal-stress sensitivity were detected in *hTPI^{170V}/TPI^{null}* animals at both early (day 3 and 4) and late (day 20 and 22) time points, indicating progressive behavioral dysfunction [Figure 23 A,B]. A slight change in thermal stress sensitivity was noted in the wild type populations, with a fraction of the population exhibiting abnormal thermal stress-dependent behavior. These effects on WT are not observed in homozygote animals, and we believe that this modest effect is likely a reflection of the heterozygote state (*hTPI^{WT}/TPI^{null}*). Interestingly, we did not detect a significant change in longevity when comparing *hTPI^{170V}/TPI^{null}* versus *hTPI^{WT}/TPI^{null}* [Figure 23C]. These results suggest *Drosophila* TPI Deficiency behavioral dysfunction and longevity phenotypes may be derived from different pathogenic sources.

4.3.2 *in vivo* TPI protein levels and enzyme activity

Having identified aberrant behavior in the $hTPI^{I170V}$ mutants, we sought to assess lysate isomerase activity and protein levels in this mutant. An analysis of wild type protein structure predicted that the I170V substitution would likely influence catalytic properties due to its positioning on the catalytic lid of the enzyme [Figure 28]. Previous studies using a transgenic expression system in yeast identified a reduction in isomerase activity due to I170V (62), and our experiments measuring $hTPI^+$ and $hTPI^{I170V}$ activity in animal lysates confirmed these observations in the native gene locus [Figure 24A]. Of note though, a previous study in *Drosophila* failed to find a link between animal metabolism and disease phenotypes (1). This former study suggested that a conformational change or depletion of cellular TPI elicited *Drosophila* TPI deficiency (1). To examine the possibility that I170V may reduce protein levels in our system, we examined TPI levels in our newly generated alleles. Western blots indicated no changes in TPI protein levels due to the I170V substitution relative to TPI^{WT} [Figure 24B,C], concluding the I170V mutation does not elicit pathology through a depletion of cellular TPI.

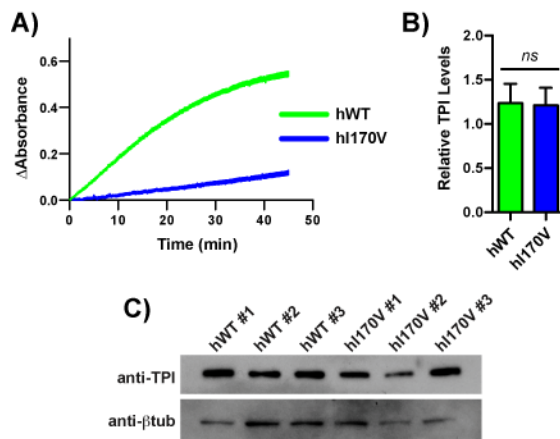


FIGURE 24. $hTPI^{I170V}$ exhibits reduced catalysis and normal cellular TPI levels. Isomerase assays reveals $hTPI^{I170V}/TPI^{null}$ reduces lysate TPI activity relative to $hTPI^{WT}/TPI^{null}$ (A), $n=3$. Independent samples

of human $hTPI^{WT}/TPI^{null}$ and $hTPI^{I170V}/TPI^{null}$ (#1,#2,#3) demonstrate similar levels of cellular TPI (C), with quantification (B), n=3. *ns* indicates no significance.

Table 3. hTPI^{WT} and hTPI^{I170V} kinetic parameters.

	hTPI ^{WT}	hTPI ^{I170V}
K_m (GAP) (mM)	1.4 ± 0.1	0.049 ± 0.014
k_{cat} (GAP) (s ⁻¹)	1623 ± 181.1	75.8 ± 2.6
k_{cat}/K_m (GAP) (M ⁻¹ s ⁻¹)	1.2×10^6	1.5×10^6

4.3.3 I170V enhances substrate affinity, stability, and dimerization *in vitro*

The only study to structurally examine a TPI deficiency mutation found that the E104D substitution altered a trans-monomeric water network; this E104D substitution resulted in reduced enzyme dimerization and stability, but did not alter enzyme activity *in vitro* (63). Recombinant human hTPI^{WT} and hTPI^{I170V} was expressed and purified, and we examined their respective kinetic properties [Table 3]. It should be noted that both enzymes displayed typical Michaelis-Menten behavior [Figure 25]. hTPI^{WT} demonstrated properties similar to those previously published (145,167,168), while hTPI^{I170V} displayed a ~20 fold reduction in catalytic turnover [Table 3] and a ~30 fold increase in substrate affinity [Table 3]. The combined reduction in turnover and increased substrate affinity suggests the enzyme is preferentially in the occupied state.

Since previous studies had indicated that dimerization was an important molecular contributor to TPI deficiency, we assessed TPI dimerization of hTPI^{I170V} using gel filtration [Figure 26]. Analyses of hTPI^{WT} at room temperature demonstrated a 80:20 equilibrium of

dimer-to-monomer, with two corresponding peaks eluting at 24 and 27 minutes [Figure 26A,B]. Comparatively, the monomer peak was absent in all analyses of hTPI^{I170V} dimerization [Figure 26A,B]. These results suggested the I170V substitution may somehow enhance TPI dimer stability. Indeed, Ralser and colleagues (62) noted that while E104D impaired WT:mut heterodimer associations in a yeast two-hybrid (Y2H) system, the I170V mutation appeared to increase these interactions. Our results suggest that their increase in Y2H signal was not likely due to aggregation or external factors, but that this TPI variant is intrinsically capable of eliciting an increase in these dimeric associations.

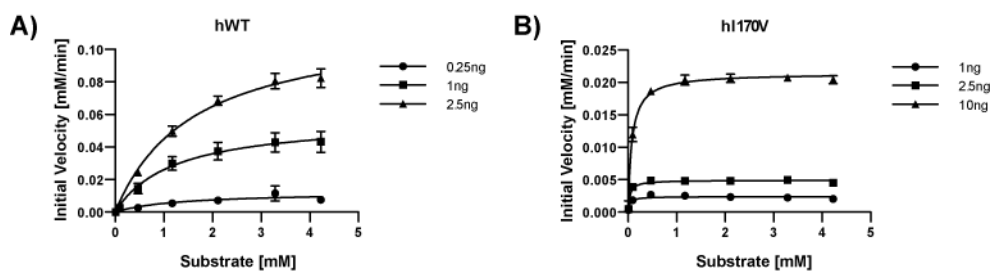


Figure 25. hTPI^{WT} and hTPI^{I170V} exhibit Michaelis-Menten behavior.

Over the past two decades several groups have characterized the folding and unfolding kinetics of TPI from numerous species (19,147,169-174). These studies have established that dimerization of TPI is a crucial determinant of protein stability, though several monomeric intermediates are also critical. Far-UV circular dichroism (CD) spectra did not identify a gross change in protein folding at 20°C [Figure 27], but an assessment of thermal denaturing at 222 nm indicated a significant change in protein stability, with hTPI^{WT} and hTPI^{I170V} exhibiting monophasic denaturation with T_m s of 46.5°C and 59.4°C respectively [Figure 26C]. Previous studies have shown that CD measurements of TPI thermal denaturing elicit monophasic transitions (167,175), lacking the capacity to resolve many of the still-folded monomeric

intermediates. Importantly, these data indicate that hTPI^{I170V} increases its dimer population through an enhancement of enzyme stability.

Occupancy of the catalytic site has been shown to stabilize the dimer (171,173). Given the enhanced substrate affinity of hTPI^{I170V}, we predicted that hTPI^{I170V} stability would be more responsive to substrate administration than hTPI^{WT}. Using DL-glycerol-3-phosphate (DL-GP), a GAP substrate analog (176-178), we measured the stability shift resulting from occupancy of the catalytic site. The addition of DL-GP to hTPI^{WT} resulted in a 3.7°C increase in stability (T_m 50.2°C), while DL-GP enhanced hTPI^{I170V} stability only 1.6°C (T_m 61.0°C). Denaturation of hTPI^{I170V} and hTPI^{WT} were both observed to be irreversible, an observation similar to that of previous studies (63,179,180).

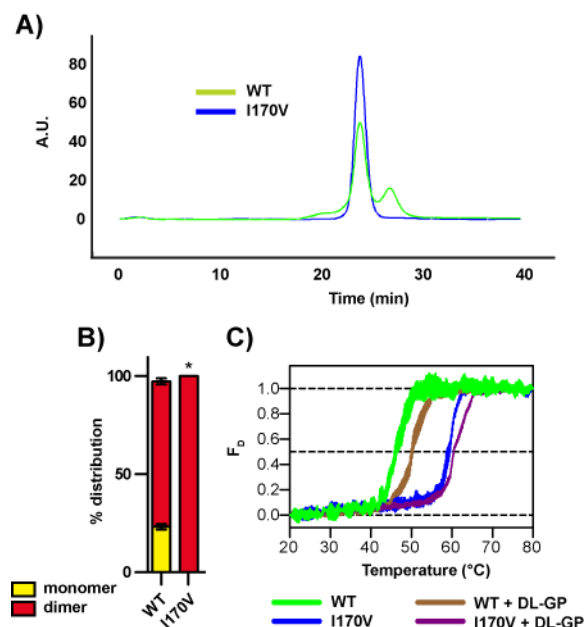


FIGURE 26. I170V increases TPI dimer stability relative to WT. Gel filtration indicates a change in monomer:dimer ratios elicited by I170V relative to WT (A) with quantification (B). CD thermal shift analyses demonstrate a stabilization of TPI due to the I170V substitution (C), and altered responsiveness to 5mM DL-GP substrate analog. * indicates $p < 0.05$, ns indicates no significance.

4.3.4 The crystal structure of I170V supports a preferentially closed catalytic pocket

TPI is a TIM barrel protein, using the β/α barrel as a base for the orientation of its accessory loops. The I170 residue is located on the rigid tip of loop 6 [Figure 28A]. Loop 6 of TPI forms a “lid” over the catalytic pocket, and its closure over the substrate has been shown to prevent the dissociation of catalytic intermediates during substrate isomerization (13). Previous studies have described loop 6 as dynamic in the unbound state, and indeed NMR studies have shown breathing motions in this loop (181). The lid is composed of three main components – an N hinge, a rigid tip, and a C hinge (182). The N hinge extends immediately from the catalytic E165 and contains a three residue sequence of P166-V167-W168 (180). The P166 provides rigidity to the hinge mechanism while the bulky hydrophobic V167 is positioned to facilitate lid movement. The N terminal hinge works in conjunction with a C terminal hinge, composed of K174-T175-A176 (179,183). Changes in phi and psi angles of T175 are believed to promote changes in lid orientation (182).

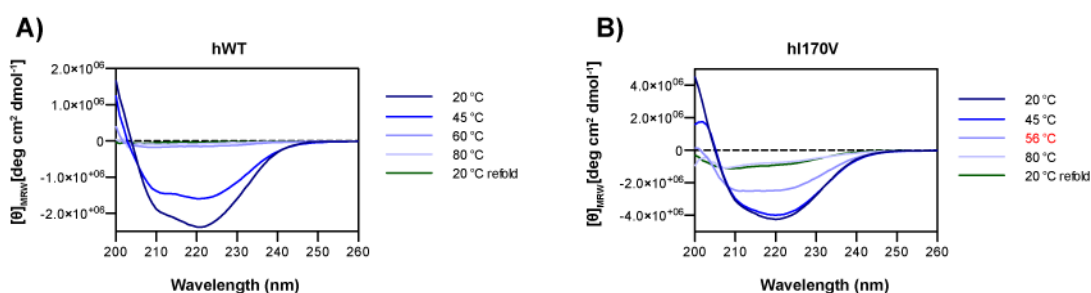


Figure 27. Averaged far-UV CD spectra of hTPI^{WT} and hTPI^{I170V} acquired during thermal denaturation.

To determine if we could visualize the molecular mechanism responsible for the altered hTPI^{I170V} catalytic properties, we purified, crystallized and analyzed the structure of hTPI^{I170V} at 2.0Å resolution. hTPI^{I170V} was crystallized in a buffer nearly identical to that of hTPI^{WT} (1.6Å), facilitating a near-atomic comparison. The overall folding of the enzymes was similar,

corroborating our previous CD analyses [Figures 27-29]. In both structures, a bromide ion from the crystallization conditions was found in the active site, as was a phosphate ion which was not added intentionally, and which presumably co-purified with TPI. The positioning of these ions directly overlap those of substrate molecules co-crystallized with other TPI structures, suggesting their inclusion helped stabilize the catalytic pocket during crystallization.

The I170V structure revealed a change in the region surrounding the N hinge; specifically a $\sim 90^\circ$ rotation of S96, moving its terminal proton 2.7\AA toward the catalytic site [Figure 28A]. S96 is known to rotate in and out of the catalytic site with the movement of the lid. In an open lid conformation, S96 rotates inward and hydrogen bonds with E165, stabilizing its localization $2\text{-}3\text{\AA}$ away from its substrate-bound position (105). However, S96 rotates out of the catalytic pocket upon lid closure, breaking the hydrogen bond with the catalytic E165 and allowing it to swing over and induce substrate isomerization. In the I170V structure, the inward rotation of S96 in the closed state is facilitated by the absence of the Ile-to-Val methyl group, and leads to increased hydrophilic interactions in the N hinge region. Previous studies have shown that the N hinge is sensitive to both bulk and hydrophilic interference (180,182), with each inducing a preferentially closed lid. The inward rotation of S96 in the I170V structure will strengthen a water network within the catalytic pocket, known to interact with substrate [Figure 28B]. This reinforced water network demonstrates a putative physical mechanism through which the enzyme turnover rate is reduced and substrate affinity increased [Table 3]. Collectively, these observations demonstrate that the shortened V170 fails to break the hydrogen bonding between E165 and S96 during lid closure, preferentially stabilizing this state and enhancing substrate affinity.

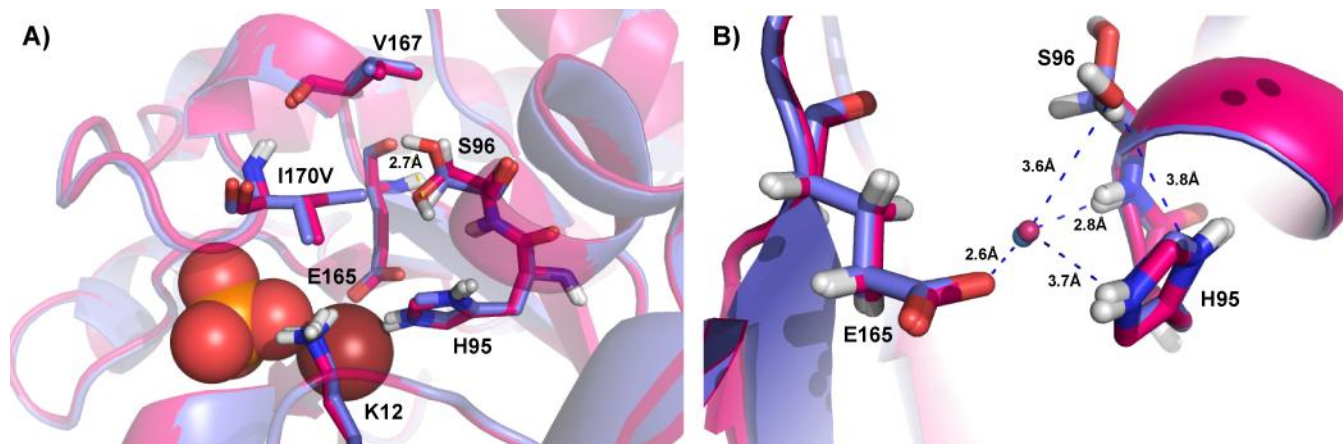


Figure 28. Structural comparisons of hWT with hI170V reveal enhanced hydrogen bonding in the catalytic site. Catalytic site of monomer A. An overlay of hWT (cyan) and hI170V (pink) reveal a 90° inward rotation of S96, moving its distal hydrogen 2.7Å (A). Movement is indicated by a yellow dashed line (A). The rotation of S96 enhances the coordination of a catalytic water and H95 (B). Polar interactions are indicated by blue dashed lines and their distances indicated (B). Both structures are shown as cartoons, with pertinent residues labeled and displayed as sticks.

4.4 DISCUSSION

Due to the rarity of the disease and dearth of model systems, little is known about the pathogenesis of TPI deficiency. We have pathologically and physically characterized a previously unstudied human disease-associated *TPI* mutation. We found that the I170V mutation was genetically homozygous viable, yet when paired with a null allele was capable of inducing behavioral dysfunction similar to a previously described pathogenic *Drosophila TPI* point mutation (50,64). These characteristic fly behaviors are enriched for neurological dysfunction, and therefore are believed to be analogs of the symptoms exhibited by human patients (74,75). A reduction in catalytic activity in these mutants was predicted based on a previous study in yeast (62). Yet oddly, *in vitro* biochemical analyses (Table 3) suggested the

I170V mutant should be as efficient as wild type, a result at odds with our *in vivo* lysate measurements [Figure 24A]. It is unclear as to why these results were not in congruence, but we cannot rule out possible effector proteins or unknown regulatory mechanisms which may be present in the lysates, but not the purified system.

Seeking a molecular explanation of *hTPI*^{I170V} pathogenesis, a high resolution crystal structure revealed clear physical changes resulting from the I170V substitution which illustrate the molecular mechanisms responsible for our altered enzyme kinetics. Specifically, the shortening of the I170 residue to V170 leads to the S96-mediated maintenance of a water network within the catalytic pocket during lid closure. This water network likely stabilizes the enzyme in the substrate-bound state, again in agreement in with our 30-fold increase in substrate affinity [Table 3]. Further, the dynamic orientation of E165, and by extension the C- and N-terminal hinges, has been linked to the breathing motions of the catalytic lid (177,184). Although our experiments lack the capacity to directly measure the rate constants of lid opening and closure, it is tempting to speculate that this catalytic water network could inhibit the opening rate of the lid. Inhibiting lid opening would reduce catalytic turnover, resulting in largely closed loop orientations, both of which are observations we have made in our crystal structure and enzyme kinetic analyses [Table 3; Figure 28].

The only previously crystallized human disease-associated TPI substitution, E104D, indicated a miscoordination of a conserved water network at the homodimer interface. This alteration of the dimer interface elicited a reduction in *hTPI*^{E104D} dimerization and stability, but not changes in catalytic activity (63). Our data establish altered catalytic properties as a function of the I170V substitution, while dimerization and stability experiments demonstrate a distinct increase in *hTPI*^{I170V} stability relative to *hTPI*^{WT} [Figure 26]. Further, although *hTPI*^{I170V}

substrate affinity is increased [Table 3], the addition of a substrate analog elicited a modest increase in protein stability ($\Delta T_m=1.6^\circ\text{C}$) relative to hTPI^{WT} ($\Delta T_m=3.7^\circ\text{C}$). These data suggest one of two possibilities: i) the I170V substitution selectively reduces DL-GP, but enhances GAP binding, or ii) hTPI^{I170V} stability is less sensitive to catalytic site occupancy. Addressing the first, the catalytic area critically affected by the I170V substitution and Ser96 rotation is the region of the catalytic pocket occupied by the phosphate. The positioning of this phosphate is conserved between DL-GP and GAP, making it unlikely that DL-GP binding would diverge from that of GAP as a function of the I170V substitution. Therefore, we believe it is far more likely that these stability data indicate that hTPI^{I170V} is mimicking the substrate-bound conformation, with similar physical mechanisms underpinning its increased stability.

Although an unanticipated and exciting result, the structure of hTPI^{I170V} does not yield any insight into why we observe changes in stability [Figure 29]. Experiments examining the relative contributions of solvent and chain entropy in this mutant would be needed to conclusively determine a molecular mechanism of I170V stability. However, the confluence of data lead us to speculate that lid orientation is likely responsible for the changes in enzyme stability. Preferential lid closure would provide additional protection from bulk solvent, and reduce overall solvent entropy; a result borne out by the substrate-induced stabilization of hTPI^{WT}. Comparatively, the preferentially closed lid of hTPI^{I170V} reduced the sensitivity to substrate-induced TPI stabilization.

Irrespective of the molecular mechanism, the findings that hTPI^{I170V} induces pathology and is characterized by decreased catalysis and increased stability demonstrates that reduced TPI dimer stability alone is not the only means to achieve pathology. These observations prompt two

new hypotheses regarding TPI Deficiency: i) TPI dimers and monomers are dynamically regulated molecules, or ii) localized, not gross TPI activity, is necessary for normal behavior.

The former hypothesis centers on the potential for TPI dimerization or stability to be purposefully regulated. In support of this hypothesis, recent reports have detailed two post-translational modifications which have been shown to influence TPI isomerase activity and protein levels *in vivo*: phosphorylation of TPI by cyclin dependent kinase 2 (cdk2) (127), and methylation of R189 by protein arginine methyl-transferase 5 (PRMT5) (128). The phosphorylation of TPI is predicted to occur at the solvent/dimer interface residue S20 (127), and we hypothesize that post-translational modifications of this residue would likely alter dimer interface morphology. Additionally, R189 participates in an entirely conserved salt bridge with D225 at the distal ends of the homodimer. This salt bridge has been shown to be a critical determinant of TPI stability (142), and methylation has been predicted to disrupt this interaction. Further work is needed to more clearly define the role of TPI post-translational modifications, but provide a tempting platform for speculation.

Alternatively, the latter hypothesis builds upon the preeminent finding that hTPI^{I170V} has a dramatic effect on enzyme kinetics. Previous work has demonstrated that a catalytically inactive TPI allele can complement the toxic TPI^{M80T} substitution. This study concluded that TPI Deficiency neurological dysfunction and reduced longevity are not correlated with metabolic stress (1), yet did not exclude the possibility of catalytic microdomains. It is currently unclear where such a microdomain could be critical, and to what end. TPI activity contributes to the glycerol synthesis pathway, glycolysis, and the glycerol 3-phosphate NADH shuttle. An assessment of human disease symptoms in each pathway fails to suggest a singular pathogenic catalytic mechanism. Additional work will be needed to explore the putative importance of

catalytic microdomains and their contribution to the unique pathology associated with TPI deficiency.

In conclusion, the data presented in this study demonstrate the pathogenic nature of a previously understudied human mutation, and illustrate the molecular mechanism responsible for its pathogenesis. These results are critical for directing future experimentation surrounding the largely understudied role of TPI in animal physiology, and the pathogenesis of TPI Deficiency.

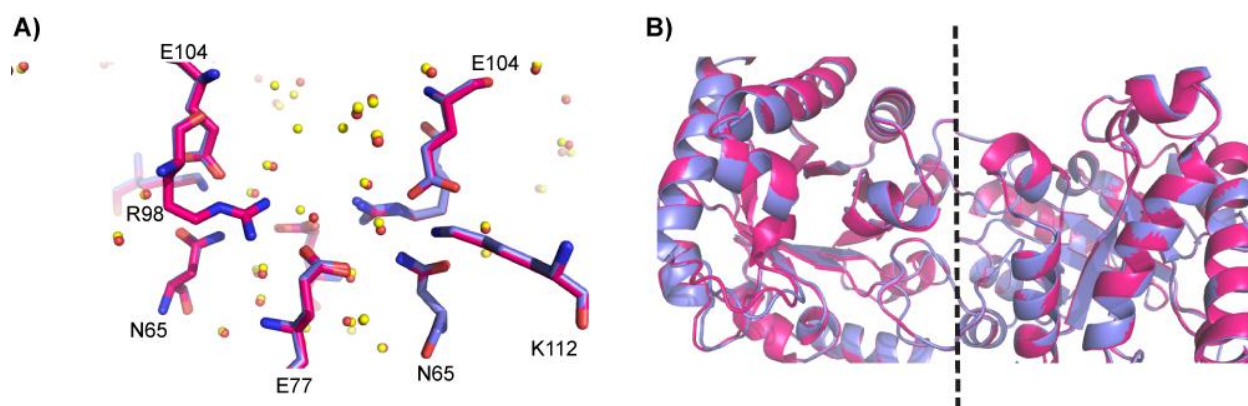


Figure 29. I170V crystal structure lacks insight regarding altered protein stability. I170V fails to alter a conserved trans-monomeric TPI water network (A) known to alter protein stability (63). Analyses of WT and I170V demonstrate similar folding and orientation of the peptide backbone (B). Residues shown as sticks, colored by element, with WT labeled blue and I170V labeled pink (A). Waters are indicated by unbound spheres, with WT in red and I170V in yellow (A). Proteins displayed a cartoon with backbones colored as before (B); dashed line indicates the dimer interface.

4.5 MATERIALS AND METHODS

4.5.1 Mutagenesis and Genomic Engineering

The *pGE-hTPI^{WT}* construct was generated using human TPI (hTPI) coding region. The hTPI sequence was synthesized and recoded for *Drosophila* codon usage, while maintaining *Drosophila* intron-exon gene architecture and splicing, to ensure appropriate expression. The synthesized hTPI was designed to include flanking restriction sites for cloning into the *pGE-attBTPI⁺* plasmid (1). Site directed mutagenesis was performed using the QuikChange Lightning Site-Directed Mutagenesis Kit (Agilent Technologies). Mutagenesis primers were generated (Integrated DNA Technologies) to introduce an Ile-to-Val codon change at position 170. Mutagenesis was performed with *pGE-hTPI^{WT}* and confirmed by sequencing. *TPI* GE was performed using previously published methods (1,99,100). Briefly, the *PGX-TPI* founder animals were mated to *vasa-phiC31^{ZH-2A}* animals expressing the integrase on the X chromosome and their progeny injected with *pGE-attBhTPI^{I170V}*. Integration events were identified via the *w⁺* phenotype and verified molecularly. The newly synthesized alleles were outcrossed to *w¹¹¹⁸* for five generations and mated to *y¹ w^{67c23} P[y[+mDint2]=Crey]1b; D^{*}/TM3, Sb¹* to reduce the engineered locus.

4.5.2 Human TPI enzyme purification

Human TPI enzyme was purified as outlined previously (1). Briefly, the coding sequence for *H.sapien TPI* was cloned into the bacterial expression vector *pLC3* using standard techniques. The resulting plasmid directs expression of TPI containing N-terminal His₆- and MBP tags, both

of which can be removed with TEV protease. TPI protein was expressed in BL21(DE3) Codon-Plus (RILP) *E. coli* (Agilent Technologies) grown in ZY auto-induction media (Studier, 2005) at room temperature for 24–30 hours. Cells were harvested by centrifugation, lysed via homogenization in 25 mM Tris pH 8.0, 500 mM NaCl, 10% glycerol, 5 mM imidazole, 1 mM β -mercaptoethanol and cleared by centrifugation at 30,000 *g*. TPI was purified by nickel affinity chromatography followed by overnight TEV protease treatment to cleave the His₆-MBP tag from TPI. A second round of nickel affinity purification was performed to separate the His₆-MBP and TEV protease. TPI protein was further purified using cation-exchange chromatography (HiTrap-QP) followed by gel filtration (Sephacryl S-200, GE Healthcare). Peak fractions were concentrated to 4–8 mg/ml in 20 mM Tris pH 8.8, 25 mM NaCl, 2.0% glycerol and 1 mM β -mercaptoethanol using a Vivaspin concentrator (GE Healthcare). The purity was >99% as verified by SDS-PAGE.

4.5.3 Gel Filtration Chromatography

Gel filtration was performed as outlined previously (85). Briefly, separations were performed with a Shimadzu high performance liquid chromatography (HPLC) system using a Superdex 75/300 GL column (Amersham Biosciences) set to a flow rate of 0.4 ml/min at room temperature. A non-denaturing mobile phase was selected consisting of 25mM NaH₂PO₄, 25mM Na₂HPO₄, 150mM NaCl; pH 7.0. The column was calibrated with a Low Molecular Weight Gel Filtration Calibration Kit (GE Healthcare Life Sciences) according to the manufacturer's instructions. Calibration standards included Aprotinin (6.5kDa), RNAase A (13.7kDa), Carbonic Anhydrase (29kDa), Ovalbumin (44kDa), and Conalbumin (75kDa). Purified TPI samples were diluted to 15 μ M in mobile phase and 100 μ l were injected and measured in triplicate, and their

elution monitored at 280nm. Chromatography traces were collected and analyzed using EZStart 7.3 (Shimadzu) to quantify the relative monomer and dimer populations. Curve integration data were compared using a one-way ANOVA with Tukey's post-hoc analysis.

4.5.4 TPI Enzyme Assays

Isomerase activity was determined using an NADH-linked assay as previously detailed (1,132). Initial velocity of the enzyme was calculated over a GAP (Sigma-Aldrich, St. Louis, MO, USA) range of 0.0094-4.23 mM; enzyme quantities as noted [Figure S1]. All kinetic measurements were performed three times in triplicate by monitoring the absorbance of NADH at 340 nm in a SpectraMax Plus 384 microplate reader (Molecular Devices). The assay was performed using 80 μ l mixtures containing varied GAP and enzyme concentrations, 0.5 mM NADH (Sigma-Aldrich), and 1 unit glycerol-3-phosphate dehydrogenase (Sigma-Aldrich) in 100 mM triethanolamine (TEA), pH 7.6. Enzyme activity curves were normalized to reactions performed without GAP. Enzyme kinetics were determined by assessing initial velocities taken during the linear phase of each reaction, and the data were fit to the Michaelis-Menten equation using nonlinear regression in Graphpad Prism 5.0b (GraphPad Software).

Lysate assays were performed similarly. Briefly, animals aged 1-3 days were collected and frozen in liquid nitrogen. Bodies lacking heads or appendages were isolated and homogenized in 100mM TEA pH 7.6 supplemented with cOmplete mini Protease Inhibitors (Roche Diagnostics). The homogenates were sonicated in an ice bath for 10min and centrifuged twice at 4°C for 5min at 5,000g to remove exoskeletal debris. Lysates were diluted to 0.1 μ g/ μ l in 100mM TEA pH 7.6 + inhibitors and enzyme activity was assessed. Reaction assays were performed using 80 μ l mixtures composed of 0.5mM NADH, 0.752mM GAP, 1 unit glycerol-3-

phosphate dehydrogenase and 1µg of lysate protein in 100mM TEA; pH 7.6. All reactions were performed in both experimental and biological triplicate. Reaction components were purchased from Sigma-Aldrich.

4.5.5 Circular dichroism and thermal stability

Circular dichroism (CD) thermal stability analysis was performed on a Jasco J-810 as outlined previously (63). Briefly, samples were diluted to 350µg/ml in 0.2µm nylon-filtered 20mM MOPS, 1mM DTT, 1mM EDTA pH 7.4, and denaturation was monitored at 222 nm over 20-80°C at a rate of 0.267°C/min with a pitch of 0.2°C. Far-UV spectra were taken in 1X PBS at indicated temperatures for better resolution (63). DL-glycerol-3-phosphate (Sigma), a TPI substrate analog (176-178), was added to a final concentration of 5mM (185) and thermal stability reassessed. All spectral data were acquired 5 times per step, and three independent replicates were run for each experimental condition.

4.5.6 Behavioral testing and lifespan analysis

Mechanical stress sensitivity was examined by vortexing the animals in a standard media vial for 20 seconds and measuring time to recovery, similar to (66,133). Thermal stress sensitivity was assessed by acutely shifting animals to 38°C and measuring time to paralysis, as previously described (65,109). Paralysis was defined as being at least a 15sec period. All behavioral responses were capped at 600 seconds. Animal lifespans were performed at 25°C as previously described (109). A nonparametric Student's t test was used to assess behavior, and lifespans were assessed with Log-rank (Mantel–Cox) survival tests.

4.5.7 Immunoblots

Animals were collected aged 1-2 days at room temperature. Ten fly heads were obtained in triplicate from each genotype and processed as outlined previously (86). Briefly, the fly heads were ground by pestle in 80 μ l 2 \times SDS-PAGE sample buffer (4% SDS, 4% β -mercaptoethanol, 130 mM Tris-HCl pH 6.8, 20% glycerol) and centrifuged for 5 minutes at 5000 **g** to pellet the exoskeleton. Proteins were resolved by SDS-PAGE and transferred onto 0.45 μ m PVDF membrane. Following treatment in 1% milk PBST, the blots were incubated with anti-TPI (1 : 5000; rabbit polyclonal FL-249; Santa Cruz Biotechnology) or anti-Beta tubulin (1 : 4,000; rabbit polyclonal d-140; Santa Cruz Biotechnology). The blots were washed in PBST, incubated in the appropriate HRP-conjugated secondary antibody, and developed using ECL (Pierce). Densitometric analyses of the scanned films were performed digitally using ImageJ software available from the National Institutes of Health. Student's unpaired t test was performed to assess differences in TPI.

4.5.8 Protein crystallization and structural determination

Recombinant human TPI and hTPI^{I170V} protein and was purified as described above. Initial TPI crystals were grown at 4 $^{\circ}$ using the sitting drop vapor diffusion method against a reservoir solution containing 34% PEG 2000 MME and 50 mM KBr. These initial crystals were improved by microseeding using a reservoir solution containing 30-34% PEG 2000 MME and 50 mM KBr. The crystals used for data collection, grew to final dimensions of \sim 100 x 100 x 150 μ m over the course of 3 days prior to harvesting. Crystals were cryoprotected by transition of the crystal into reservoir solution supplemented to 40% PEG 2000 MME and 20% glycerol followed

by flash freezing in liquid nitrogen. Diffraction data for wild type TPI were collected at the National Synchrotron Light Source on beamline X25 using a Pilatus 6M detector. Diffraction data were integrated, scaled, and merged using HKL2000 (186). Wild-type crystals belong to the space group $P2_1$ ($a = 47.92 \text{ \AA}$, $b = 48.85 \text{ \AA}$, $c = 93.97 \text{ \AA}$; $\beta = 103.66^\circ$) and contain a dimer in the asymmetric unit. Crystals of hTPI^{I170V} belong to space group $P2_12_12_1$ ($a = 64.92 \text{ \AA}$, $b = 73.64 \text{ \AA}$, $c = 91.77 \text{ \AA}$), and also contain a dimer in the asymmetric unit. Initial phases for both wild-type and hTPI^{I170V} were estimated via molecular replacement using a search model derived from an independent structure of human TPI (2VOM) (63). The model was then refined against native data and improved by manual rebuilding within Coot (187) combined with simulated annealing, positional, and anisotropic B factor refinement within Phenix. For hTPI^{I170V}, isotropic B-factor and TLS refinement was used. Model quality for both structures was assessed using MolProbity (188). Structural figures were generated using PyMol (PyMOL Molecular Graphics System, Version 1.5.0.4, Schrödinger, LLC.).

5.0 DISCUSSION

Prior to the initiation of my thesis work, very little was known about the pathogenic nature of TPI deficiency. Due to the rarity of the disease and disparate patient allelic combinations, it was not entirely clear which TPI mutations were sufficient to cause neurological phenotypes. Work in this field was often limited to description due to the dearth of primary tissue samples and a lack of robust model systems. Yet in the past few years of my graduate work I have helped establish a genomic engineering system for the *Drosophila* TPI locus, and this system facilitated hypothesis-driven experimentation on the pathogenesis of TPI deficiency. Establishing this system, I used these resources to examine whether the presence of the enzyme or its catalysis were most critical to the behavioral phenotypes seen in our animals. In these initial studies I found that an inactive variant of TPI was capable of fully complementing our disease mutant, and biochemical data supported this conclusion, revealing that this complementation occurred without gross changes in enzyme catalysis or alleviating metabolic stress. These data suggested that it was unlikely that TPI deficiency was being caused by a general metabolic defect, and instead pointed to the possibility that it could be due to a conformational change in the protein. To test this hypothesis, I worked in collaboration with the VanDemark lab to purify and characterize the TPI^{M80T} protein.

Physical analyses revealed a dimerization defect associated with TPI^{M80T}, a characteristic shared by the highly toxic human disease-associated mutation, TPI^{E104D} (63). Independent

mutations at the dimer interface of TPI, TPI^{I74R} and TPI^{G75E} , further underlined the relationship between dimer conformations and disease. These mutations exhibited more severe phenotypes than our previously characterized TPI^{M80T} allele, and their behaviors suggested the possibility of underlying conductive or synaptic dysfunction. Indeed, vesicle recycling experiments indicate synaptic dysfunction, and although I have not established a precise biochemical mechanism for these effects, they demonstrate that the neurological dysfunction seen in TPI Deficiency patients arises from a vesicle recycling defect. Further work will clearly be needed to establish the exact mechanism of the pathogenesis, but my observations are the first to establish a synaptic phenotype in TPI deficiency.

Finally, the last of my dissertation work sought to focus our GE system on an understudied human disease-associated mutation. As mentioned earlier, prior to my work it was not understood whether certain human TPI mutations were sufficient for pathology. One such mutation, a TPI^{I170V} missense mutation, has now been established as sufficient for eliciting neurological dysfunction in *Drosophila*. Further, a detailed structural and biochemical analysis of this protein indicated a unique increase in substrate affinity, homodimerization, and thermal stability. Structural analyses revealed that the I170V substitution facilitated the internal rotation of S96 into the catalytic pocket of TPI^{I170V} . The rotation of this S96 residue stabilized a hydrogen bond network within the catalytic pocket, and is responsible for the increase in substrate affinity and reduction in catalytic turnover. Data from the crystal structure and stability assays suggest that TPI^{I170V} is preferentially in the closed lid conformation, and this closed lid is likely the mechanism responsible for the observed increase in enzyme stability. These observations are provocative in their implications regarding cellular recognition of enzyme activity and protein regulation.

5.1 TPI PROTEIN CONFORMATION AND DISEASE

In the last two decades several reviews have been written summarizing the collective observations of the community and literature surrounding TPI deficiency (26,45,48,189). With the dearth of model experimental systems, these reviews have relied heavily on the initial clinical characterizations of the disease and a few descriptive studies of erythrocytes derived from patients. This research has been critical for understanding the relationship between TPI mutations and the human disease, yet lacked the hypothesis-driven approaches found in controlled systems. The authors of these reviews should be commended for highlighting of the poorly understood link between TPI activity and disease, with many citing the diverse observations of protein activity, cellular metabolism and protein levels. Indeed, a review which structurally plotted all of the known human mutations was the first to propose the idea that protein conformation could be the basis of TPI deficiency pathology (45). This hypothesis was followed up by a yeast molecular study by the Krobitch lab and structural/biochemical analyses by the Torres-Larios lab which determined the TPI^{E104D} human mutation affected protein dimerization and therefore quaternary structure (62,63). These articles were the first to lend substantial support to the hypothesis that TPI deficiency is a conformational disease.

Many conformational diseases are elicited by changes in protein quaternary structure, with the most common being gain-of-function changes leading to aggregation (138). However, it has been well-established that conformational loss-of-function diseases are also possible, with the most prevalent being mutations in the tumor-suppressor p53. p53 is a highly regulated transcription factor, intimately related to DNA repair and cell cycle progression (190,191). Conformational changes in p53 can result in an inability to appropriately tetramerize and bind DNA (192), an alteration of binding to regulatory proteins (193), changes in localization signals

(194), etc. Mutations of p53 are found in approximately 50% of cancers, and almost all cancers influence either it or members of its network, underlining the protein's relevance to human disease (195). I propose that TPI deficiency could be elicited by a similar loss-of-function due to protein conformation – likely through changes in enzyme transport to distal cellular locations.

The TPI reviews were critical in shaping my understanding of the field as I was initiating my experiments. I was fortunate to be working with a whole animal model of TPI deficiency which allowed for such analyses, and these inspirations directed me to question whether gross activity and metabolism were truly necessary contributors to the behavioral and longevity phenotypes we saw in our *Drosophila*. To this end, my initial studies focused on whether a depletion of TPI protein or catalytic activity were more critical determinants of *Drosophila* TPI deficiency. I engineered a constitutively inactive variant of TPI and sought to assess complementation of our *TPI*^{M80T} mutant allele; a general strategy employed in the evaluation of several molecular fields (196-198). The results of these experiments indicated the inactive TPI was able to fully complement *TPI*^{M80T}. Further experiments established that this was not due to changes in gross lysate TPI activity, *TPI*^{M80T} protein levels, or an insect marker of metabolic stress. Later experiments established that the *TPI*^{M80T} mutation reduced dimerization of TPI, and independent mutations of TPI at the dimer interface were also sufficient to elicit disease. These same experiments established that some of the most toxic TPI alleles were characterized by dramatically more lysate isomerase activity than completely healthy animals, firmly establishing that gross catalytic activity is not predictive of disease presence or severity, and instead suggesting that protein conformations are more likely the critical determinants of disease.

To contrast these results, I selected a human disease-associated mutation at the catalytic site for further evaluation. This point mutation, *TPI*^{I170V}, was examined in the context of the

human protein in *Drosophila* for its sufficiency to elicit pathology, as it had only ever been identified in a *trans*-heterozygote state in humans, paired with a TPI^{E104D} allele. We again saw pathology in these $hTPI^{I170V}$ animals as contrasted by $hTPI^{WT}$. Detailed characterization of enzyme kinetics revealed that the mutation elicited a marked change in enzyme activity, with I170V eliciting an increase in substrate affinity and a decrease in catalytic turnover. Noting that dimerization can influence catalytic activity, we sought to examine the converse relationship – whether changes in the catalytic site could influence dimerization and stability. Gel filtration results indicated that $hTPI^{I170V}$ exhibited an increase in dimerization and enzyme stability. In collaboration with the VanDemark lab, X-ray crystal structures of each protein were generated and analyzed. Resolutions of 1.6 and 2.0Å were achieved in the WT and I170V structures, respectively, allowing near-atomic comparisons of protein conformations. The crystal structure indicated that the shortening of the I170 residue to V170 facilitated the rotation of a proximal S96 into the catalytic site, reinforcing a water network within the catalytic pocket. This water network increased substrate affinity, reduced enzyme turnover, and led to a generally closed lid conformation. The crystal structure failed to reveal any obvious changes at the dimer interface. Indeed, the only changes observed at the critical dimer interface loop 3 revealed backbone and therefore residue shifts of 0.4-0.6Å, just outside the cumulative resolution error of 0.4Å for any pairwise comparison of these structures. However, thermal stability experiments suggested that the I170V substitution elicited a protein conformation also induced by catalytic site occupancy. These data collectively suggest that an occupied or closed catalytic lid yields a more stable enzyme. The basic implications of active site conformation and putative changes in stability are intriguing, and could be a means for a protein to autonomously regulate its own turnover. Extending this type of analysis to similar soluble, oligomeric, cytosolic proteins could have

stimulating implications on the turnover of cytosolic substrates, as comparatively little is known these regulatory mechanisms versus that of the endoplasmic reticulum.

5.2 DIMERIC COOPERATION AT THE CATALYTIC SITE

One of the key results that I have struggled with during the course of my thesis has been the inexplicable differences in pathology as a result of various TPI structural modifications and allelic combinations. In particular, I have found it difficult to explain the healthy behavior of $TPI^{T74R}/TPI^{\Delta cat}$ and $TPI^{M80T}/TPI^{\Delta cat}$, versus the moderate behavioral dysfunction of $TPI^{G75E}/TPI^{\Delta cat}$ and the complex behavioral and longevity phenotypes of $TPI^{T74R,G75E}/TPI^{\Delta cat}$. The capacity of an inactive enzyme to rescue two severe mutant *TPI* alleles is astonishing. Yet an inability for this same inactive allele to similarly complement two other dimer mutations has led me to conclude that $TPI^{\Delta cat}$ is not alone sufficient for adult rescue, suggesting requisite interactions within the heterodimer. Again, the pathology does not seem to be determined by gross isomerase activity, and an analysis of heterodimer populations failed to suggest an underlying mechanism. Further, the capacity of a catalytic site mutation, TPI^{I170V} , to similarly elicit pathology cumulatively suggests the importance of microdomains of activity as a pathological mechanism. Indeed, a conformational change in the protein could merely affect trafficking and/or stabilization of small pools of active heterodimers at a requisite site. However, if one proposed that the inactive enzyme rescued pathology through increased trafficking of the still-active allele ($TPI^{T74R}/TPI^{\Delta cat}$ for example), then it would follow that this interaction would likely be stronger than a comparatively poorly rescued variant ($TPI^{G75E}/TPI^{\Delta cat}$) [Figure 30]. However, coimmunoprecipitation experiments detailed almost the opposite phenomenon.

Clearly physical interactions alone do not explain the complementation of the disease phenotypes. Yet if activity is to be achieved by the heterodimer, how could this occur in TPI^{T74R}:TPI^{Δcat} and TPI^{M80T}:TPI^{Δcat} but not TPI^{T74R,G75E}:TPI^{Δcat}?

To address putative changes in heterodimer catalysis I sought to analyze the crystal structures and known mechanisms of dimeric cooperation and TPI catalysis. The dimer interface of TPI is composed of a mixture of hydrophobic and hydrogen bond interactions which ultimately contribute toward the rigidification of the catalytic site of each monomer (199,200). Hydrogen bonds established by water molecules sequestered at the dimer interface further facilitate this dimeric cooperation, and are themselves participants in the catalytic process (201). To help explain this cooperation, the monomers involved in this interplay will be referred to as A and B.

The cooperative nature of TPI catalysis is best exemplified by the extension of the 3rd loop of TPI[A] toward the catalytic site of its partner [B]. The residues of this loop are entirely conserved and catalytic simulations suggest that T74[A] flips “in” and “out” toward its dimer partner’s catalytic site, alternating the coordination of a catalytic H95[B] (21). The alternating nature of this interaction allows the substrate to facilitate rapid de- and re-protonation of E165[B] and H95[B] in sequence. This shuttling of protons between these catalytic residues is fundamental to the isomerization mechanism (202). Additionally, hydrophobic interactions provided by non-polar members of the 3rd loop [A] support the appropriate alignment of a catalytic N10[B] and K12[B] which are required for substrate binding and stabilization of substrate transition states (18). Without these hydrophobic support mechanisms it has been demonstrated that the active site of the monomer becomes highly flexible, resulting in dramatic reductions in substrate affinity and catalytic capacity (18).

Each catalytic site within the [A]:[B] dimer is independent of the other; inactivation of one catalytic site does not influence the substrate affinity or catalysis of the other unless the dimer interface is perturbed (203). This observation is important considering the nature of the proposed orientation of the TPI^{T74R} mutation. When first described, the T74R[A] mutant was predicted to fit within the bottom of the catalytic site of the [B] monomer when a dimer was forced by a modeling algorithm (19). Experimentally it was determined that the T74R mutation conveyed a strong disruption of the dimer interface leading to a largely monomeric population of TPI *in vitro*. To obtain a fully monomeric population of protein to examine, the authors generated an additional mutation at the G75 position, and the double mutant was confirmed to be completely monomeric (19).

I believe that the nuances in the positioning of these dimer interface mutations could ultimately be responsible for the complete phenotypic rescue via a catalytically inactive TPI to the TPI^{M80T} and TPI^{T74R}, but not the TPI^{G75E} and TPI^{T74R,G75E} alleles. Of the three mutations examined, M80T[A] and T74R[A] would be predicted to elicit their catalytic defects by i) reducing dimer affinity and ii) modulating the integrity of the catalytic pocket of TPI[B]. Conversely, G75E[A] is hypothesized to i) disrupt the 3rd loop flexibility provided by the G75 (21) thereby conveying stress back into TPI[A] upon dimerization, and ii) project into and displace important waters sequestered in the dimer interface which contribute to the catalysis of both [A] and [B]. These alternative positions, when heterodimerized with an inactive TPI[B], would lead to various catalytic outcomes for [A]. Importantly, both M80T[A] and T74R[A] would be left with an intact catalytic site [A] which if localized appropriately could contribute a modicum of isomerase activity [Figure 27]. Further, the displacement of K12[B] from Δ cat[B] may actually generate an amenable pocket for T74R[A]. Conversely, TPI isoforms containing

the G75E[A] mutation would continue to exhibit a dearth of local activity even when paired with an inactive partner[B].

5.3 SYNAPTIC TPI DEFICIENCY AND BEHAVIOR

Measurements of lysate isomerase activity have firmly established that gross isomerase activity is not predictive of presence or severity of TPI Deficiency, yet allelic interactions suggest some role for catalytic activity in this disease. These data could indicate the formation of catalytic microdomains [Figure 30] or differential enrichment of activity within specific tissues, both of which would be impossible to discriminate using our lysate isomerase assay. FlyAtlas – a tissue-based microarray survey of *Drosophila* gene expression – failed to detect a dramatic enrichment of TPI mRNA in the larval or adult CNS relative to the fly as a whole (204), suggesting that if tissue-specific differences in TPI activity were the culprit then regulation of these differences would occur at a translational or protein stability level. Based on the ubiquity of TPI expression, I would more simply suggest that if tissue-specific effects are occurring it is more likely that unknown secondary factors are contributing to these events, possibly forming microdomains of necessary activity. For example, aldolase is another glycolytic enzyme which is expressed ubiquitously and at relatively consistent levels (204). However, its localization to the endosome is required for vacuolar H⁺-ATPase (V-ATPase) assembly and function (119,120,205). Though V-ATPase function is important in all tissues, a loss of rapid acidification of vesicles, or poor maintenance of the proton gradient in endosomes could lead to dysfunction in receptor dynamics as well as vesicle loading.

Previously, the only secondary factors known to directly interact with TPI were the cytoskeletal protein cofilin and the sodium-potassium exchanging ATPase (Na,K-ATPase). Work in mammalian systems described the localization of TPI at the Na,K-ATPase by cofilin, and concluded that this was to establish a glycolytic complex to feed the ATPase (206). Experiments performed in the lab prior to my integration were unable to identify cofilin:TPI complexes [data not shown]. Additionally, my TPI::Na,K-ATPase genetic interactions yielded unclear results. Interestingly though, previous studies in our lab have detailed the sequestration of TPI^{M80T} by heat shock proteins 70 and 90 (Hsp70, Hsp90) (86). In this way, it is possible that the differences in TPI^{Δcat} complementation could be due to changes in this sequestration. Indeed, my discussion in Chapter 3 centered on the possibility of sequestration and degradation of TPI dimer mutations prior to their distal transport [Figure 30]. These assertions were based largely on *in vitro* analyses which demonstrated that these substitutions altered protein stability. Future experiments could focus on the capacity of TPI^{Δcat} to protect TPI mutants from sequestration by chaperones. Additionally, changes in enzyme stability could be assessed *in vivo* through cotransformation of yeast with differently tagged variants of TPI dimer mutants and TPI^{Δcat}. Finally, restored distal trafficking could be measured *in vivo* using genetic complementation of fluorescently-tagged mutants.

To identify candidate tissues and subcellular locations where TPI function could be most critical, I turned to the mutant phenotypes. The vacuolar neuropathology of our TPI^{M80T} mutant *Drosophila* suggested the possibility of either neural or glial dysfunction, while their behavior left open the possibility of a muscular component. As described earlier, mechanical stress sensitivity and thermal stress sensitivity are phenotypes enriched for neurological dysfunction (72); several mutations that affect primarily glia or neurons have been shown to result in these

behaviors. Conversely, few mutations specifically influencing muscles have been established to do the same, with one of the few being a mutation in the sarco/endoplasmic reticulum calcium ATPase (SERCA) (207). Though *SERCA* mutations elicit thermal stress sensitivity, the hallmarks of this SERCA phenotype are basal hypoactivity, which is slowly exacerbated at the non-permissive temperature with no accompanying mechanical stress paralysis or seizures.

Therefore the confluence of both thermal- and mechanical dependant phenotypes, as well as the neuropathology provided the basis for looking specifically at the nervous system. Tissue-specific rescue experiments, often a strength of the *Drosophila* model system, were also examined. However, it was found that the initial transposon-mediated placement of the UAS-TPI transgenes exhibited substantial leak expression, confounding the rescue data. These results were unfortunate and precluded a proper genetic anatomical dissection. Recently, the McCabe laboratory has developed a new *attB*-mediated transgenic vector with gypsy insulator sequences to help protect the construct from chromatin positional effects and *cis*-regulatory elements (208). The *attB* sequences facilitate directed transgene placement in previously established locations in the genome (97,98). Additionally, noting the propensity for insulators to enhance leak when combined with the widely used UAS *hsp70* promoter (209,210), the authors leveraged a synthetic promoter construct in conjunction with the UAS system (211). Using these constructs, the authors established exquisite transgenic regulatory control in a number of diverse tissues, with transgenes positioned on different chromosomes (208). This system would likely be perfect for addressing our previous transgenic difficulties, facilitating a proper analysis of tissue-specific requirements of TPI and its relationship to longevity and behavior.

Though our anatomic transgenic strategies failed to establish a tissue-specific source of dysfunction, the extreme thermal stress dependant phenotype of *TPI^{T74R}* suggested a neuronal

source. As mentioned earlier, this type of acute phenotype has only been described in mutants which influence neural conductance or synaptic properties. An analysis of vesicle recycling at the synapse revealed a conditional inhibition of endocytosis under thermal stress [Chapter 3]. This progressive reduction in recycling was not observed at room temperature, and could be complemented by *TPI^{Δcat}*, much like the adult thermal stress-dependent paralysis [Chapter 3]. These data are the first to demonstrate that TPI Deficiency elicits neurologic dysfunction through a reduction in synaptic vesicle recycling. TPI has not previously been directly linked to any of the endocytic machinery, but a recent study indicated that vesicle recycling was the largest consumer of ATP at the synapse (135). This study established that glycolysis was a strong facilitator of vesicle recycling, and that glycolytic inhibition resulted in a quick cessation of vesicle endocytosis (135). I lacked the experimental time necessary to identify the exact biochemical mechanism, but predict that if TPI mutations reduce vesicle endocytosis through an inhibition of synaptic glycolytic flux, we should be able to phenocopy our mutant results in *TPI^{WT}* animals through the administration of glycolytic inhibitors such as 2-deoxyglucose. Similarly, bath applications of ATP or GTP with the addition of membrane pore-forming antibiotics should facilitate a conditional rescue of the mutant phenotypes.

Interestingly, Rangaraju and colleagues found that glycolytic inhibition had a greater influence over vesicle recycling than inhibition of OXPHOS (135). The conclusions of this study were hinted at previously by Verstreken and colleagues, wherein the authors were able to inhibit synaptic mitochondrial transport, yet still achieve normal vesicle recycling (212). Finally, previous work performed by the Littleton group also indicated a reduction in vesicle recycling through a mutation in phosphoglycerate kinase, an ATP-producing step of glycolysis (158).

Collectively, these studies suggest that glycolytic ATP is the primary energy source for vesicle recycling, and these findings strongly support a catalytic role for TPI in vesicle recycling.

As mentioned previously, *Drosophila* TPI Deficiency is a multi-phenotype condition, consisting of both mechanical- and thermal-stress induced seizure and paralytic phenotypes. The work presented in Chapter 3 demonstrates a physiologic mechanism responsible for the thermal-stress induced paralysis, but does not clarify the pathogenesis of the mechanical-stress induced seizures. A survey of mechanical-stress sensitive mutants reveals they are enriched for metabolic and mitochondrial mutants, including genes encoding citrate synthase (213), ethanolamine kinase (214), a mitochondrial ribosomal protein (215), ATP6 of the electron transport chain (216), mitochondrial superoxide dismutase 2 (217), triosephosphate isomerase (50), and the adenosine nucleotide translocase (218). Many of these reports originally focused on the bioenergetic effects of these mutations, but an emerging theme among these alleles has been an increasingly prevalent thread of altered cellular redox chemistry.

In the *TPI*^{M80T} mutant it has been shown that lysate NAD⁺/NADH ratios shift toward an oxidative state (35). A buildup of cytosolic NAD⁺ or NADP⁺ could have dramatic consequences on general excitability through their capacity to regulate various K⁺ channels and TRPM2. Mutations in GAPDH, the primary cytosolic source of NADH, have not been identified as a source of disease in human patients. This lack of disease-association, coupled with the central importance of GAPDH as a regulator of vesicle transport (219), cytosolic NADH production, its contributions as a transcription factor (123) and regulator of apoptosis (220) all suggest lethality. However, inhibiting TPI function would have a clear impact in NADH production through its restriction of glycolysis. In this way, it is possible that TPI dysfunction may specifically restrict NADH production. Accumulation of NAD⁺ in the cytosol could activate K⁺ or TRP channels,

thereby altering circuit excitability. Two-electrode voltage clamp experiments at the *Drosophila* neuromuscular junction would facilitate the analysis of mini excitatory post-junctional currents, as well as summation properties of excitability at the presynaptic terminal. Failure rates when following train stimuli could also suggest conductance defects. Finally, if an aberrant phenotype is revealed, the nature of these preparations would allow the introduction of pharmacologic redox modifications, facilitating an examination of redox status in these specific mutants.

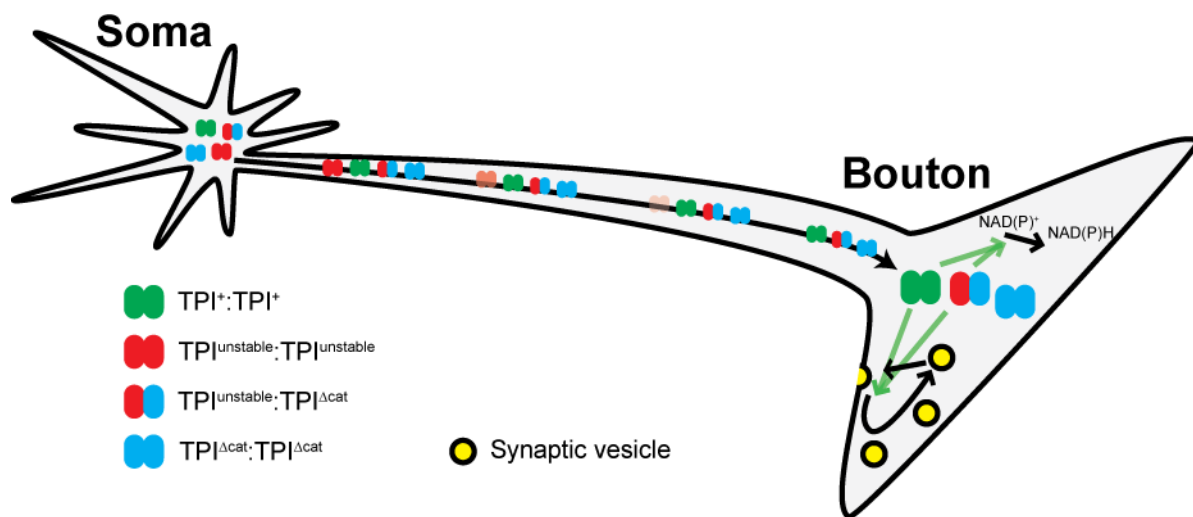


Figure 30. Hypothesized model of TPI behavioral pathogenesis. Long-distance transport of glycolytic proteins is required for their delivery to the boutons. **Wild type TPI (green)** is transported to the terminal, enhances glycolytic flux, maintains cellular redox potential, and facilitates **synaptic vesicle endocytosis**. Conversely, an **unstable (red)** and **inactive (blue)** TPI are sequestered and degraded, and/or unable to support chronic endocytosis and appropriate redox chemistry. I hypothesize that the genetic complementation of the **inactive** and **unstable** variants are likely capable of restoring transport and localized activity at the bouton (**red/blue**).

To support any potential synaptic redox data, measurements of NAD⁺ and NADH have been performed optically *in vivo* and in *in vitro* cell cultures (221-223). These strategies could be a means to link the complementation of TPI mutants with a biochemical mechanism. The

capacity of an inactive allele of *TPI* to fully complement the behavioral defects of two dimer interface *TPI* mutants (*TPI*^{T74R}, *TPI*^{M80T}), but incompletely attenuate two others (*TPI*^{G75E}, *TPI*^{T74R,G75E}) suggested the necessity of heterodimer interactions. Yet coimmunoprecipitation experiments assessing heterodimer populations suggested no obvious role for heterodimers. Lysate measurements of protein levels, enzyme activity, and protein-protein interactions may not reflect the events occurring at a distal element like the synapse. It is possible that the inactive allele provides complementation through a small population of heterodimers exhibiting a structural interaction – as outlined previously – to restore localized catalytic activity [Figure 30]. This type of catalytic influence could provide the means to restore robust production of cytosolic NADH at critical microdomains at the synapse or in the axon [Figure 30]. Indeed, future experiments will require examination of localization and quantification of *TPI* populations at the nerve terminal. This will be accomplished by optical measurements of C-terminal CFP tags I have recently added to each of the *TPI* dimer interface mutations. Further, genetic interactions with the inactive allele could be assessed for the capacity to modulate the presence of the active *TPI* variants at the synapse, perhaps through small changes in stability, increased trafficking, or protection from sequestration.

5.4 EVOLUTIONARY MAINTENANCE OF *TPI* DYSFUNCTION

An interesting observation made by Arthur Schneider, the patriarch of *TPI* deficiency research, has been the wide-spread persistence of loss-of-function mutations within the *TPI* gene (26). Dr. Schneider's work has detailed up to a 40% prevalence of promoter mutations in African-American populations, and roughly 2-4% in European and Asian populations (55). The

pervasiveness of these mutations in the face of their homozygous lethality and disease has been extremely curious, resulting in several epidemiologists to suggest an advantage – though clearly not a selection – for the heterozygous condition. My studies have established a definitive survival advantage for *Drosophila* heterozygous for a loss-of-function mutation at the dimer interface. These experiments were initially meant to probe possible dominant negative effects of the dimer interface mutations, yet their data reveal the first demonstration of a distinct heterozygote advantage.

Given the role of TPI in metabolism, it is likely that this extension in longevity is achieved through a well-established means of caloric restriction. Indeed, a population survey of glycolytic loss-of-function revealed a relatively high level of genetic maintenance for TPI and pyruvate kinase dysfunction in particular (56). Decades of work supports this idea that caloric restriction extends longevity, though the mechanisms responsible for this extension have been hotly debated. It has been proposed that caloric restriction extends longevity by several possible means: reduced oxidative stress, reduced DNA damage, and hormesis. Based on TPI's established ability to reroute glycolytic intermediates through the pentose phosphate pathway (PPP), I would contend the partial loss-of-function likely reduced oxidative stress in our animals, though I have no experimental data to support this assertion.

5.5 NEW FRONTIERS IN GENOMIC ENGINEERING

Little of the science presented here would have been possible if not for genomic engineering (GE). The GE used in these studies is an incredibly powerful technique for the evaluation of a single gene. As has been shown previously, the true value of this approach is its rapid generation

of diverse alleles once the founder line has been established. Importantly, all of these newly generated alleles utilize endogenous regulatory mechanisms to achieve normal spatial, quantal, and temporal regulation. These alleles can then be compared in similar genetic backgrounds to facilitate beautiful genetic experiments featuring the perfect controls. Further, the use of endogenous promoter elements ensures that your work will not be complicated by possible overexpression or misexpression artifacts. Transgenic overexpression is a well-established danger for any molecular geneticist, as you are biasing the evaluation of your molecule in the face of its poorly understood mechanisms of action. For example, if your protein of interest were to form stoichiometric protein complexes, the overexpression of said transgene could have deleterious effects on the purposeful regulation of its partners. Scaffolding molecules such as the sodium-hydrogen regulatory exchange factor1 (NHERF1) (224) and post-synaptic density protein 95 (PSD95) (225) are difficult to study in part due to the importance of stoichiometry. Further, overexpression of wild type could fail to achieve its desired effect without compensatory amplification of its complex partners, resulting in a falsely negative result. A simple example of these principles can be seen in the expression of the Na,K-ATPase. The Na,K-ATPase is composed of two primary subunits, an alpha and a beta. The alpha subunit is the primary catalytic component of the ATPase, yet it will not leave the endoplasmic reticulum without complexing with beta for transport (226). In this way, overexpression of alpha without beta could result in false negative results.

Another pitfall of traditional transgenic expression is the use of linked expression systems, wherein you leverage an independent promoter to drive the expression of your transgene. Using a linked expresser system exposes you to misexpression of your molecule in tissues for which it may lack a function or elicit a new one. For example, genes such

hemoglobin perform diverse roles depending on the tissue in which it is expressed. Hemoglobin's function as an oxygen-carrier in erythrocytes is well-defined. However, its ability to bind other gas molecules has recently implicated hemoglobin as a regulator of nitric oxide signaling between the vasculature and muscle (9-11). Additionally, its function as a metal chelator could deplete important tissues of vital cofactors necessary for other protein functions. In this manner, conclusions made from an incompletely characterized promoter could achieve off-target effects, necessitating the utilization of multiple redundant drivers for the confirmation of tissue-specificity. However, all of these concerns have been anticipated in the genomic engineering system, as the critical viral integration site was knocked into the endogenous gene locus.

Yet there are definite drawbacks to the implementation of the genomic engineering technology. In particular, the inefficiencies of homologous recombination have been well-documented, and often discourage the inexperienced from utilizing these powerful genetic technologies. Upon initiating an HR project, a scientist has little way of knowing how amenable the targeted gene locus will be to recombination. To this end, leveraging a genetic lesion technology in conjunction with the *attP* knock-in could be a tremendous tool for enhancing the efficiency of founder line generation. The new CRISPR system utilizes an RNA-Cas9 methodology to elicit guided double strand breaks in the genome (227,228). This system has been lauded as a new and highly efficient means of generating targeted gene knockouts, yet its leverage toward genomic engineering would be of much greater utility.

The introduction of both 5' and 3' double strand breaks within the genomic engineering homology arms would dramatically increase the rate of homologous repair, thus increasing the knock-in rate to generate the founder lines (229,230). The challenges of such a strategy are the

generation and administration of the targeted guide strand RNAs, necessitating embryonic co-injection of these constructs with linearized *pGX* constructs for the initial recombination event (229,230). Incredibly, the authors utilized two guide RNA-targeted Cas9s to cleave 5' and 3' their desired 4.6kb gene locus, and used a simple 160 nucleotide (nt) single stranded donor with 50nt homology arms to mediate a 3.3% replacement of their gene (229). This combinatorial strategy could have dramatic effects on the time and monetary investments required for genomic engineering. However, this is clearly a mutagenesis-based, reductionist approach, and thus has inherent limitations.

5.6 MUTAGENESIS: FORWARD, REVERSE, AND EVERYTHING IN BETWEEN

Since the establishment of modern genetic research by Thomas Hunt Morgan and his students, mutagenesis has been a tool for the investigation of genome organization as well as its content. Much of the fundamental work on the organization of chromosomes, genes, and heredity was first performed using phenotypic markers derived from mutations. Yet upon the establishment of the gene as a discrete entity, forward genetics has been a means to expand our understanding of biology. Through the induction of both gain-of-function and loss-of-function mutations, generations of scientists have probed the biological functions of our increasingly broad catalog of genes. This forward genetic strategy has consistently pushed the boundaries of our understanding and remains one of the primary mechanisms of discovery-based science.

Yet as molecular technology has advanced, we have developed and refined our understanding of genetic architecture, as well as the molecules responsible for its persistence. The identification of nucleic acids and the genetic code, the polymerases responsible for its

replication, and the repair mechanisms which maintain integrity were all landmark discoveries which have facilitated our current understanding of the gene. In turn scientists have taken these discoveries and leveraged them into technologies with which to intentionally modulate the gene with the goal of intentionally changing its content, yielding the field of reverse genetics.

In the course of my thesis work I have utilized observations and techniques owing from both forward and reverse genetic principles. The impetus for my thesis work, the *TPI^{M80T}* (*sugarkill* – *TPI^{sgk}*) allele, was first identified in a forward genetic screen. Yet the entirety of my dissertation research has been a tour de force in reverse genetics – utilizing a structure-function-physiology-behavior experimental paradigm. I have endeavored as a reductionist to relate changes in protein structure to important phenotypic consequences. I have felt that working within a model system which allowed me to observe obvious whole-animal phenotypes was an important strategy for ensuring the impact of my experiments, maintaining their biological importance. Yet in reflection on my thesis work, I feel that I relied too heavily on these reverse genetic principles, at times to the exclusion of good observation-based investigative science.

My experience with reverse genetic approaches has left me with an intimate understanding of its strengths and weaknesses. I have leaned heavily on structural biology to develop hypotheses surrounding physical TPI regions of putative biological importance. Yet from my mutagenesis experiments I have found that there are seemingly endless ways of disrupting function, and the means to define uniting principles are not always obvious. The core of this problem is inherent in the complexity of my *in vivo* system. Genes are not singly demarcated entities within a larger framework of the chromosome. Genes are integrated components of biology which cumulatively lead to a complex interactive system. Genomic modifications of a single nucleotide within the framework of an organism will lead to

complications arising from not only its particular alteration, but that of its effectors and effectors. Reverse genetics is the most appropriate approach when asking questions with clearly defined players. How does protein X interact with protein Y? How does enzyme Q catalyze the isomerization of substrate R? Yet in my case, I was making observations not merely at the biochemical level, but within the context of biology.

I was performing experiments with reductionist approaches, yet my initial observation of complementation with a catalytically inactive allele clearly demonstrated an ignorance of all the effectors and effectors of TPI. I continued my reverse genetic approach, establishing that dimerization defects were sufficient to elicit pathology, but spent too much time in this mindset as I struggled with interpreting my genetic interactions. It was not until the end of my dissertation work that I retooled and took an observation-based investigative angle. I consider it extremely unfortunate that it took me so long to initiate my experiments looking at synaptic dynamics, though I consider it one of the more important turning points for my science and my development as a scientist. Observation-based science is extremely valuable in generating questions with testable hypotheses, which can then utilize reverse approaches; and the role of forward genetics is simply the means to make novel observations. Clearly there is no one experimental approach that is more valuable than the others – each has its strengths and weaknesses – and in reflection, I think good science is simply the recognition and application of whatever approach is necessary to address the question at hand. ...with appropriate controls of course.

BIBLIOGRAPHY

1. Roland, B. P., Stuchul, K. A., Larsen, S. B., Amrich, C. G., Vandemark, A. P., Celotto, A. M., and Palladino, M. J. (2013) Evidence of a triosephosphate isomerase non-catalytic function crucial to behavior and longevity. *J Cell Sci* **126**, 3151-3158
2. Nagano, N., Orengo, C. A., and Thornton, J. M. (2002) One fold with many functions: the evolutionary relationships between TIM barrel families based on their sequences, structures and functions. *J Mol Biol* **321**, 741-765
3. Hosfield, D. J., Guan, Y., Haas, B. J., Cunningham, R. P., and Tainer, J. A. (1999) Structure of the DNA repair enzyme endonuclease IV and its DNA complex: double-nucleotide flipping at abasic sites and three-metal-ion catalysis. *Cell* **98**, 397-408
4. Gulbis, J. M., Mann, S., and MacKinnon, R. (1999) Structure of a voltage-dependent K⁺ channel beta subunit. *Cell* **97**, 943-952
5. Moser, J., Gerstel, B., Meyer, J. E., Chakraborty, T., Wehland, J., and Heinz, D. W. (1997) Crystal structure of the phosphatidylinositol-specific phospholipase C from the human pathogen *Listeria monocytogenes*. *J Mol Biol* **273**, 269-282
6. Kim, J. W., and Dang, C. V. (2005) Multifaceted roles of glycolytic enzymes. *Trends Biochem Sci* **30**, 142-150
7. Ashizawa, K., and Cheng, S. Y. (1992) Regulation of thyroid hormone receptor-mediated transcription by a cytosol protein. *Proc Natl Acad Sci U S A* **89**, 9277-9281
8. Kato, H., Fukuda, T., Parkison, C., McPhie, P., and Cheng, S. Y. (1989) Cytosolic thyroid hormone-binding protein is a monomer of pyruvate kinase. *Proc Natl Acad Sci U S A* **86**, 7861-7865
9. Jia, L., Bonaventura, C., Bonaventura, J., and Stamler, J. S. (1996) S-nitrosohaemoglobin: a dynamic activity of blood involved in vascular control. *Nature* **380**, 221-226
10. Gladwin, M. T., Lancaster, J. R., Jr., Freeman, B. A., and Schechter, A. N. (2003) Nitric oxide's reactions with hemoglobin: a view through the SNO-storm. *Nat Med* **9**, 496-500
11. Straub, A. C., Lohman, A. W., Billaud, M., Johnstone, S. R., Dwyer, S. T., Lee, M. Y., Bortz, P. S., Best, A. K., Columbus, L., Gaston, B., and Isakson, B. E. (2012) Endothelial cell expression of haemoglobin alpha regulates nitric oxide signalling. *Nature* **491**, 473-477
12. Alagona, G., Ghio, C., and Kollman, P. A. (1986) Simple model for the effect of Glu165---Asp165 mutation on the rate of catalysis in triose phosphate isomerase. *J Mol Biol* **191**, 23-27
13. Pompliano, D. L., Peyman, A., and Knowles, J. R. (1990) Stabilization of a reaction intermediate as a catalytic device: definition of the functional role of the flexible loop in triosephosphate isomerase. *Biochemistry* **29**, 3186-3194

14. Thornalley, P. J. (2008) Protein and nucleotide damage by glyoxal and methylglyoxal in physiological systems--role in ageing and disease. *Drug Metabol Drug Interact* **23**, 125-150
15. Banner, D. W., Bloomer, A. C., Petsko, G. A., Phillips, D. C., Pogson, C. I., Wilson, I. A., Corran, P. H., Furth, A. J., Milman, J. D., Offord, R. E., Priddle, J. D., and Waley, S. G. (1975) Structure of chicken muscle triose phosphate isomerase determined crystallographically at 2.5 angstrom resolution using amino acid sequence data. *Nature* **255**, 609-614
16. Wierenga, R. K., Kapetaniou, E. G., and Venkatesan, R. (2010) Triosephosphate isomerase: a highly evolved biocatalyst. *Cell Mol Life Sci* **67**, 3961-3982
17. Borchert, T. V., Kishan, K. V., Zeelen, J. P., Schliebs, W., Thanki, N., Abagyan, R., Jaenicke, R., and Wierenga, R. K. (1995) Three new crystal structures of point mutation variants of monoTIM: conformational flexibility of loop-1, loop-4 and loop-8. *Structure* **3**, 669-679
18. Schliebs, W., Thanki, N., Eritja, R., and Wierenga, R. (1996) Active site properties of monomeric triosephosphate isomerase (monoTIM) as deduced from mutational and structural studies. *Protein Sci* **5**, 229-239
19. Schliebs, W., Thanki, N., Jaenicke, R., and Wierenga, R. K. (1997) A double mutation at the tip of the dimer interface loop of triosephosphate isomerase generates active monomers with reduced stability. *Biochemistry* **36**, 9655-9662
20. Blacklow, S. C., Raines, R. T., Lim, W. A., Zamore, P. D., and Knowles, J. R. (1988) Triosephosphate isomerase catalysis is diffusion controlled. Appendix: Analysis of triose phosphate equilibria in aqueous solution by ³¹P NMR. *Biochemistry* **27**, 1158-1167
21. Aqvist, J., and Fothergill, M. (1996) Computer simulation of the triosephosphate isomerase catalyzed reaction. *J Biol Chem* **271**, 10010-10016
22. Thakur, S. S., Deepalakshmi, P. D., Gayathri, P., Banerjee, M., Murthy, M. R., and Balaram, P. (2009) Detection of the protein dimers, multiple monomeric states and hydrated forms of Plasmodium falciparum triosephosphate isomerase in the gas phase. *Protein Eng Des Sel* **22**, 289-304
23. Perez-Montfort, R., Garza-Ramos, G., Alcantara, G. H., Reyes-Vivas, H., Gao, X. G., Maldonado, E., de Gomez-Puyou, M. T., and Gomez-Puyou, A. (1999) Derivatization of the interface cysteine of triosephosphate isomerase from Trypanosoma brucei and Trypanosoma cruzi as probe of the interrelationship between the catalytic sites and the dimer interface. *Biochemistry* **38**, 4114-4120
24. Berg, J. M., Tymoczko, J. L., and Stryer, L. (2012) *Biochemistry*, 7th ed., W.H. Freeman, New York
25. McKenna, M. C., Waagepetersen, H. S., Schousboe, A., and Sonnewald, U. (2006) Neuronal and astrocytic shuttle mechanisms for cytosolic-mitochondrial transfer of reducing equivalents: current evidence and pharmacological tools. *Biochem Pharmacol* **71**, 399-407
26. Schneider, A. S. (2000) Triosephosphate isomerase deficiency: historical perspectives and molecular aspects. *Baillieres Best Pract Res Clin Haematol* **13**, 119-140
27. Houtkooper, R. H., Canto, C., Wanders, R. J., and Auwerx, J. (2010) The secret life of NAD⁺: an old metabolite controlling new metabolic signaling pathways. *Endocr Rev* **31**, 194-223

28. Houtkooper, R. H., Williams, R. W., and Auwerx, J. (2010) Metabolic networks of longevity. *Cell* **142**, 9-14
29. Sauve, A. A., Wolberger, C., Schramm, V. L., and Boeke, J. D. (2006) The biochemistry of sirtuins. *Annu Rev Biochem* **75**, 435-465
30. Kaerberlein, M., McVey, M., and Guarente, L. (1999) The SIR2/3/4 complex and SIR2 alone promote longevity in *Saccharomyces cerevisiae* by two different mechanisms. *Genes Dev* **13**, 2570-2580
31. Lin, S. J., Kaerberlein, M., Andalis, A. A., Sturtz, L. A., Defossez, P. A., Culotta, V. C., Fink, G. R., and Guarente, L. (2002) Calorie restriction extends *Saccharomyces cerevisiae* lifespan by increasing respiration. *Nature* **418**, 344-348
32. Howitz, K. T., Bitterman, K. J., Cohen, H. Y., Lamming, D. W., Lavu, S., Wood, J. G., Zipkin, R. E., Chung, P., Kisielewski, A., Zhang, L. L., Scherer, B., and Sinclair, D. A. (2003) Small molecule activators of sirtuins extend *Saccharomyces cerevisiae* lifespan. *Nature* **425**, 191-196
33. Tissenbaum, H. A., and Guarente, L. (2001) Increased dosage of a sir-2 gene extends lifespan in *Caenorhabditis elegans*. *Nature* **410**, 227-230
34. Rogina, B., and Helfand, S. L. (2004) Sir2 mediates longevity in the fly through a pathway related to calorie restriction. *Proc Natl Acad Sci U S A* **101**, 15998-16003
35. Hrizo, S. L., Fisher, I. J., Long, D. R., Hutton, J. A., Liu, Z., and Palladino, M. J. (2013) Early mitochondrial dysfunction leads to altered redox chemistry underlying pathogenesis of TPI deficiency. *Neurobiol Dis* **54**, 289-296
36. Kilfoil, P. J., Tipparaju, S. M., Barski, O. A., and Bhatnagar, A. (2013) Regulation of ion channels by pyridine nucleotides. *Circ Res* **112**, 721-741
37. Tamsett, T. J., Picchione, K. E., and Bhattacharjee, A. (2009) NAD⁺ activates KNa channels in dorsal root ganglion neurons. *J Neurosci* **29**, 5127-5134
38. Liu, S. Q., Jin, H., Zacarias, A., Srivastava, S., and Bhatnagar, A. (2001) Binding of pyridine nucleotide coenzymes to the beta-subunit of the voltage-sensitive K⁺ channel. *J Biol Chem* **276**, 11812-11820
39. Pan, Y., Weng, J., Cao, Y., Bhosle, R. C., and Zhou, M. (2008) Functional coupling between the Kv1.1 channel and aldo-ketoreductase Kvbeta1. *J Biol Chem* **283**, 8634-8642
40. Tipparaju, S. M., Saxena, N., Liu, S. Q., Kumar, R., and Bhatnagar, A. (2005) Differential regulation of voltage-gated K⁺ channels by oxidized and reduced pyridine nucleotide coenzymes. *Am J Physiol Cell Physiol* **288**, C366-376
41. Hara, Y., Wakamori, M., Ishii, M., Maeno, E., Nishida, M., Yoshida, T., Yamada, H., Shimizu, S., Mori, E., Kudoh, J., Shimizu, N., Kurose, H., Okada, Y., Imoto, K., and Mori, Y. (2002) LTRPC2 Ca²⁺-permeable channel activated by changes in redox status confers susceptibility to cell death. *Mol Cell* **9**, 163-173
42. Sano, Y., Inamura, K., Miyake, A., Mochizuki, S., Yokoi, H., Matsushime, H., and Furuichi, K. (2001) Immunocyte Ca²⁺ influx system mediated by LTRPC2. *Science* **293**, 1327-1330
43. Kolisek, M., Beck, A., Fleig, A., and Penner, R. (2005) Cyclic ADP-ribose and hydrogen peroxide synergize with ADP-ribose in the activation of TRPM2 channels. *Mol Cell* **18**, 61-69
44. Schneider, A. S., Valentine, W. N., Hattori, M., and Heins, H. L., Jr. (1965) Hereditary Hemolytic Anemia with Triosephosphate Isomerase Deficiency. *N Engl J Med* **272**, 229-235

45. Orosz, F., Olah, J., and Ovadi, J. (2006) Triosephosphate isomerase deficiency: facts and doubts. *IUBMB Life* **58**, 703-715
46. Jogl, G., Rozovsky, S., McDermott, A. E., and Tong, L. (2003) Optimal alignment for enzymatic proton transfer: structure of the Michaelis complex of triosephosphate isomerase at 1.2-Å resolution. *Proc Natl Acad Sci U S A* **100**, 50-55
47. Humphries, A., Ationu, A., Wild, B., and Layton, D. M. (1999) The consequence of nucleotide substitutions in the triosephosphate isomerase (TPI) gene promoter. *Blood Cells Mol Dis* **25**, 210-217
48. Orosz, F., Olah, J., and Ovadi, J. (2009) Triosephosphate isomerase deficiency: new insights into an enigmatic disease. *Biochim Biophys Acta* **1792**, 1168-1174
49. Rosa, R., Prehu, M. O., Calvin, M. C., Daffos, F., and Forestier, F. (1986) Possibility of prenatal diagnosis of hereditary triose phosphate isomerase deficiency. *Prenat Diagn* **6**, 231-234
50. Celotto, A. M., Frank, A. C., Seigle, J. L., and Palladino, M. J. (2006) Drosophila model of human inherited triosephosphate isomerase deficiency glycolytic enzymopathy. *Genetics* **174**, 1237-1246
51. Clark, A. C., and Szobolotzky, M. A. (1985) Triose phosphate isomerase deficiency: prenatal diagnosis. *J Pediatr* **106**, 417-420
52. Zingg, B. C., Pretsch, W., and Mohrenweiser, H. W. (1995) Molecular analysis of four ENU induced triosephosphate isomerase null mutants in *Mus musculus*. *Mutat Res* **328**, 163-173
53. Schneider, A., Westwood, B., Yim, C., Cohen-Solal, M., Rosa, R., Labotka, R., Eber, S., Wolf, R., Lammi, A., and Beutler, E. (1996) The 1591C mutation in triosephosphate isomerase (TPI) deficiency. Tightly linked polymorphisms and a common haplotype in all known families. *Blood Cells Mol Dis* **22**, 115-125
54. Schneider, A., Westwood, B., Yim, C., Prchal, J., Berkow, R., Labotka, R., Warriar, R., and Beutler, E. (1995) Triosephosphate isomerase deficiency: repetitive occurrence of point mutation in amino acid 104 in multiple apparently unrelated families. *Am J Hematol* **50**, 263-268
55. Schneider, A., Forman, L., Westwood, B., Yim, C., Lin, J., Singh, S., and Beutler, E. (1998) The relationship of the -5, -8, and -24 variant alleles in African Americans to triosephosphate isomerase (TPI) enzyme activity and to TPI deficiency. *Blood* **92**, 2959-2962
56. Satoh, C., Neel, J. V., Yamashita, A., Goriki, K., Fujita, M., and Hamilton, H. B. (1983) The frequency among Japanese of heterozygotes for deficiency variants of 11 enzymes. *Am J Hum Genet* **35**, 656-674
57. Hollan, S., Fujii, H., Hirono, A., Hirono, K., Karro, H., Miwa, S., Harsanyi, V., Gyodi, E., and Inselt-Kovacs, M. (1993) Hereditary triosephosphate isomerase (TPI) deficiency: two severely affected brothers one with and one without neurological symptoms. *Hum Genet* **92**, 486-490
58. Hollan, S., Magocsi, M., Fodor, E., Horanyi, M., Harsanyi, V., and Farkas, T. (1997) Search for the pathogenesis of the differing phenotype in two compound heterozygote Hungarian brothers with the same genotypic triosephosphate isomerase deficiency. *Proc Natl Acad Sci U S A* **94**, 10362-10366
59. Orosz, F., Wagner, G., Liliom, K., Kovacs, J., Baroti, K., Horanyi, M., Farkas, T., Hollan, S., and Ovadi, J. (2000) Enhanced association of mutant triosephosphate

- isomerase to red cell membranes and to brain microtubules. *Proc Natl Acad Sci U S A* **97**, 1026-1031
60. Charles, D. J., and Pretsch, W. (1987) Linear dose-response relationship of erythrocyte enzyme-activity mutations in offspring of ethylnitrosourea-treated mice. *Mutat Res* **176**, 81-91
 61. Pretsch, W. (2009) Triosephosphate isomerase activity-deficient mice show haemolytic anaemia in homozygous condition. *Genet Res (Camb)* **91**, 1-4
 62. Ralser, M., Heeren, G., Breitenbach, M., Lehrach, H., and Krobitsch, S. (2006) Triose phosphate isomerase deficiency is caused by altered dimerization--not catalytic inactivity--of the mutant enzymes. *PLoS One* **1**, e30
 63. Rodriguez-Almazan, C., Arreola, R., Rodriguez-Larrea, D., Aguirre-Lopez, B., de Gomez-Puyou, M. T., Perez-Montfort, R., Costas, M., Gomez-Puyou, A., and Torres-Larios, A. (2008) Structural basis of human triosephosphate isomerase deficiency: mutation E104D is related to alterations of a conserved water network at the dimer interface. *J Biol Chem* **283**, 23254-23263
 64. Gnerer, J. P., Kreber, R. A., and Ganetzky, B. (2006) Wasted away, a *Drosophila* mutation in triosephosphate isomerase, causes paralysis, neurodegeneration, and early death. *Proc Natl Acad Sci U S A* **103**, 14987-14993
 65. Palladino, M. J., Hadley, T. J., and Ganetzky, B. (2002) Temperature-sensitive paralytic mutants are enriched for those causing neurodegeneration in *Drosophila*. *Genetics* **161**, 1197-1208
 66. Ganetzky, B., Loughney, K., and Wu, C. F. (1986) Analysis of mutations affecting sodium channels in *Drosophila*. *Ann N Y Acad Sci* **479**, 325-337
 67. Ganetzky, B., and Wu, C. F. (1986) Neurogenetics of membrane excitability in *Drosophila*. *Annu Rev Genet* **20**, 13-44
 68. Wu, C. F., and Ganetzky, B. (1992) Neurogenetic studies of ion channels in *Drosophila*. *Ion Channels* **3**, 261-314
 69. Wu, C. F., Ganetzky, B., Jan, L. Y., Jan, Y. N., and Benzer, S. (1978) A *Drosophila* mutant with a temperature-sensitive block in nerve conduction. *Proc Natl Acad Sci U S A* **75**, 4047-4051
 70. Jackson, F. R., Wilson, S. D., Strichartz, G. R., and Hall, L. M. (1984) Two types of mutants affecting voltage-sensitive sodium channels in *Drosophila melanogaster*. *Nature* **308**, 189-191
 71. Siddiqi, O., and Benzer, S. (1976) Neurophysiological defects in temperature-sensitive paralytic mutants of *Drosophila melanogaster*. *Proc Natl Acad Sci U S A* **73**, 3253-3257
 72. Vijayakrishnan, N., and Broadie, K. (2006) Temperature-sensitive paralytic mutants: insights into the synaptic vesicle cycle. *Biochem Soc Trans* **34**, 81-87
 73. Zhang, Y. Q., Bailey, A. M., Matthies, H. J., Renden, R. B., Smith, M. A., Speese, S. D., Rubin, G. M., and Broadie, K. (2001) *Drosophila fragile X*-related gene regulates the MAP1B homolog Futsch to control synaptic structure and function. *Cell* **107**, 591-603
 74. Parker, L., Howlett, I. C., Rusan, Z. M., and Tanouye, M. A. (2011) Seizure and epilepsy: studies of seizure disorders in *Drosophila*. *Int Rev Neurobiol* **99**, 1-21
 75. Song, J., and Tanouye, M. A. (2008) From bench to drug: human seizure modeling using *Drosophila*. *Prog Neurobiol* **84**, 182-191

76. Celotto, A. M., Chiu, W. K., Van Voorhies, W., and Palladino, M. J. (2011) Modes of metabolic compensation during mitochondrial disease using the *Drosophila* model of ATP6 dysfunction. *PLoS One* **6**, e25823
77. Howlett, I. C., and Tanouye, M. A. (2009) Neurocircuit assays for seizures in epilepsy mutants of *Drosophila*. *J Vis Exp*
78. Kuebler, D., Zhang, H., Ren, X., and Tanouye, M. A. (2001) Genetic suppression of seizure susceptibility in *Drosophila*. *J Neurophysiol* **86**, 1211-1225
79. Song, J., and Tanouye, M. A. (2006) Seizure suppression by shakB2, a gap junction mutation in *Drosophila*. *J Neurophysiol* **95**, 627-635
80. Glasscock, E., and Tanouye, M. A. (2005) *Drosophila* couch potato mutants exhibit complex neurological abnormalities including epilepsy phenotypes. *Genetics* **169**, 2137-2149
81. Hekmat-Scafe, D. S., Dang, K. N., and Tanouye, M. A. (2005) Seizure suppression by gain-of-function escargot mutations. *Genetics* **169**, 1477-1493
82. Hekmat-Scafe, D. S., Mercado, A., Fajilan, A. A., Lee, A. W., Hsu, R., Mount, D. B., and Tanouye, M. A. (2010) Seizure sensitivity is ameliorated by targeted expression of K⁺-Cl⁻ cotransporter function in the mushroom body of the *Drosophila* brain. *Genetics* **184**, 171-183
83. Howlett, I. C., and Tanouye, M. A. (2013) Seizure-Sensitivity in *Drosophila* Is Ameliorated by Dorsal Vessel Injection of the Antiepileptic Drug Valproate. *J Neurogenet*
84. Kuebler, D., and Tanouye, M. (2002) Anticonvulsant valproate reduces seizure-susceptibility in mutant *Drosophila*. *Brain Res* **958**, 36-42
85. Seigle, J. L., Celotto, A. M., and Palladino, M. J. (2008) Degradation of functional triose phosphate isomerase protein underlies sugarkill pathology. *Genetics* **179**, 855-862
86. Hrizo, S. L., and Palladino, M. J. (2010) Hsp70- and Hsp90-mediated proteasomal degradation underlies TPI sugarkill pathogenesis in *Drosophila*. *Neurobiol Dis* **40**, 676-683
87. Schuster, R., and Holzhutter, H. G. (1995) Use of mathematical models for predicting the metabolic effect of large-scale enzyme activity alterations. Application to enzyme deficiencies of red blood cells. *Eur J Biochem* **229**, 403-418
88. Olah, J., Orosz, F., Puskas, L. G., Hackler, L., Jr., Horanyi, M., Polgar, L., Hollan, S., and Ovadi, J. (2005) Triosephosphate isomerase deficiency: consequences of an inherited mutation at mRNA, protein and metabolic levels. *Biochem J* **392**, 675-683
89. Orosz, F., Vertessy, B. G., Hollan, S., Horanyi, M., and Ovadi, J. (1996) Triosephosphate isomerase deficiency: predictions and facts. *J Theor Biol* **182**, 437-447
90. Ralser, M., Wamelink, M. M., Kowald, A., Gerisch, B., Heeren, G., Struys, E. A., Klipp, E., Jakobs, C., Breitenbach, M., Lehrach, H., and Krobitsch, S. (2007) Dynamic rerouting of the carbohydrate flux is key to counteracting oxidative stress. *J Biol* **6**, 10
91. Gruning, N. M., Rinnerthaler, M., Bluemlein, K., Mulleder, M., Wamelink, M. M., Lehrach, H., Jakobs, C., Breitenbach, M., and Ralser, M. (2011) Pyruvate kinase triggers a metabolic feedback loop that controls redox metabolism in respiring cells. *Cell Metab* **14**, 415-427
92. Godon, C., Lagniel, G., Lee, J., Buhler, J. M., Kieffer, S., Perrot, M., Boucherie, H., Toledano, M. B., and Labarre, J. (1998) The H₂O₂ stimulon in *Saccharomyces cerevisiae*. *J Biol Chem* **273**, 22480-22489

93. Ahmed, N., Battah, S., Karachalias, N., Babaei-Jadidi, R., Horanyi, M., Baroti, K., Hollan, S., and Thornalley, P. J. (2003) Increased formation of methylglyoxal and protein glycation, oxidation and nitrosation in triosephosphate isomerase deficiency. *Biochim Biophys Acta* **1639**, 121-132
94. Miyazawa, N., Abe, M., Souma, T., Tanemoto, M., Abe, T., Nakayama, M., and Ito, S. (2010) Methylglyoxal augments intracellular oxidative stress in human aortic endothelial cells. *Free Radic Res* **44**, 101-107
95. Wang, H., Liu, J., and Wu, L. (2009) Methylglyoxal-induced mitochondrial dysfunction in vascular smooth muscle cells. *Biochem Pharmacol* **77**, 1709-1716
96. Rong, Y. S., and Golic, K. G. (2000) Gene targeting by homologous recombination in *Drosophila*. *Science* **288**, 2013-2018
97. Bischof, J., Maeda, R. K., Hediger, M., Karch, F., and Basler, K. (2007) An optimized transgenesis system for *Drosophila* using germ-line-specific phiC31 integrases. *Proc Natl Acad Sci U S A* **104**, 3312-3317
98. Groth, A. C., Fish, M., Nusse, R., and Calos, M. P. (2004) Construction of transgenic *Drosophila* by using the site-specific integrase from phage phiC31. *Genetics* **166**, 1775-1782
99. Huang, J., Zhou, W., Dong, W., Watson, A. M., and Hong, Y. (2009) From the Cover: Directed, efficient, and versatile modifications of the *Drosophila* genome by genomic engineering. *Proc Natl Acad Sci U S A* **106**, 8284-8289
100. Huang, J., Zhou, W., Watson, A. M., Jan, Y. N., and Hong, Y. (2008) Efficient ends-out gene targeting in *Drosophila*. *Genetics* **180**, 703-707
101. Huang, J., Huang, L., Chen, Y. J., Austin, E., Devor, C. E., Roegiers, F., and Hong, Y. (2011) Differential regulation of adherens junction dynamics during apical-basal polarization. *J Cell Sci* **124**, 4001-4013
102. Arya, R., Laloz, M. R., Bellingham, A. J., and Layton, D. M. (1997) Evidence for founder effect of the Glu104Asp substitution and identification of new mutations in triosephosphate isomerase deficiency. *Hum Mutat* **10**, 290-294
103. Daar, I. O., Artymiuk, P. J., Phillips, D. C., and Maquat, L. E. (1986) Human triosephosphate isomerase deficiency: a single amino acid substitution results in a thermolabile enzyme. *Proc Natl Acad Sci U S A* **83**, 7903-7907
104. Lodi, P. J., Chang, L. C., Knowles, J. R., and Komives, E. A. (1994) Triosephosphate isomerase requires a positively charged active site: the role of lysine-12. *Biochemistry* **33**, 2809-2814
105. Zhang, Z., Sugio, S., Komives, E. A., Liu, K. D., Knowles, J. R., Petsko, G. A., and Ringe, D. (1994) Crystal structure of recombinant chicken triosephosphate isomerase-phosphoglycolohydroxamate complex at 1.8-Å resolution. *Biochemistry* **33**, 2830-2837
106. Lambeir, A. M., Opperdoes, F. R., and Wierenga, R. K. (1987) Kinetic properties of triose-phosphate isomerase from *Trypanosoma brucei brucei*. A comparison with the rabbit muscle and yeast enzymes. *Eur J Biochem* **168**, 69-74
107. Norledge, B. V., Lambeir, A. M., Abagyan, R. A., Rottmann, A., Fernandez, A. M., Filimonov, V. V., Peter, M. G., and Wierenga, R. K. (2001) Modeling, mutagenesis, and structural studies on the fully conserved phosphate-binding loop (loop 8) of triosephosphate isomerase: toward a new substrate specificity. *Proteins* **42**, 383-389
108. Gong, W. J., and Golic, K. G. (2003) Ends-out, or replacement, gene targeting in *Drosophila*. *Proc Natl Acad Sci U S A* **100**, 2556-2561

109. Palladino, M. J., Bower, J. E., Kreber, R., and Ganetzky, B. (2003) Neural dysfunction and neurodegeneration in *Drosophila* Na⁺/K⁺ ATPase alpha subunit mutants. *J Neurosci* **23**, 1276-1286
110. Viant, M. R., Rosenblum, E. S., and Tjeerdema, R. S. (2001) Optimized method for the determination of phosphoarginine in abalone tissue by high-performance liquid chromatography. *J Chromatogr B Biomed Sci Appl* **765**, 107-111
111. Watanabe, M., Zingg, B. C., and Mohrenweiser, H. W. (1996) Molecular analysis of a series of alleles in humans with reduced activity at the triosephosphate isomerase locus. *Am J Hum Genet* **58**, 308-316
112. Pollarolo, G., Schulz, J. G., Munck, S., and Dotti, C. G. (2011) Cytokinesis remnants define first neuronal asymmetry in vivo. *Nat Neurosci* **14**, 1525-1533
113. Venken, K. J., Simpson, J. H., and Bellen, H. J. (2011) Genetic manipulation of genes and cells in the nervous system of the fruit fly. *Neuron* **72**, 202-230
114. Orosz, F., Olah, J., Alvarez, M., Keseru, G. M., Szabo, B., Wagner, G., Kovari, Z., Horanyi, M., Baroti, K., Martial, J. A., Hollan, S., and Ovadi, J. (2001) Distinct behavior of mutant triosephosphate isomerase in hemolysate and in isolated form: molecular basis of enzyme deficiency. *Blood* **98**, 3106-3112
115. Raines, R. T., Sutton, E. L., Straus, D. R., Gilbert, W., and Knowles, J. R. (1986) Reaction energetics of a mutant triosephosphate isomerase in which the active-site glutamate has been changed to aspartate. *Biochemistry* **25**, 7142-7154
116. Nickbarg, E. B., Davenport, R. C., Petsko, G. A., and Knowles, J. R. (1988) Triosephosphate isomerase: removal of a putatively electrophilic histidine residue results in a subtle change in catalytic mechanism. *Biochemistry* **27**, 5948-5960
117. Casteleijn, M. G., Alahuhta, M., Groebel, K., El-Sayed, I., Augustyns, K., Lambeir, A. M., Neubauer, P., and Wierenga, R. K. (2006) Functional role of the conserved active site proline of triosephosphate isomerase. *Biochemistry* **45**, 15483-15494
118. Go, M. K., Koudelka, A., Amyes, T. L., and Richard, J. P. (2010) Role of Lys-12 in catalysis by triosephosphate isomerase: a two-part substrate approach. *Biochemistry* **49**, 5377-5389
119. Lu, M., Sautin, Y. Y., Holliday, L. S., and Gluck, S. L. (2004) The glycolytic enzyme aldolase mediates assembly, expression, and activity of vacuolar H⁺-ATPase. *J Biol Chem* **279**, 8732-8739
120. Lu, M., Ammar, D., Ives, H., Albrecht, F., and Gluck, S. L. (2007) Physical interaction between aldolase and vacuolar H⁺-ATPase is essential for the assembly and activity of the proton pump. *J Biol Chem* **282**, 24495-24503
121. Pastorino, J. G., Shulga, N., and Hoek, J. B. (2002) Mitochondrial binding of hexokinase II inhibits Bax-induced cytochrome c release and apoptosis. *J Biol Chem* **277**, 7610-7618
122. Majewski, N., Nogueira, V., Bhaskar, P., Coy, P. E., Skeen, J. E., Gottlob, K., Chandel, N. S., Thompson, C. B., Robey, R. B., and Hay, N. (2004) Hexokinase-mitochondria interaction mediated by Akt is required to inhibit apoptosis in the presence or absence of Bax and Bak. *Mol Cell* **16**, 819-830
123. Zheng, L., Roeder, R. G., and Luo, Y. (2003) S phase activation of the histone H2B promoter by OCA-S, a coactivator complex that contains GAPDH as a key component. *Cell* **114**, 255-266

124. Niinaka, Y., Paku, S., Haga, A., Watanabe, H., and Raz, A. (1998) Expression and secretion of neuroleukin/phosphohexose isomerase/maturation factor as autocrine motility factor by tumor cells. *Cancer Res* **58**, 2667-2674
125. Coma, M., Guix, F. X., Uribesalgo, I., Espuna, G., Sole, M., Andreu, D., and Munoz, F. J. (2005) Lack of oestrogen protection in amyloid-mediated endothelial damage due to protein nitrotyrosination. *Brain* **128**, 1613-1621
126. Guix, F. X., Ill-Raga, G., Bravo, R., Nakaya, T., de Fabritiis, G., Coma, M., Miscione, G. P., Villa-Freixa, J., Suzuki, T., Fernandez-Busquets, X., Valverde, M. A., de Strooper, B., and Munoz, F. J. (2009) Amyloid-dependent triosephosphate isomerase nitrotyrosination induces glycation and tau fibrillation. *Brain* **132**, 1335-1345
127. Lee, W. H., Choi, J. S., Byun, M. R., Koo, K. T., Shin, S., Lee, S. K., and Surh, Y. J. (2010) Functional inactivation of triosephosphate isomerase through phosphorylation during etoposide-induced apoptosis in HeLa cells: potential role of Cdk2. *Toxicology* **278**, 224-228
128. Kim, C., Lim, Y., Yoo, B. C., Won, N. H., Kim, S., and Kim, G. (2010) Regulation of post-translational protein arginine methylation during HeLa cell cycle. *Biochim Biophys Acta* **1800**, 977-985
129. Khurana, V., and Feany, M. B. (2007) Connecting cell-cycle activation to neurodegeneration in Drosophila. *Biochim Biophys Acta* **1772**, 446-456
130. Yang, Y., Geldmacher, D. S., and Herrup, K. (2001) DNA replication precedes neuronal cell death in Alzheimer's disease. *J Neurosci* **21**, 2661-2668
131. Studier, F. W. (2005) Protein production by auto-induction in high density shaking cultures. *Protein Expr Purif* **41**, 207-234
132. Williams, J. C., Zeelen, J. P., Neubauer, G., Vriend, G., Backmann, J., Michels, P. A., Lambeir, A. M., and Wierenga, R. K. (1999) Structural and mutagenesis studies of leishmania triosephosphate isomerase: a point mutation can convert a mesophilic enzyme into a superstable enzyme without losing catalytic power. *Protein Eng* **12**, 243-250
133. Ganetzky, B., and Wu, C. F. (1982) Indirect Suppression Involving Behavioral Mutants with Altered Nerve Excitability in DROSOPHILA MELANOGASTER. *Genetics* **100**, 597-614
134. Morrison, J. F., Griffiths, D. E., and Ennor, A. H. (1957) The purification and properties of arginine phosphokinase. *Biochem J* **65**, 143-153
135. Rangaraju, V., Calloway, N., and Ryan, T. A. (2014) Activity-driven local ATP synthesis is required for synaptic function. *Cell* **156**, 825-835
136. Dietzl, G., Chen, D., Schnorrer, F., Su, K. C., Barinova, Y., Fellner, M., Gasser, B., Kinsey, K., Oettel, S., Scheiblauer, S., Couto, A., Marra, V., Keleman, K., and Dickson, B. J. (2007) A genome-wide transgenic RNAi library for conditional gene inactivation in Drosophila. *Nature* **448**, 151-156
137. Aguirre, Y., Cabrera, N., Aguirre, B., Perez-Montfort, R., Hernandez-Santoyo, A., Reyes-Vivas, H., Enriquez-Flores, S., de Gomez-Puyou, M. T., Gomez-Puyou, A., Sanchez-Ruiz, J. M., and Costas, M. (2013) Different contribution of conserved amino acids to the global properties of triosephosphate isomerases. *Proteins*
138. Uversky, V. N., and Fink, A. L. (2007) *Protein misfolding, aggregation and conformational diseases. Part B, Molecular mechanisms of conformational diseases*, Springer, New York ; London

139. Zhang, X., Smith, D. L., Meriin, A. B., Engemann, S., Russel, D. E., Roark, M., Washington, S. L., Maxwell, M. M., Marsh, J. L., Thompson, L. M., Wanker, E. E., Young, A. B., Housman, D. E., Bates, G. P., Sherman, M. Y., and Kazantsev, A. G. (2005) A potent small molecule inhibits polyglutamine aggregation in Huntington's disease neurons and suppresses neurodegeneration in vivo. *Proc Natl Acad Sci U S A* **102**, 892-897
140. Brent, J. R., Werner, K. M., and McCabe, B. D. (2009) Drosophila larval NMJ dissection. *J Vis Exp*
141. Verstreken, P., Ohyama, T., and Bellen, H. J. (2008) FM 1-43 labeling of synaptic vesicle pools at the Drosophila neuromuscular junction. *Methods Mol Biol* **440**, 349-369
142. Kursula, I., Partanen, S., Lambeir, A. M., and Wierenga, R. K. (2002) The importance of the conserved Arg191-Asp227 salt bridge of triosephosphate isomerase for folding, stability, and catalysis. *FEBS Lett* **518**, 39-42
143. Borchert, T. V., Zeelen, J. P., Schliebs, W., Callens, M., Minke, W., Jaenicke, R., and Wierenga, R. K. (1995) An interface point-mutation variant of triosephosphate isomerase is compactly folded and monomeric at low protein concentrations. *FEBS Lett* **367**, 315-318
144. Mainfroid, V., Mande, S. C., Hol, W. G., Martial, J. A., and Goraj, K. (1996) Stabilization of human triosephosphate isomerase by improvement of the stability of individual alpha-helices in dimeric as well as monomeric forms of the protein. *Biochemistry* **35**, 4110-4117
145. Mainfroid, V., Terpstra, P., Beauregard, M., Frere, J. M., Mande, S. C., Hol, W. G., Martial, J. A., and Goraj, K. (1996) Three hTIM mutants that provide new insights on why TIM is a dimer. *J Mol Biol* **257**, 441-456
146. Hinault, M. P., Ben-Zvi, A., and Goloubinoff, P. (2006) Chaperones and proteases: cellular fold-controlling factors of proteins in neurodegenerative diseases and aging. *J Mol Neurosci* **30**, 249-265
147. Lambeir, A. M., Backmann, J., Ruiz-Sanz, J., Filimonov, V., Nielsen, J. E., Kursula, I., Norledge, B. V., and Wierenga, R. K. (2000) The ionization of a buried glutamic acid is thermodynamically linked to the stability of Leishmania mexicana triose phosphate isomerase. *Eur J Biochem* **267**, 2516-2524
148. Suzuki, D. T., Grigliatti, T., and Williamson, R. (1971) Temperature-sensitive mutations in Drosophila melanogaster. VII. A mutation (para-ts) causing reversible adult paralysis. *Proc Natl Acad Sci U S A* **68**, 890-893
149. Kawasaki, F., Felling, R., and Ordway, R. W. (2000) A temperature-sensitive paralytic mutant defines a primary synaptic calcium channel in Drosophila. *J Neurosci* **20**, 4885-4889
150. Pallanck, L., Ordway, R. W., and Ganetzky, B. (1995) A Drosophila NSF mutant. *Nature* **376**, 25
151. Dickman, D. K., Lu, Z., Meinertzhagen, I. A., and Schwarz, T. L. (2006) Altered synaptic development and active zone spacing in endocytosis mutants. *Curr Biol* **16**, 591-598
152. McCabe, B. D., Marques, G., Haghghi, A. P., Fetter, R. D., Crotty, M. L., Haerry, T. E., Goodman, C. S., and O'Connor, M. B. (2003) The BMP homolog Gbb provides a retrograde signal that regulates synaptic growth at the Drosophila neuromuscular junction. *Neuron* **39**, 241-254

153. Fuentes-Medel, Y., Ashley, J., Barria, R., Maloney, R., Freeman, M., and Budnik, V. (2012) Integration of a retrograde signal during synapse formation by glia-secreted TGF-beta ligand. *Curr Biol* **22**, 1831-1838
154. Packard, M., Koo, E. S., Gorczyca, M., Sharpe, J., Cumberledge, S., and Budnik, V. (2002) The Drosophila Wnt, wingless, provides an essential signal for pre- and postsynaptic differentiation. *Cell* **111**, 319-330
155. Budnik, V., and Salinas, P. C. (2011) Wnt signaling during synaptic development and plasticity. *Curr Opin Neurobiol* **21**, 151-159
156. Scott, D. A., Das, U., Tang, Y., and Roy, S. (2011) Mechanistic logic underlying the axonal transport of cytosolic proteins. *Neuron* **70**, 441-454
157. Boulanger, A., Farge, M., Ramanoudjame, C., Wharton, K., and Dura, J. M. (2012) Drosophila motor neuron retraction during metamorphosis is mediated by inputs from TGF-beta/BMP signaling and orphan nuclear receptors. *PLoS One* **7**, e40255
158. Wang, P., Saraswati, S., Guan, Z., Watkins, C. J., Wurtman, R. J., and Littleton, J. T. (2004) A Drosophila temperature-sensitive seizure mutant in phosphoglycerate kinase disrupts ATP generation and alters synaptic function. *J Neurosci* **24**, 4518-4529
159. Beernink, P. T., and Tolan, D. R. (1996) Disruption of the aldolase A tetramer into catalytically active monomers. *Proc Natl Acad Sci U S A* **93**, 5374-5379
160. Zhang, E., Brewer, J. M., Minor, W., Carreira, L. A., and Lebioda, L. (1997) Mechanism of enolase: the crystal structure of asymmetric dimer enolase-2-phospho-D-glycerate/enolase-phosphoenolpyruvate at 2.0 Å resolution. *Biochemistry* **36**, 12526-12534
161. Steitz, T. A., Fletterick, R. J., Anderson, W. F., and Anderson, C. M. (1976) High resolution x-ray structure of yeast hexokinase, an allosteric protein exhibiting a non-symmetric arrangement of subunits. *J Mol Biol* **104**, 197-122
162. Fredriksson, L., Li, H., and Eriksson, U. (2004) The PDGF family: four gene products form five dimeric isoforms. *Cytokine Growth Factor Rev* **15**, 197-204
163. Schlessinger, J. (2002) Ligand-induced, receptor-mediated dimerization and activation of EGF receptor. *Cell* **110**, 669-672
164. Dominguez, R., and Holmes, K. C. (2011) Actin structure and function. *Annu Rev Biophys* **40**, 169-186
165. Sutton, R. B., Fasshauer, D., Jahn, R., and Brunger, A. T. (1998) Crystal structure of a SNARE complex involved in synaptic exocytosis at 2.4 Å resolution. *Nature* **395**, 347-353
166. Fernandez, I., Ubach, J., Dulubova, I., Zhang, X., Sudhof, T. C., and Rizo, J. (1998) Three-dimensional structure of an evolutionarily conserved N-terminal domain of syntaxin 1A. *Cell* **94**, 841-849
167. Peimbert, M., Dominguez-Ramirez, L., and Fernandez-Velasco, D. A. (2008) Hydrophobic repacking of the dimer interface of triosephosphate isomerase by in silico design and directed evolution. *Biochemistry* **47**, 5556-5564
168. Hernandez-Alcantara, G., Torres-Larios, A., Enriquez-Flores, S., Garcia-Torres, I., Castillo-Villanueva, A., Mendez, S. T., de la Mora-de la Mora, I., Gomez-Manzo, S., Torres-Arroyo, A., Lopez-Velazquez, G., Reyes-Vivas, H., and Oria-Hernandez, J. (2013) Structural and functional perturbation of giardia lamblia triosephosphate isomerase by modification of a non-catalytic, non-conserved region. *PLoS One* **8**, e69031

169. Chanez-Cardenas, M. E., Fernandez-Velasco, D. A., Vazquez-Contreras, E., Coria, R., Saab-Rincon, G., and Perez-Montfort, R. (2002) Unfolding of triosephosphate isomerase from *Trypanosoma brucei*: identification of intermediates and insight into the denaturation pathway using tryptophan mutants. *Arch Biochem Biophys* **399**, 117-129
170. Chanez-Cardenas, M. E., Perez-Hernandez, G., Sanchez-Rebollar, B. G., Costas, M., and Vazquez-Contreras, E. (2005) Reversible equilibrium unfolding of triosephosphate isomerase from *Trypanosoma cruzi* in guanidinium hydrochloride involves stable dimeric and monomeric intermediates. *Biochemistry* **44**, 10883-10892
171. Gonzalez-Mondragon, E., Zubillaga, R. A., and Hernandez-Arana, A. (2007) Effect of a specific inhibitor on the unfolding and refolding kinetics of dimeric triosephosphate isomerase: establishing the dimeric and similarly structured nature of the main transition states on the forward and backward reactions. *Biophys Chem* **125**, 172-178
172. Mixcoha-Hernandez, E., Moreno-Vargas, L. M., Rojo-Dominguez, A., and Benitez-Cardoza, C. G. (2007) Thermal-unfolding reaction of triosephosphate isomerase from *Trypanosoma cruzi*. *Protein J* **26**, 491-498
173. Tellez, L. A., Blancas-Mejia, L. M., Carrillo-Nava, E., Mendoza-Hernandez, G., Cisneros, D. A., and Fernandez-Velasco, D. A. (2008) Thermal unfolding of triosephosphate isomerase from *Entamoeba histolytica*: dimer dissociation leads to extensive unfolding. *Biochemistry* **47**, 11665-11673
174. Thanki, N., Zeelen, J. P., Mathieu, M., Jaenicke, R., Abagyan, R. A., Wierenga, R. K., and Schliebs, W. (1997) Protein engineering with monomeric triosephosphate isomerase (monoTIM): the modelling and structure verification of a seven-residue loop. *Protein Eng* **10**, 159-167
175. Benitez-Cardoza, C. G., Rojo-Dominguez, A., and Hernandez-Arana, A. (2001) Temperature-induced denaturation and renaturation of triosephosphate isomerase from *Saccharomyces cerevisiae*: evidence of dimerization coupled to refolding of the thermally unfolded protein. *Biochemistry* **40**, 9049-9058
176. Fenn, R. H., and Marshall, G. E. (1972) The stereochemical structure of disodium DL-glycerol 3-phosphate hexahydrate, the D isomer of which is an inhibitor of triose phosphate isomerase. *Biochem J* **130**, 1-10
177. Rozovsky, S., and McDermott, A. E. (2001) The time scale of the catalytic loop motion in triosephosphate isomerase. *J Mol Biol* **310**, 259-270
178. Nickbarg, E. B., and Knowles, J. R. (1988) Triosephosphate isomerase: energetics of the reaction catalyzed by the yeast enzyme expressed in *Escherichia coli*. *Biochemistry* **27**, 5939-5947
179. Sun, J., and Sampson, N. S. (1998) Determination of the amino acid requirements for a protein hinge in triosephosphate isomerase. *Protein Sci* **7**, 1495-1505
180. Xiang, J., Sun, J., and Sampson, N. S. (2001) The importance of hinge sequence for loop function and catalytic activity in the reaction catalyzed by triosephosphate isomerase. *J Mol Biol* **307**, 1103-1112
181. Massi, F., Wang, C., and Palmer, A. G., 3rd. (2006) Solution NMR and computer simulation studies of active site loop motion in triosephosphate isomerase. *Biochemistry* **45**, 10787-10794
182. Kursula, I., Salin, M., Sun, J., Norledge, B. V., Haapalainen, A. M., Sampson, N. S., and Wierenga, R. K. (2004) Understanding protein lids: structural analysis of active hinge mutants in triosephosphate isomerase. *Protein Eng Des Sel* **17**, 375-382

183. Sun, J., and Sampson, N. S. (1999) Understanding protein lids: kinetic analysis of active hinge mutants in triosephosphate isomerase. *Biochemistry* **38**, 11474-11481
184. Rozovsky, S., Jogl, G., Tong, L., and McDermott, A. E. (2001) Solution-state NMR investigations of triosephosphate isomerase active site loop motion: ligand release in relation to active site loop dynamics. *J Mol Biol* **310**, 271-280
185. Johnson, L. N., and Wolfenden, R. (1970) Changes in absorption spectrum and crystal structure of triose phosphate isomerase brought about by 2-phosphoglycollate, a potential transition state analogue. *J Mol Biol* **47**, 93-100
186. Otwinowski, Z., and Minor, W. (1997) Processing of X-ray diffraction data collected in oscillation mode. *Method Enzymol* **276**, 307-326
187. Emsley, P., Lohkamp, B., Scott, W. G., and Cowtan, K. (2010) Features and development of Coot. *Acta Crystallogr D Biol Crystallogr* **66**, 486-501
188. Davis, I. W., Leaver-Fay, A., Chen, V. B., Block, J. N., Kapral, G. J., Wang, X., Murray, L. W., Arendall, W. B., 3rd, Snoeyink, J., Richardson, J. S., and Richardson, D. C. (2007) MolProbity: all-atom contacts and structure validation for proteins and nucleic acids. *Nucleic Acids Res* **35**, W375-383
189. Orosz, F., Olah, J., and Ovadi, J. (2011) Reappraisal of triosephosphate isomerase deficiency. *Eur J Haematol* **86**, 265-267
190. Vogelstein, B., Lane, D., and Levine, A. J. (2000) Surfing the p53 network. *Nature* **408**, 307-310
191. Ryan, K. M., Phillips, A. C., and Vousden, K. H. (2001) Regulation and function of the p53 tumor suppressor protein. *Curr Opin Cell Biol* **13**, 332-337
192. Clore, G. M., Omichinski, J. G., Sakaguchi, K., Zambrano, N., Sakamoto, H., Appella, E., and Gronenborn, A. M. (1994) High-resolution structure of the oligomerization domain of p53 by multidimensional NMR. *Science* **265**, 386-391
193. Momand, J., Wu, H. H., and Dasgupta, G. (2000) MDM2--master regulator of the p53 tumor suppressor protein. *Gene* **242**, 15-29
194. Stommel, J. M., Marchenko, N. D., Jimenez, G. S., Moll, U. M., Hope, T. J., and Wahl, G. M. (1999) A leucine-rich nuclear export signal in the p53 tetramerization domain: regulation of subcellular localization and p53 activity by NES masking. *EMBO J* **18**, 1660-1672
195. Hainaut, P., and Hollstein, M. (2000) p53 and human cancer: the first ten thousand mutations. *Adv Cancer Res* **77**, 81-137
196. Huang, Z., Wu, Q., Guryanova, O. A., Cheng, L., Shou, W., Rich, J. N., and Bao, S. (2011) Deubiquitylase HAUSP stabilizes REST and promotes maintenance of neural progenitor cells. *Nat Cell Biol* **13**, 142-152
197. Ruault, M., and Pillus, L. (2006) Chromatin-modifying enzymes are essential when the *Saccharomyces cerevisiae* morphogenesis checkpoint is constitutively activated. *Genetics* **174**, 1135-1149
198. Rauch, J., Volinsky, N., Romano, D., and Kolch, W. (2011) The secret life of kinases: functions beyond catalysis. *Cell Commun Signal* **9**, 23
199. Wierenga, R. K., Noble, M. E., Postma, J. P., Groendijk, H., Kalk, K. H., Hol, W. G., and Opperdoes, F. R. (1991) The crystal structure of the "open" and the "closed" conformation of the flexible loop of trypanosomal triosephosphate isomerase. *Proteins* **10**, 33-49

200. Wierenga, R. K., Noble, M. E., Vriend, G., Nauche, S., and Hol, W. G. (1991) Refined 1.83 Å structure of trypanosomal triosephosphate isomerase crystallized in the presence of 2.4 M-ammonium sulphate. A comparison with the structure of the trypanosomal triosephosphate isomerase-glycerol-3-phosphate complex. *J Mol Biol* **220**, 995-1015
201. Zhang, Z., Komives, E. A., Sugio, S., Blacklow, S. C., Narayana, N., Xuong, N. H., Stock, A. M., Petsko, G. A., and Ringe, D. (1999) The role of water in the catalytic efficiency of triosephosphate isomerase. *Biochemistry* **38**, 4389-4397
202. Albery, W. J., and Knowles, J. R. (1976) Free-energy profile of the reaction catalyzed by triosephosphate isomerase. *Biochemistry* **15**, 5627-5631
203. Sun, A. Q., Yuksel, K. U., and Gracy, R. W. (1992) Interactions between the catalytic centers and subunit interface of triosephosphate isomerase probed by refolding, active site modification, and subunit exchange. *J Biol Chem* **267**, 20168-20174
204. Chintapalli, V. R., Wang, J., and Dow, J. A. (2007) Using FlyAtlas to identify better *Drosophila melanogaster* models of human disease. *Nat Genet* **39**, 715-720
205. Lu, M., Holliday, L. S., Zhang, L., Dunn, W. A., Jr., and Gluck, S. L. (2001) Interaction between aldolase and vacuolar H⁺-ATPase: evidence for direct coupling of glycolysis to the ATP-hydrolyzing proton pump. *J Biol Chem* **276**, 30407-30413
206. Jung, J., Yoon, T., Choi, E. C., and Lee, K. (2002) Interaction of cofilin with triosephosphate isomerase contributes glycolytic fuel for Na,K-ATPase via Rho-mediated signaling pathway. *J Biol Chem* **277**, 48931-48937
207. Sanyal, S., Consoulas, C., Kuromi, H., Basole, A., Mukai, L., Kidokoro, Y., Krishnan, K. S., and Ramaswami, M. (2005) Analysis of conditional paralytic mutants in *Drosophila* sarco-endoplasmic reticulum calcium ATPase reveals novel mechanisms for regulating membrane excitability. *Genetics* **169**, 737-750
208. Wang, J. W., Beck, E. S., and McCabe, B. D. (2012) A modular toolset for recombination transgenesis and neurogenetic analysis of *Drosophila*. *PLoS One* **7**, e42102
209. Zhu, Q., and Halfon, M. S. (2007) Vector-dependent gene expression driven by insulated P-element reporter vectors. *Fly (Austin)* **1**, 55-56
210. Markstein, M., Pitsouli, C., Villalta, C., Celniker, S. E., and Perrimon, N. (2008) Exploiting position effects and the gypsy retrovirus insulator to engineer precisely expressed transgenes. *Nat Genet* **40**, 476-483
211. Pfeiffer, B. D., Jenett, A., Hammonds, A. S., Ngo, T. T., Misra, S., Murphy, C., Scully, A., Carlson, J. W., Wan, K. H., Laverty, T. R., Mungall, C., Svirskas, R., Kadonaga, J. T., Doe, C. Q., Eisen, M. B., Celniker, S. E., and Rubin, G. M. (2008) Tools for neuroanatomy and neurogenetics in *Drosophila*. *Proc Natl Acad Sci U S A* **105**, 9715-9720
212. Verstreken, P., Ly, C. V., Venken, K. J., Koh, T. W., Zhou, Y., and Bellen, H. J. (2005) Synaptic mitochondria are critical for mobilization of reserve pool vesicles at *Drosophila* neuromuscular junctions. *Neuron* **47**, 365-378
213. Fergestad, T., Bostwick, B., and Ganetzky, B. (2006) Metabolic disruption in *Drosophila* bang-sensitive seizure mutants. *Genetics* **173**, 1357-1364
214. Pavlidis, P., Ramaswami, M., and Tanouye, M. A. (1994) The *Drosophila* easily shocked gene: a mutation in a phospholipid synthetic pathway causes seizure, neuronal failure, and paralysis. *Cell* **79**, 23-33

215. Royden, C. S., Pirrotta, V., and Jan, L. Y. (1987) The tko locus, site of a behavioral mutation in *D. melanogaster*, codes for a protein homologous to prokaryotic ribosomal protein S12. *Cell* **51**, 165-173
216. Celotto, A. M., Frank, A. C., McGrath, S. W., Fergestad, T., Van Voorhies, W. A., Buttle, K. F., Mannella, C. A., and Palladino, M. J. (2006) Mitochondrial encephalomyopathy in *Drosophila*. *J Neurosci* **26**, 810-820
217. Celotto, A. M., Liu, Z., Vandemark, A. P., and Palladino, M. J. (2012) A novel *Drosophila* SOD2 mutant demonstrates a role for mitochondrial ROS in neurodevelopment and disease. *Brain Behav* **2**, 424-434
218. Zhang, Y. Q., Roote, J., Brogna, S., Davis, A. W., Barbash, D. A., Nash, D., and Ashburner, M. (1999) stress sensitive B encodes an adenine nucleotide translocase in *Drosophila melanogaster*. *Genetics* **153**, 891-903
219. Zala, D., Hinckelmann, M. V., Yu, H., Lyra da Cunha, M. M., Liot, G., Cordelieres, F. P., Marco, S., and Saudou, F. (2013) Vesicular glycolysis provides on-board energy for fast axonal transport. *Cell* **152**, 479-491
220. Hara, M. R., Agrawal, N., Kim, S. F., Cascio, M. B., Fujimuro, M., Ozeki, Y., Takahashi, M., Cheah, J. H., Tankou, S. K., Hester, L. D., Ferris, C. D., Hayward, S. D., Snyder, S. H., and Sawa, A. (2005) S-nitrosylated GAPDH initiates apoptotic cell death by nuclear translocation following Siah1 binding. *Nat Cell Biol* **7**, 665-674
221. Baraghis, E., Devor, A., Fang, Q., Srinivasan, V. J., Wu, W., Lesage, F., Ayata, C., Kasischke, K. A., Boas, D. A., and Sakadzic, S. (2011) Two-photon microscopy of cortical NADH fluorescence intensity changes: correcting contamination from the hemodynamic response. *J Biomed Opt* **16**, 106003
222. Asfour, H., Wengrowski, A. M., Jaimes, R., 3rd, Swift, L. M., and Kay, M. W. (2012) NADH fluorescence imaging of isolated biventricular working rabbit hearts. *J Vis Exp*
223. Walsh, A. J., Poole, K. M., Duvall, C. L., and Skala, M. C. (2012) Ex vivo optical metabolic measurements from cultured tissue reflect in vivo tissue status. *J Biomed Opt* **17**, 116015
224. Ardura, J. A., and Friedman, P. A. (2011) Regulation of G protein-coupled receptor function by Na⁺/H⁺ exchange regulatory factors. *Pharmacol Rev* **63**, 882-900
225. Feng, W., and Zhang, M. (2009) Organization and dynamics of PDZ-domain-related supramodules in the postsynaptic density. *Nat Rev Neurosci* **10**, 87-99
226. Geering, K. (2001) The functional role of beta subunits in oligomeric P-type ATPases. *J Bioenerg Biomembr* **33**, 425-438
227. Jinek, M., Chylinski, K., Fonfara, I., Hauer, M., Doudna, J. A., and Charpentier, E. (2012) A programmable dual-RNA-guided DNA endonuclease in adaptive bacterial immunity. *Science* **337**, 816-821
228. Jinek, M., East, A., Cheng, A., Lin, S., Ma, E., and Doudna, J. (2013) RNA-programmed genome editing in human cells. *Elife* **2**, e00471
229. Gratz, S. J., Cummings, A. M., Nguyen, J. N., Hamm, D. C., Donohue, L. K., Harrison, M. M., Wildonger, J., and O'Connor-Giles, K. M. (2013) Genome engineering of *Drosophila* with the CRISPR RNA-guided Cas9 nuclease. *Genetics* **194**, 1029-1035
230. Gratz, S. J., Wildonger, J., Harrison, M. M., and O'Connor-Giles, K. M. (2013) CRISPR/Cas9-mediated genome engineering and the promise of designer flies on demand. *Fly (Austin)* **7**

